STRENGTHENING MECHANISMS IN STEEL

MORRIS COHEN, S. C. MOSS, D. W. HOFFMAN, B. A. MacDONALD,
G. LANGFORD, U. H. LINDBORG, and B. L. AVERBACH

MASSACHUSETTS INSTITUTE OF TECHNOLOGY

*** Export controls have been removed ***

This technical report has been reviewed and is approved.

I. PERLMUTTER
Chief, Physical Metallurgy Branch
Metals and Ceramics Division
Air Force Materials Laboratory

TABLE OF CONTENTS

v

LIST OF TABLES

Contrails

I. GENERAL INTRODUCTION

This report represents the culmination of a three-year research program on five aspects of strengthening mechanisms in steel: (1) atomic displacements in martensite, (2) ausforming of iron-nickel-carbon martensites, (3) strain tempering of iron-carbon martensites, (4) strain hardening of body-centered cubic versus face-centered cubic metals at very high strains, and (5) modes of fracture in martensite. The underlying reason for these five investigations was to provide further basic understanding of the strengthening processes at play in virgin and tempered martensites, with and without thermomechanical treatments.

II. GENERAL SUMMARY

A. Atomic Displacements in Martensite

With the aid of x-ray intensity measurements, an attempt has been made to determine the local distortions around interstitial carbon atoms in iron-carbon body-centered tetragonal martensite, taking into account the anisotropy of both the static and thermal displacements. The local distortions are of special importance in the theory of the solid-solution strengthening of martensite. In order to rationalize the anisotropy of the thermal displacements with the observed anisotropy in the thermal-expansion coefficients, it is necessary to assume that the static displacements vary with temperature, which is in line with the known temperature-dependence of Poisson's ratio. However, these effects are minor compared to the static displacements.

In the 1.33 percent carbon martensite investigated, the RMS static displacement is $0.24\mathring{A}$ in the c-direction, but it is less than $0.09 \mathring{A}$ in the a-direction; this represents a much higher degree of anisotropy than previously reported. These quantities can be used to compute the displacements of iron atoms next to carbon atoms and the corresponding local tetragonal strain ($\epsilon_c - \epsilon_a$). The resulting values are $0.68 \mathring{A}$ in the c-direction, $-0.17 \mathring{A}^\circ$ in the a-direction, and $\epsilon_c - \epsilon_a = 0.57$. Considering the calculations involved, these values should be regarded essentially as upper limits, but the method seems capable of eventually yielding just the quantities needed to test the theory of solid-solution strengthening of iron-carbon martensites.

B. Ausforming of Iron-Nickel-Carbon Martensites

The magnitude and mechanisms of ausform-strengthening in an iron - 23 percent nickel - 0.4 percent carbon martensite were examined in detail, with particular regard to (a) the state of the deformed parent austenite, (b) the correction for retained austenite present with the ausformed martensite, and (c) the role of subsequent aging or tempering.

In the virgin martensite the yield stress (flow stress at low strains in a tensile test) is relatively low whether the martensite

1

is ausformed or not. During tempering from -100°C to slightly a-
bove room temperature, the yield strength rises rapidly with both
types of martensite, but the increment of ausform-strengthening re-
mains the same, and is attributable mainly to the lattice imperfec-
tions introduced into the parent austenite by the prior plastic
deformation.

When the tempering temperature approaches 200°C, however, the
increment of ausform-strengthening becomes quite large because the
ausformed martensite resists softening on tempering more effective-
ly than does the regular martensite. Strain-aging and electrical-
resistivity experiments show that the rate of carbide precipitation
on tempering is significantly retarded in the ausformed martensite,
thereby suggesting that a larger component of interstitial solid-
solution strengthening prevails than in the tempering of regular
martensite. This difference in tempering kinetics is ascribed to
the trapping and stabilization of carbon atoms at lattice imperfec-
tions in the ausformed martensite.

C. Strain Tempering of Iron-Carbon Martensites

Martensites in the range of 0.18 - 0.80 percent carbon, with
and without pretempering, have been subjected to systematic combin-
ations of strain tempering by conical brale indentations and subse-
quent retempering. Such plastic deformation of as-quenched marten-
site tends to suppress the precipitation of epsilon carbide during
the first stage of tempering; in fact, if epsilon carbide is al-
ready present due to pretempering, this carbide actually dissolves
as a result of plastic straining and retempering at temperatures
where epsilon carbide would normally form. It is deduced (a) that
lattice vacancies as well as dislocations are generated by the plas-
tic deformation, (b) that dislocations and lattice vacancies pro-
vide more stable sites for the carbon atoms than exist in the epsi-
lon-carbide lattice, and (c) that dislocation movements are im-
peded by carbon clusters at strategic points. Thus, the observed
hardening is attributed to dislocation locking by carbon atoms, a
state which can persist up to higher-than-usual tempering tempera-
tures because the driving force for epsilon-carbide precipitation
is nullified by the carbon-atom traps.

If the tempering after plastic straining is carried above 250°C,
cementite precipitation ensues as might be expected in the third
stage of tempering, but there is evidence that the nucleation rate
is retarded while the spheroidization rate is enhanced. These phe-
nomena are explained by a reduced driving force for cementite pre-
cipitation, and the availability of excess vacancies when the car-
bon atoms transfer from the vacancy traps to the carbide lattice.
As the cementite particles coalesce on further tempering, the dis-
locations introduced by the plastic deformation anneal out progres-
sively, and the hardness increment due to strain tempering gradually
disappears.

When the pretempering of the martensite causes cementite to
form, the general hardness levels are relatively low, but a sub-
stantial response to strain tempering is still found. In this
case, however, the cementite is not noticeably redissolved (like

2

the epsilon carbide) by plastic deformation and retempering.   Instead, ordinary strain aging is encountered in which the dislocation arrays are first locked by carbon atmospheres and then pinned by actual carbide precipitation; the carbon for these effects appears to come from the low-carbon ferritic matrix of the pretempered steel.

D.   Strain Hardening of Body-Centered Cubic vs Face-Centered Cubic Metals at Very High Strains

The strain hardenability of BCC iron (0.006 percent carbon), FCC austenite (iron - 31.9 percent nickel - 0.008 percent carbon), and BCC martensite of the latter composition has been studied by wire-drawing experiments, with particular attention to the attainment of homogeneous deformation at natural strains up to about 7. The iron and martensite were wire drawn at room temperature, but the austenite was drawn at 130°C to avoid the formation of martensite due to the plastic deformation.   Tensile tests were carried out as a function of plastic strain, care being taken to minimize strain-aging effects.   The strain-hardened structures were examined on longitudinal sections by transmission electron microscopy.

Substructures comprised mainly of elongated cells with walls of entangled dislocations are generated by the wire drawing in all three materials, and the strength is found to vary inversely with the square root of the average transverse dimension of the cells, as in the Petch relation for grain-size strengthening.   However, the transverse dimension of the cells varies in a complex way with the drawing strain.   In the austenite, the cells seem to undergo axially symmetric flow, but reach a limiting cross section due to migration of the cell walls (dynamic recovery) at a strain of about 2, after which no further strain hardening ensues.   In contrast, the cells in the iron and martensite first become ribbon-shaped, and then undergo axial flow while the cellular cross section continues to be reduced up to largest strains attained.   Correspondingly, both the iron and martensite maintain a high rate of strain hardening throughout the wire drawing, although there is a slight decrease in the hardening rate of the martensite, perhaps caused by some dynamic recovery or by the generation of austenite due to the high hydrostatic pressures set up in the drawing process.

Nevertheless, the iron and martensite strain harden at approximately the same rate, but the martensite attains higher strength levels inasmuch as it has a higher friction stress and achieves a smaller transverse cell size because of its finer starting structure.   The k_y values obtained for the iron and martensite through these measurements suggest that the cell walls are effective barriers to slip, but somewhat less so than regular grain boundaries. Notwithstanding such strengthening by strain hardening, the attendant substructural changes do not seem to be operative in the quench hardening of steel, and therefore are not considered responsible for the strength of regular tetragonal martensite.

It is concluded that the differences in strain-hardening characteristics between the BCC and FCC metals are attributable, not to any basic difference in the plastic flow of the two lattices, but to whether or not the cell walls are inhibited from migrating by interstitial impurities.

3

E. **Modes of Fracture in Martensite**

The modes of fracture in as-quenched and tempered martensite
containing 0.3 percent carbon were investigated by transmission
electron microscopy. The specimens consisted of foils 5 - 10μ
thick, and they were fractured at room temperature and at -195°C
by indentation with a needle. Due to plastic deformation in vary-
ing degree along the fracture path, sufficient thinning occurred
to produce electron-transparent zones for electron microscopy and
selected-area diffraction. These zones became wider with increas-
ing tempering temperature.

The fracture path in martensite is found to be transgranular
with respect to the martensitic crystallites, but there are many
fracture segments across each crystallite. Analysis of the ori-
entation distribution of the segments shows that certain crystal-
lographic planes are favored in the fracturing process. At room
temperature, fracture in as-quenched martensite takes place on
multiple planes, with some preference for {100} which is a likely
cleavage mode. Consideration of the coherency strains due to ε -
carbide precipitation on tempering reveals no preference for any
of the main competing fracture planes. However, after tempering
to the stage where cementite starts to form, fracture on {211} and
{321} planes becomes more prevalent, these being shear modes of
fracture enhanced by cementite coherency strains. At higher tem-
pering temperatures, and in ferrite, fracture on {110} planes
dominates.

On fracturing at -195°C, martensite fractures on multiple
planes as at room temperature, but the fracture plane in ferrite
switches from {110} to {100}, or from the shear mode to cleavage.
Thus, unlike ferrite, martensite is not subject to a sudden transi-
tion in mode of fracture at test temperatures down to -195°C.

Although the general path of fracture is comprised of many
crystallographically oriented segments, the over-all direction of
propagation is probably more sensitive to the state of stress and
the concommitant plastic flow than to the orientation of the mar-
tensitic crystallites. A strong correlation is found between the
width of the electron-transparent zone along the fracture and the
general direction of the fracture. When the fracture direction is
such that {111} slip directions have a high resolved shear stress,
plastic flow can occur readily, and a wide transparent zone is de-
veloped.

4

III. ATOMIC DISPLACEMENTS IN MARTENSITE

S. C. Moss

A. Introduction

Although as-quenched martensites contain substructures of appreciable complexity involving transformation twinning and high densities of dislocations, the static iron-atom displacements caused by carbon atoms in interstitial solid solution are of unquestionable importance in the high strength exhibited by iron-carbon martensites.[1] Therefore, it was considered desirable to determine the magnitude of these iron-atom displacements, taking into account their anisotropy in the body-centered tetragonal lattice and the dynamic displacements due to thermal motion.

The presence of large c-axis distortions of the iron atoms in a 1.57 percent carbon martensite was demonstrated some years ago by Lipson and Parker,[2] who made densitometer traces of a Debye-Scherrer photograph taken of a moderately fast-quenched specimen. There have also been several related Russian papers, summarized by Kurdjumov,[3] the latest of which on electrolytically extracted martensite[4] reported that the mean-square static displacement in the c-direction was twice that in the a-direction of the body-centered tetragonal lattice.

B. Diffraction Theory

The x-ray theory underlying the measurement of atomic displacements is now well established, aside from a few points of interpretation which will receive further attention later. It is known from the work of James[5] and Borie[6] that, neglecting the effects of extinction, the integrated x-ray intensities from a monoatomic powder sample are given by:

$$I_{hkl} = \text{const.} \ |F_{hkl}|^2 \ e^{-2M_{hkl}} \ \times \text{L.P.} \ \times P_{hkl}$$

$$= I'_{hkl} \ |F_{hkl}|^2 \ \times \text{L.P.} \ \times P_{hkl} \qquad \text{(III-1)}$$

where F_{hkl} is the structure factor for a particular (hkl) reflection, P_{hkl} is the planar multiplicity associated with that reflection, and L.P. is the combined Lorentz and polarization factors which in this case had to be slightly modified from the usual tabulated values because a monochromator crystal was employed. The factor $e^{-2M_{hkl}}$ may be rewritten as

5

$$\exp \left\{ \left[-2B_{hkl} \right] \left[\frac{\sin^2 \Theta_{hkl}}{\lambda^2} \right] \right\}$$

B_{hkl} is then equal to:

$$B_{hkl} = 8\pi^2 \left[\overline{\mu^2}_{th} + \overline{\mu^2}_{st} \right]_{hkl} \qquad \text{(III-2)}$$

where the $\overline{\mu^2}$'s are, respectively, the mean-square thermal displacement and mean-square static displacement in a direction normal to the (hkl) plane. These displacements are taken about the mean atomic positions as defined by the lattice constants.

Since we are dealing with tetragonal martensite, it may also be shown that if the values of $\overline{\mu^2}$ differ along the a- and c-axes:

$$\overline{\mu^2}_{hkl} = \overline{\mu^2} (\vec{a}) \sin^2 \phi + \overline{\mu^2} (\vec{c}) \cos^2 \phi \qquad \text{(III-3)}$$

where ϕ is the angle between the c-axis and the [hkl] direction.

The two sets of diffraction peaks measured were the tetragonal doublets (200,020 - 002) and (211,121 - 112), for which the values of $\overline{\mu^2}$ are:

$$\overline{\mu^2}_{200,020} = \overline{\mu^2} (\vec{a})$$

$$\overline{\mu^2}_{002} = \overline{\mu^2} (\vec{c})$$

$$\overline{\mu^2}_{211,121} = 0.849 \,\overline{\mu^2} (\vec{a}) + 0.151 \,\overline{\mu^2} (\vec{c})$$

$$\overline{\mu^2}_{112} = 0.360 \,\overline{\mu^2} (\vec{a}) + 0.640 \,\overline{\mu^2} (\vec{c})$$

$$\text{(III-4)}$$

These equations apply to both the static and thermal displacements. The coefficients shown are based on an axial ratio of c/a = 1.06 which is appropriate for the 1.33 percent carbon martensite to be examined in this section.

FeK_α radiation was chosen in order to achieve maximum resolution of the martensite doublets. The measurement technique was the so-called "peak-to-peak" procedure wherein the intensity ratio of a single peak at two temperatures was obtained to determine the thermal displacements. In order to make use of this method, it must be assumed that B_{st} (or $\overline{\mu^2}_{st}$) is not a function of temperature.

One may then write, for any particular reflection, the following ratio:

$$\ln\left\{\frac{I'(T_2)}{I'(T_1)}\right\} = 2\left[(B_{th}\frac{\sin^2\Theta}{\lambda^2})_{T_1} - (B_{th}\frac{\sin^2\Theta}{\lambda^2})_{T_2}\right] \qquad \text{(III-5)}$$

where λ is the x-ray wavelength, and Θ is the Bragg angle.

Also, since $B_{st}(T_2) = B_{st}(T_1)$, B_{th} is likewise given by:

$$B_{th} = 8\pi^2\overline{\mu^2}_{th} = \frac{6h^2 T}{m\,k\,\Theta_M^2}\left\{\phi(x) + \frac{x}{4}\right\} \qquad \text{(III-6)}$$

where the x-ray Debye temperature (Θ_M) is taken to be independent of temperature, m is the mass of the iron atom, x is the temperature ratio, Θ_M/T, and $\phi(x)$ is a tabulated function of x. For the two temperatures of measurement used here:

$$B_{th}(295°K) = \frac{63.01}{\Theta_m^2} \times 10^{-13} \qquad \text{(III-7)}$$

$$B_{th}(92°K) = \frac{25.88}{\Theta_M^2} \times 10^{-13}$$

For the ratio in Eq.(III-5):

$$\ln\left\{\frac{I'(92°K)}{I'(295°K)}\right\} = \frac{2}{\Theta_M^2}\left\{(63.01\frac{\sin^3\Theta}{\lambda^2})_{295°K} - (25.88\frac{\sin^2\Theta}{\lambda^2})_{92°K}\right\} \qquad \text{(III-8)}$$

In accordance with Eq.(III-1), the intensities (I') are the observed intensities (I) divided by the factors $|F|^2$, L.P. and P, the first two of which vary slightly with temperature because of their dependence on the Bragg angle. The atomic scattering factors for iron were taken from Volume III of the International Tables for X-ray Crystallography. Henceforth, only the reduced intensities (I') are necessary for this discussion.

Through the aid of the foregoing equations, one can experimentally evaluate B_{th}, Θ_M, and μ^2_{th} in both the a- and c-directions of the martensite as long as the tetragonal doublets are resolvable.

With regard to the static displacements, it is possible to de-

termine these parameters[2] by taking the following ratio* at either temperature:

$$\frac{1}{2}\ln\left\{\frac{I'_{200}\ (295^\circ K)}{I'_{002}\ (295^\circ K)}\right\} = \left\{\left(B_{th}[002]\ \frac{\sin^2\theta}{\lambda^2}\right)_{002} -\left(B_{th}[200]\frac{\sin^2\theta}{\lambda^2}\right)_{200}\right\}$$

$$+\left\{\left(B_{st}\ [002]\ \frac{\sin^2\theta}{\lambda^2}\right)_{002} -\left(B_{st}[200]\frac{\sin^2\theta}{\lambda^2}\right)_{200}\right\} \quad \text{(III-9)}$$

When B_{th} (002) and B_{th} (200) are known, we are left with a difference measurement of essentially $\overline{\mu_{st}^2}(\vec{c}) - \overline{\mu_{st}^2}(\vec{a})$. Because the static displacements encountered in martensite are very large, it turns out that their determination is relatively insensitive to the magnitude of B_{th}. There are also certain restrictions in the range of variation that the ratio $\overline{\mu_{st}^2}(\vec{a})/\overline{\mu_{st}^2}(\vec{c})$ can take, and thus a much more unambiguous value for $\overline{\mu_{st}^2}(\vec{c})$ can be obtained than might seem possible at first glance from Eq. (III-9).

C. Experimental Details

The alloy chosen for this study was a solid sample of a 1.33 percent carbon steel whose composition is given in Table III-I. Flat x-ray specimens were machined from the center of a 5/8-inch hot-worked bar, and were austenitized at 970°C for 1/2 hour in evacuated Vycor tubes which were then rapidly quenched and broken in an iced-brine solution. The steel samples were further cooled in liquid nitrogen and brought back to room temperature. After metallographic polishing and etching, very fine-grained martensite and some retained austenite were revealed. The flat surfaces were then given an additional light polish and etch in a 1 percent nital solution. Hardness measurements indicated that the extent of aging resulting from these room-temperature operations was quite small.

Preliminary x-ray measurements with unfiltered radiation and a Laue back-reflection camera showed continuous Debye rings of nearly even intensity, indicating that a random fine-grained martensitic structure had been produced. These exposures were taken at both normal and oblique incidence, and the specimen area illuminated was about 1/20 of the beam size to be used in the subsequent intensity measurements.

The diffractometer was set up with an iron-target line-focus x-ray tube, and monochromatic FeKα radiation was obtained with a singly bent and ground LiF crystal. Narrow entrance slits and very careful adjustment of the monochromator eliminated the Kα_2

---

*A similar ratio can be written for the (211,121 - 112)doublet.

TABLE III-I

Composition of Steel Used for X-ray Intensity Measurements

(Weight Percent)

C	Mn	P	S	Si	Cu	Ni	Cr	N
1.33	< 0.01	0.004	0.003	0.037	0.005	0.020	0.002	0.001

component entirely, as confirmed by the high-angle reflections from a relatively perfect silicon single crystal. The latter crystal gave an instrumental broadening of about six minutes of arc, this being approximately the same width as derived from a pure carbonyl-iron powder standard.

The diffractometer was operated with a very narrow receiving slit (which permitted the sharp iron-powder peaks to pass through) and Soller slits to decrease the vertical-divergence broadening. The intensities were measured with a low-noise scintillation counter and pulse-height selector, set to eliminate completely any $\lambda/2$ contamination from the LiF monochromator. The iron-target x-ray tube was operated at 30 KV and 15 ma, which yielded appreciable intensities for the pure iron standard ($\sim$ 50,000 counts/min. peak intensity for the (211) reflection).

A liquid-nitrogen sample holder was mounted concentric with the diffractometer axis and, with the instrument completely aligned, 2θ positions for the peaks of the iron-powder standard were recorded to calibrate the martensite peaks. All of these precautions were considered essential for attaining good resolution of the martensite doublets, high accuracy of the absolute lattice constants, symmetrical peak profiles (no $K\alpha_2$ component), and very high signal-to-noise ratios.

When the doublets were well resolved, the corresponding diffraction peaks appeared quite symmetrical. This circumstance permitted the direct measurement of the lattice constants by recording the peak maximum in each case. It also allowed a direct and accurate determination of the relative integrated intensity merely by sitting at the maximum position and taking a 20-minute count. The background was counted on either side of each entire doublet, and the peak measurements were appropriately corrected. This technique depended solely on being able to resolve the peaks, with the peaks having a well-defined shape. As will be discussed later, these requirements were more completely met with the (200,020 - 002) than with the (211,121 - 112) reflections.

All the x-ray determinations made at 295° and 92°K were reversible in the sense that they could be repeated with any sequence of these two temperatures. This signified that the initial specimen preparation and handling at room temperature probably led to some aging of the martensite and thereby minimized any further aging which might otherwise have occurred during the subsequent x-ray runs at room temperature.

D. Experimental Results

Figure III-1 illustrates the two sets of (200,020 - 002) and (211,121 - 112) doublets at room temperature. The full-scale intensity amounted to 2000 counts/min. in both cases. It is obvious that the (200,020 - 002) doublet was completely separated, permitting a direct determination of both the c- and a-parameters. Here, the angular scale was accurately calibrated by means of the (200) reflection from pure iron. The (211,121 - 112) doublet, even though at a higher Bragg angle, was less well resolved. The small overlap

in this case (of perhaps 10 percent) affected the lattice-constant determinations and, more importantly, the peak-intensity measurements. Hence, although the (211,121 - 112) data are included here for comparative purposes, the main weight should be given to the (200,020 - 002) data.

The c- and a-parameters and the c/a ratio were determined at both liquid nitrogen (actually 92°K) and room temperature (295°K). Table III-2 lists the values obtained. Based on the relationship: $c/a = 1.000 + 0.045$ wt.%C, given by Roberts[7] and corroborated by Winchell,[8] the carbon content calculated from the (200,020 - 002) doublet at 295°K was 1.32 percent, in close agreement with the chemical analysis (Table III-1). The other doublet yielded 1.30 percent carbon, suggesting that the measured line separation in this case was slightly too small because of the overlap.

The thermal coefficients of expansion along the c- and a-axes could be derived from the lattice parameters at 295° and 92°K, as shown in Table III-2. Here again, the (200,020 - 002) measurements should be considered as being more dependable; on this basis, the thermal coefficient of expansion was much larger in the c-direction than in the a-direction.

Next, the mean-square amplitudes of thermal vibration were determined. As previously described, the intensity counts at the peak positions were recorded at 295° and 92°K, and two runs apiece were made alternatively at each temperature. Such duplicate runs agreed to within $\pm$ 1 percent of each other. The results are summarized in Table III-3. According to the thermal-expansion values in Table III-2, $\overline{\mu^2_{th}}(\vec{c})$ would be expected to be larger than $\mu^2_{th}(\vec{a})$, and, while this was indicated by the (211,121 - 112) data, the more valid (200,020 - 002) data showed the opposite. At the same time, the mean Debye temperature of 365°C based on the (200,020 - 002) measurements was found to be in good agreement with those reported by the Russian investigators[3] on martensites of about the same composition, in contrast to a mean Debye temperature of 435°K calculated from the (211,121 - 112) data.

In addition to the diffraction-peak overlap which rendered the (211,121 - 112) measurements questionable, errors due to thermal-diffuse scattering may have entered the picture at the higher Bragg angles involved. The resulting correction, if applied, would tend to bring the higher-angle data into line with the lower-angle data. In other words, the (211,121 - 112) observations were undoubtedly distorted by the fact that the thermal-diffuse tail of the (211,121) peak overlapped the (112) peak more at 295° than at 92°K. Thus, we must conclude that only the (200-020 - 002) measurements should be relied on for serious analysis and interpretation. This will be done in the next section.

We come now to the static displacements in the martensite. As mentioned in connection with Eq. (III-9), differences of the kind $\left\{ \overline{\mu^2_{st}}(\vec{c}) - \mu^2_{st}(\vec{a}) \right\}$ could be obtained from the intensity ratios I'_{200}/I'_{002} and I'_{211}/I'_{112}, on the assumption that these static

FIGURE III-1. Room-Temperature Diffractometer Tracings of the (200,020 - 002) and (211,121 - 112) Tetragonal Doublets from As-quenched 1.33 Percent Carbon Martensite. X-radiation = FeK_{α_1}. Full-Scale Intensity = 2000 Counts Per Minute.

12a

TABLE III-2
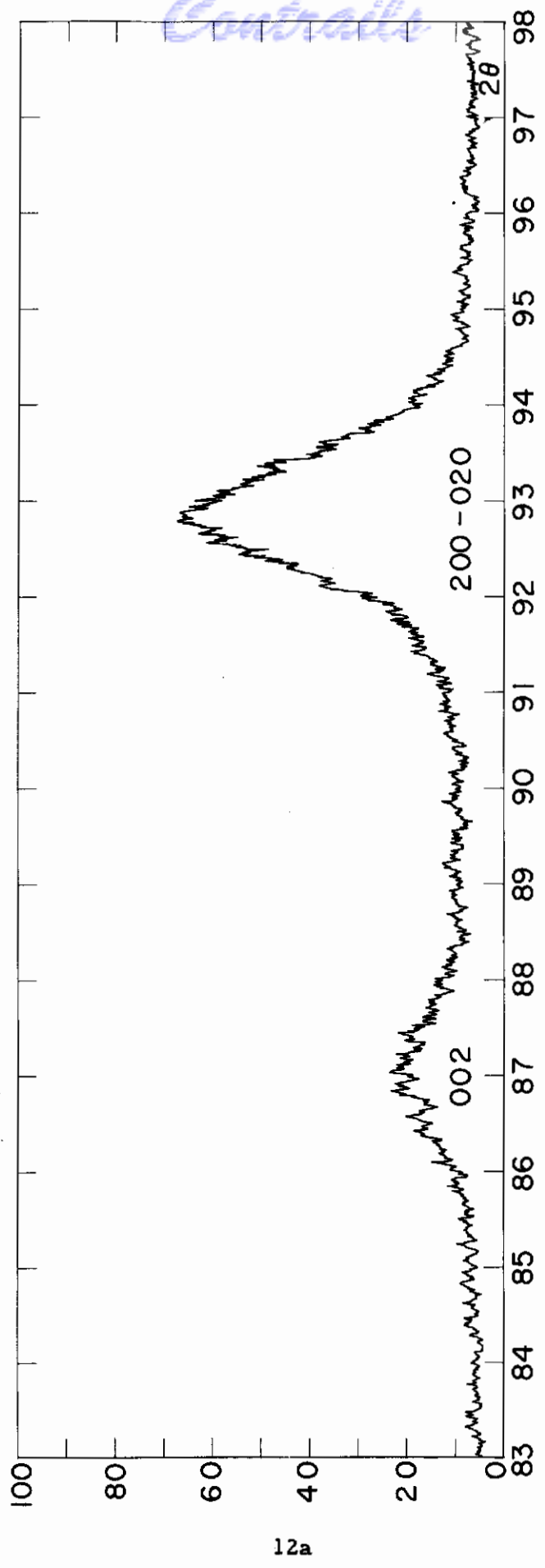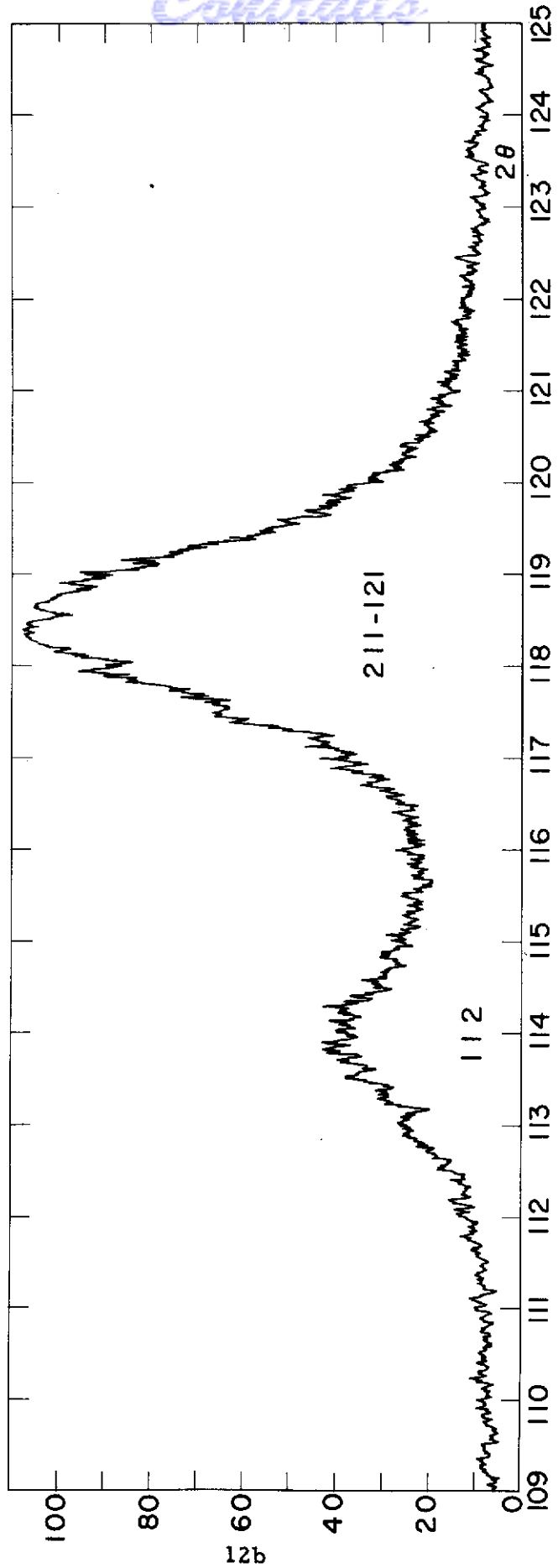
Lattice Constants, Axial Ratios, and Coefficients of Thermal
Expansion for 1.33 Percent Carbon Martensite

Diffraction Doublet	a,A°		c, A°		c/a		$\alpha_a \times 10^6$	$\alpha_c \times 10^6$
	295°K	92°K	295°K	92°K	295°K	92°K	per °C*	per °C**
200,020 002	2.854_6	2.849_6	3.024_5	3.016_0	1.059_5	1.058_4	8.63	13.0
211,121 112	2.851_6	2.846_1	3.018_8	3.012_6	1.058_6	1.058_5	9.52	9.82

$$\text{*} \quad \alpha_a = \frac{\Delta a}{a_{295°K}} \left(\frac{1}{295° - 92°K}\right)$$

$$\text{**} \quad \alpha_c = \frac{\Delta c}{c_{295°K}} \left(\frac{1}{295° - 92°K}\right)$$

TABLE III-3

Mean-Square Amplitudes of Thermal Vibration and Debye Temperatures for 1.33% C Martensite*

Diffraction Doublet	a-axis		c-axis	
	$\overline{\mu^2_{th}}$ ($\overset{\circ}{a}$)	Θ_M ($\overset{\circ}{a}$)	$\overline{\mu^2_{th}}$ ($\overset{\circ}{c}$)	Θ_M ($\overset{\circ}{c}$)
200,020 002	0.0068 $\overset{\circ}{A}{}^2$	342°K	0.0052 $\overset{\circ}{A}{}^2$	389°K
211,121 112	0.0039 $\overset{\circ}{A}{}^2$	450°K	0.0047 $\overset{\circ}{A}{}^2$	418°K

* Both the Debye temperatures and static displacements are assumed to be independent of temperature in this tabulation.

14

displacements were independent of temperature. It was then found that the mean-square static displacements (0.040 - 0.100 Å^2) were an order of magnitude larger than the mean-square thermal displacements (0.004 - 0.007 Å^2). Consequently, the thermal displacements could be neglected in Eq. III-9 without significant error. Because only the differences $\left\{ \overline{\mu^2}_{st}(\vec{c}) - \overline{\mu^2}_{st}(\vec{a}) \right\}$ were obtained in this way, various assumptions for the anisotropy in static displacements rangfrom $\mu^2_{st}(\vec{a})/\mu^2 st(\vec{c}) = 0$ to 1/2 were tried. The results are presented in Table III-4 in terms of the root-mean-square (RMS) static displacements.

Once more, the (200,020 - 002) results should be regarded with greater confidence than the (211,121 - 112), but the discrepancy here was only about 10 percent and could be entirely accounted for by the postulated overlap in the latter pair of peaks. Accordingly, it was possible to rule out preferred orientation of the martensitic plates as the cause of the discrepancies arising from the two sets of doublets. Lipson and Parker[2] reported $\sqrt{\overline{\mu^2}(\vec{c})} = 0.20$ Å for a 1.57 percent carbon martensite, based on the assumption that the static displacements in the a-direction were nil. This figure is somewhat lower than the corresponding 0.23 Å value given in Table III-4, perhaps because of inadvertent tempering in the Lipson and Parker specimen. On the other hand, the results summarized by Kurdjumov[3] indicate much less anisotropy in the static displacements, namely, $\sqrt{\mu^2_{st}(\vec{a})} = 0.16$Å and

$$\sqrt{\overline{\mu^2}_{st}(\vec{c})} = 0.23 \text{ Å} \quad \text{or} \quad \overline{\mu^2}_{st}(\vec{a})/\overline{\mu^2}_{st}(\vec{c}) \approx 1/2.$$ For this ratio, the present measurements would give $\sqrt{\overline{\mu^2}(\vec{c})} = 0.34$ Å, (Table III-4, last column), which turns out to be unreasonably high. The relevance of these comparisons will be discussed in the next section.

E. Discussion of Results

It follows from these x-ray diffraction measurements on BCT martensite that the root-mean-square static displacement $\sqrt{\mu^2_{st}}$ of the iron atoms is very large in the c-direction. However, as we have seen, the numerical quantity depends on what is assumed for its relation to the RMS displacement in the a-direction. These orthogonal static displacements are each averaged over the entire lattice, and represent fluctuations about the mean BCT lattice sites as defined by the c- and a-parameters. Undoubtedly, the iron-atom displacements are a consequence of the local distortions around individual carbon atoms trapped in the octahedral interstitial sites, and it is these local distortions which are believed to be responsible (through their interaction with the strain fields of dislocations) for the solid-solution strengthening of virgin martensite.

15

TABLE III-4

Root-Mean-Square Static Displacements of the Iron Atoms Along the C-axis of 1.33 Percent Carbon Martensite

Tabulated values of $\sqrt{\overline{\mu^2_{st}}(\vec{c})}$

Assumed Anisotropy — Diffraction Doublet	$\overline{\mu^2_{st}}(\vec{a})=0$	$\overline{\mu^2_{st}}(\vec{a})=\frac{1}{10}\overline{\mu^2_{st}}(\vec{c})$	$\overline{\mu^2_{st}}(a)=\frac{1}{5}\overline{\mu^2_{st}}(\vec{c})$	$\overline{\mu^2_{st}}(\vec{a})=\frac{1}{2}\overline{\mu^2_{st}}(\vec{c})$
200,020 002	0.23 Å	0.24 Å	0.26 Å	0.34 Å
211,121 112	0.20 Å	0.21 Å	0.22 Å	0.30 Å

The fact that the a-parameter decreases linearly with in-
creasing carbon content, while the c-parameter increases linearly,[7,8]
suggests that the mean distortion field arising from all the inter-
stitial carbon atoms may be considered as a linear superposition
of the distortions around the individual carbon atoms, and also
that the local contraction along the a-axis may be regarded as a
Poisson-type contraction accompanying the expansion along the c-
axis.   Recent elastic-constant data on iron[9] gives a Poisson
ratio of $\upsilon = -c_{12}/(c_{11} + c_{12}) = -0.37$, which places an upper limit
on the local $\Delta a/a /\!/ \Delta c/c$ ratio around a carbon atom because the
local displacements within the lattice are probably more constrained
than is the response of the bulk metal to external forces.   Hence,
we can say that

$$\sqrt{\overline{\mu^2}_{st}(\vec{a})} \leq 0.37\sqrt{\overline{\mu^2}_{st}(\vec{c})}, \quad \text{or} \quad \overline{\mu^2}_{st}(\vec{a}) \leq 0.14\,\overline{\mu^2}_{st}(\vec{c})$$

which is not in agreement with the findings of Arbuzov et al.[4]
Based on these arguments, the best RMS static displacement in the
c-direction of the 1.33 percent carbon martensite studied here
comes out to be 0.24 Å, while the RMS value in the a-direction is
less than 0.24 X 0.37 or 0.09 Å.

Before analyzing the significance of the static displacements
in the problem of martensite strengthening, we now turn to the de-
rived temperature parameters: thermal expansion (Table III-2) and
thermal displacements (Table III-3).   Inasmuch as the thermal-
expansion coefficient in the c-direction is appreciably larger than
in the a-direction, marked anisotropy must exist in the anharmonic
vibrations of the iron atoms about their equilibrium positions.
For the thermal displacements, however, there really is no single
zero-point equilibrium position, and what has been measured in the
present investigation is both space-averaged and time-averaged.

As mentioned earlier, a comparison of the thermal-expansion
coefficients, α_c and α_a, would indicate that the thermal displace-
ments in the c-direction should be larger than in the a-direction.
Yet, the more reliable measurements on the (200,020 - 002) lines
show the reverse.   This anomaly forces a re-examination of the
assumptions implicit in the calculation of the thermal displace-
ments, and it now appears that the static displacements may not be
completely independent of temperature over the range of measure-
ments.   In fact, one may obtain a qualitative appreciation for the
change in the static displacements by examining the corresponding
variation in Poisson's ratio over the same temperature interval.
Using the model developed by Fisher,[10] $\varepsilon_a/\varepsilon_c$ (the ratio of the
orthogonal strains associated with a single carbon atom in an octa-
hedral site of the BCC iron lattice) is given at low temperatures by
$-C_{12}/(C_{11} + C_{12})$, or Poisson's ratio.   From the data of Lord and
Beshers,[9] $\upsilon = -0.367$ at 298°K and -0.362 at 77°K.   In other
words, there must be a relative change in the a-axis and c-axis lo-
cal static distortions with decreasing temperature.   By allowing
$\sqrt{\overline{\mu^2}_{st}}$ to become a function of temperature, we would then expect to

17

observe a greater change in $\sqrt{\overline{\mu^2}_{st}}$ $(\vec{a})$ than in $\sqrt{\overline{\mu^2}_{st}}$ $(\vec{c})$.

Experimentally, it is observed that $I'200$ $(92°K)/I'200$ $(295°K)$ is greater than $I'002$ $(92°K)/I'002$ $(295°K)$. If, as we have previously assumed, $\overline{\mu^2}_{st} \neq f(T)$, then $\overline{\mu^2}_{th}$ $(\vec{a}) > \overline{\mu^2}_{th}$ $(\vec{c})$, as listed in Table III-3. Alternatively, the x-ray intensity data may be disclosing some anisotropy in the change of $\sqrt{\overline{\mu^2}_{st}}$ with temperature, in line with the variation in Poisson's ratio.

The same limitations apply to the Russian results, as summarized by Kurdjumov.[2] Unfortunately, once the possibility of a change in $\sqrt{\overline{\mu^2}_{st}}$ with temperature is admitted, the x-ray intensity measurements do not afford a quantitative sorting-out of the thermal displacements from the static displacements, and it could even be that $\overline{\mu^2}_{th}$ $(\vec{c})$ is actually greater than $\overline{\mu^2}_{th}$ $(\vec{a})$, in contrast to what has been calculated before. Then, the anisotropy in the thermal amplitudes would conform with the anisotropy in the thermal-expansion coefficients.

Be that as it may, $\sqrt{\overline{\mu^2}_{st}}$ $(\vec{c})$ is quite large compared to the temperature-dependent effects, whether the latter are ascribed to thermal or static displacements. The mean iron-carbon distance in the 1.33 percent carbon martensite is $c/2 = 1.512$ Å, whereas in cementite it is 2.01 Å.[11] Thus, the local displacement of an iron atom next to an interstitial carbon atom in the BCT martensite only has to be about twice the observed RMS displacement $\sqrt{\overline{\mu^2}_{st}}$ $(\vec{c}) = 0.24$ Å) in order to accommodate the carbon atom, if the interatomic distances in cementite can be taken as a guide.

With regard to the problem of martensite strengthening by interstitial carbon, we now make use of the RMS static displacements in order to deduce the local displacements of iron atoms adjacent to carbon atoms. The difference $\varepsilon_o - \varepsilon_a = \Delta\varepsilon$ enters into the Fleischer model,[12] the carbon-dependent strengthening at 0°K being $\frac{G\Delta\varepsilon}{3} N_c^{1/2}$, where G is the shear modulus and N_c is the atomic fraction of carbon. In this expression $\Delta\varepsilon$ is the difference between the c-axis and a-axis strains (the so-called tetragonal strain or dipole distortion) in the immediate vicinity of a carbon atom, and has previously been evaluated as 0.41 from lattice-constant data.[12] However, this is a questionable procedure because it is risky to estimate the local strain field around a carbon atom from bulk-lattice properties. Hence, we shall now try to invoke the measured RMS static displacements.

Fisher[10] has suggested a way of calculating the local distortions from the RMS distortion. using the bulk elastic constants

for pure iron. Unfortunately, even if the elastic constants were available for BCT martensite, the local displacement field is not necessarily determined by the bulk elastic properties. More recently, Gielen[13] has extended the Fisher calculations by incorporating the interatomic force constants obtained from the phonon-dispersion curves in neutron inelastic-scattering experiments on BCC iron.[14] He computed the entire set of distortions for a lattice of 40 iron atoms containing one carbon atom (2.5 atomic percent carbon). When the resulting values are normalized by applying the c-direction RMS displacement measured in the present work (scaled down proportionally from the 6 atomic percent carbon of the experimental alloy to the 2.5 atomic percent of the calculated model), the local displacement (x_1) in the c-direction of an iron atom next to a carbon atom turns out to be 0.68 Å, relative to the original BCC lattice.

This displacement in the c-direction of an iron atom next to a carbon atom is the maximum encountered in the lattice, and is so large that the exact relationship between x_1 and $\sqrt{\overline{\mu_{st}^2}}\,(\vec{c})$ becomes very insensitive to the details of the rest of the displacement field. In fact, Kaplow[15] has suggested that x_1 may be estimated directly from the RMS value by assuming that only the maximum displacement contributes to the RMS displacement in averaging over all

the atoms. Thus, $x_1 = \sqrt{\dfrac{N}{2}\,\overline{\mu_{st}^2}\,(\vec{c})}$, where N is the number of iron atoms per carbon atom, and the averaging is taken over one-half this number because there are two x_1 displacements in the $\pm$ c-direction for each carbon atom. From this calculation, x_1 again equals 0.68 Å.

According to either the Fisher[10] or Gielen[13] methods of computation, a given value of x_1 fixes the entire set of iron-atom displacements, even those in the a-direction. The local displacement (y_5) in the a-direction is then found to be -0.17 Å. The ratio $y_5/x_1 = -0.25$, which is appreciably less than the bulk Poisson ratio, as we suspected. Therefore, the RMS static displacement of 0.09 Å in the a-direction, which we calculated before from $\sqrt{\overline{\mu_{st}^2}}\,(\vec{c})$ and Poisson's ratio, must represent a maximum figure, notwithstanding the still higher values reported elsewhere.[4]

If the iron atoms adjacent to the carbon atoms in martensite are now regarded as being displaced 0.68 Å in the c-direction off the original BCC lattice, the iron-carbon distance is then $a_o/2 + 0.68 = 2.11$ Å, compared to 2.01 Å in cementite. This difference suggests that the derived displacement of 0.68 Å may be too large. Another difficulty is that an iron-carbon distance of 2.11 Å would cause an increase in the a-parameter of the martensite, whereas a decrease is actually observed. This means that the carbon atom does not seem to interact in a symmetrical way with its six nearest-neighbor iron atoms. Further refinements in the RMS determinations and in the local-distortion calculations may lead to

smaller values for x_1, thus bringing the iron-carbon distance in martensite into line with that in cementite. For the time being, then, it seems best to regard 0.68 Å as an upper limit for the dipole displacement in martensite.

Correspondingly, an upper limit for the local tetragonal strain in the Fleischer model[12] can now be established as

$$\Delta\epsilon = \epsilon_c - \epsilon_a = \frac{x_1}{c/2} - \frac{y_5}{a/2} = \frac{0.68}{1.51} - \frac{-0.17}{1.43} = 0.57, \text{ which is}$$

slightly larger than the 0.41 previously used. There is now hope of evaluating $\Delta\epsilon$ with fair accuracy by applying the experimental and computational procedures described here to a series of iron-carbon martensites.

F. Conclusions

1. The thermal-expansion coefficients of BCT martensite suggest that the interstitial carbon atoms loosen the lattice along the c-direction, giving rise to the anisotropy, $\alpha_c > \alpha_a$.

2. Although the above anisotropy indicates that the thermal displacements in the c-direction should be greater than in the a-direction, the opposite turns out to be the case if it is assumed that the static displacements are invariant with temperature. In order to rationalize these findings, it is concluded that the static displacements do change with temperature, although this variation is quite small compared to the large static displacements.

3. On the basis of the RMS static displacements thus deduced, upper limits have been computed for the local displacements of iron atoms adjacent to carbon atoms, and from this, the local tetragonal strain around the carbon atoms. These quantities are fundamental to the solution-hardening of martensite by interstitial carbon.

G. References

1. Morris Cohen, "The Strengthening of Steel," Trans.Met.Soc. AIME 224 (1962) 638.

2. H.Lipson and A.M.B. Parker, "Structure of Martensite," J.Iron and Steel Inst. 149 (1944) 123.

3. G.J.Kurdjumov, "Phenomena Occurring in the Quenching and Tempering of Steel," J.Iron and Steel Inst. 195 (1960) 26.

4. M.P.Arbuzov, L.I.Lysak and Ye.G.Nesterenko, "On the Structure of Martensite in Hardened Steel," Doklady Acad. Nauk SSSR 90 (1953) 375.

5. R.W.James, "The Optical Principles of the Diffraction of X-rays, London, G.Bell and Sons, Ltd. (1954).

6. Bernard Borie, "X-ray Diffraction Effects of Atomic Size in Alloys," Acta Cryst. 10 (1957) 89.

7. C.S.Roberts, "Effect of Carbon on the Volume Fractions and Lattice Parameters of Retained Austenite and Martensite," Trans. AIME 197 (1953) 203.

8. P.G.Winchell and M.Cohen, "The Strength of Martensite," Trans.ASM. 55 (1962) 347.

9. A.E.Lord and D.N.Beshers, "Elastic Stiffness Coefficients of Iron from 77° to 673°K," J.Appl.Phys. 36 (1965) 1620.

10. J.C.Fisher, "Elastic Interaction of Interstitial Atoms in Body-Centered Cubic Crystals," Acta Met. 6 (1958) 13.

11. E.J.Fasiska, G.A.Jeffrey, and L.Zwell, "On the Cementite Structure," to be published in Acta Cryst.

12. Robert L. Fleisher, "Rapid Solution Hardening, Dislocation Mobility, and the Flow Stress of Crystals," J.Appl.Phys. 33 (1962) 3504.

13. Paul Gielen, "Mossbauer Effect in Iron-Carbon and Iron-Nitrogen Solid Solutions," MIT Doctoral Thesis (1965)

14. G.G.E.Low, "Some Measurements of Phonon Dispersion Relations in Iron," Proc.Phys.Soc. 79 (1962) 479.

15. R.Kaplow, private communication.

D. W. Hoffman

A. Introduction

In the development of materials with higher strength levels, the thermomechanical treatment of steel has been actively explored. Since 1957, the most intensively studied treatment along these lines has been that of ausforming, in which the parent austenite is plastically deformed just before transformation to martensite. Research in this field has proceeded concurrently on both the developmental and theoretical fronts, and a number of comprehensive reviews have appeared describing both the properties obtained in various steels through ausforming and the ideas advanced to explain the observations.[1,2,3]   These reviews also discuss the influence of the processing variables which are basic to an understanding of the ausforming phenomenon.

The effectiveness of ausforming is dependent on steel composition.   In very low-carbon alloys (e.g., 0.006 percent carbon), the response to ausforming is relatively small.[4]   But if the carbon content is increased to only 0.3 percent the incremental strengthening produced by ausforming becomes quite marked.   Although further raising of the carbon content increases the absolute strength, the response to ausforming tends to level off.[5] The presence of strong carbide-forming elements such as chromium, molybdenum and vanadium further enhances the ausform-strengthening, provided that these elements are dissolved in the austenite prior to its deformation.[6]

The yield strength of ausformed martensite is, in general, an increasing function of the amount of deformation imposed on the austenite, in the absence of recrystallization.   Some investigators have found that the strengthening is directly proportional to the reduction in thickness or cross section.[7]   Consequently, the ausform-strengthening of a given steel is often divided by the percent deformation in order to provide an index of the response to ausforming.   Typical values of this index run from 1000 to 1500 psi/%, with the majority of values being closer to the lower end.[1,2] Increasing the deformation temperature causes a decrease in the response to ausforming,[8] even when recrystallization or gross decomposition of the austenite is not allowed to occur.

The tempering behavior of martensite, as evidenced by the strength properties, is influenced by ausforming in a variety of ways.   In some cases, there appears to be little change in the over-all trends, the yield strength vs tempering curves of the ausformed and unausformed martensites being generally parallel but separated by the ausform-strengthening increment.[7]   With steels normally displaying secondary hardening, ausforming may eliminate the intermediate softening on tempering and thereby obscure the hardening peak.[9] However, at least one instance has been reported in which ausforming gives rise to a secondary-hardening peak where none existed before.[10]   In the examples where ausforming alters the strength behavior on tempering, it appears likely that the un-

22

derlying carbide-precipitation reactions are altered. Other processing variables such as rate of deformation, time at deformation temperature, and method of deformation, do not have a primary influence on the ausforming response.

Several hypotheses have been suggested to account for the phenomenon of ausform-strengthening. Those considered to be of major importance are the following:

1. Strain hardening (lattice defects and substructural changes) inherited by the martensite from the austenite.[11]*

2. Dispersion hardening due to precipitation of fine carbides during austenite deformation, the carbide-hardening effects being transferred to the martensite formed subsequently.[9]

3. Increased density of imperfections retaining more carbon in solution in the martensite for solid-solution hardening during tempering.[5]

4. Dispersion hardening due to carbon-rich clusters segregated around dislocations in the austenite and inherited by the martensite.[12]

5. Enhanced dispersion hardening during tempering due to the precipitation of fine carbides on the substructure inherited by the martensite.[5]

Of course, these mechanisms are not mutually exclusive. For example, the first may depend on the second, in that the fine structure inherited by the ausformed martensite may be influenced by the prior precipitation of carbides in the plastically deformed austenite. It has been proposed that alloy carbides precipitated during the austenite deformation increase the concurrent rate of dislocation multiplication and then stabilize the dislocation network as it is transmitted to the martensite.[6] Possibly, additional dislocations are accumulated during the transformation from the moving dislocation arrays and accommodation strains. It has been pointed out that glide dislocations on certain variants of the austenite slip systems should become sessile with a type <100> Burgers vector in the martensite.[13]

The third and fourth mechanisms are interrelated inasmuch as both are based on the interactions between interstitial carbon atoms and the strain fields around dislocations. The fifth mechanism goes a step beyond the fourth, with the dislocation locking being attributed to the formation of distinguishable carbide particles. The latter two processes may operate simultaneously at some step of the tempering sequence.

All of the explanations except the first are dependent upon the presence of carbon, and as mentioned, even the first may be greatly enhanced by the concomitant precipitation of alloy carbides. The known importance of dissolved carbon implies that at least one

---

* Although each of these hypotheses has been discussed by several investigators, only a single key reference is given here.

23

of the carbon-dependent mechanisms is active in any steel containing carbon. Only the last hypothesis depends upon the migration of carbon in the martensite.

It is likely that more than one of these processes may be operative at the same time, and they may contribute to the ausform-strengthening in different degrees depending on the alloy system. In a recent investigation of steels containing strong carbide-forming solutes,[6] the ausform-strengthening was explained by an additive combination of mechanisms 1, 2 and a reduced amount of the regular solid-solution hardening by carbon interstitials. A salient feature of this hypothesis was that the alloy carbides precipitated during the austenite deformation promote the retention of very high dislocation densities in the ausformed martensite. Nevertheless, significant ausform-strengthening does occur in alloys not containing strong carbide-forming elements.

The present investigation was undertaken to learn more about the magnitude and mechanisms of ausform-strengthening in a steel containing 23 percent nickel and 0.4 percent carbon. In this case, the carbon-dependent strengthening cannot be linked to the presence of carbide-forming elements and, therefore, certain simplifications in interpretation become possible. At the same time, since the M_s temperature of this alloy lies below the ambient, the parent austenite can be studied in detail, with and without plastic deformation.

B. Experimental Procedures

1. Specimen Preparation - Stock for all the experiments in this part of the program was prepared from a 5/8-inch diameter bar of air-melted iron - 23 percent nickel - 0.4 percent carbon alloy. The bar was alternately swaged and annealed (1000°C) to insure homogenization and to reach an appropriate size for ausforming by wire drawing. Before each heat treatment, the rod surface was carefully cleaned by machining, grinding, and/or electropolishing to remove contamination and defects. The rods were then sealed in evacuated Vycor capsules for the annealing or final austenitizing. At one stage after several cycles of reduction and annealing, all the rods were sealed in a single capsule and held at 1000°C for 24 hours for homogenizing purposes. After the final austenitizing for 1 hour at 1000°C, the individual encapsulated specimens were water quenched to room temperature, retaining 100 percent austenite.

Wire drawing was selected as the mode of deformation for ausforming because (a) the temperature of deformation could be easily controlled, (b) the extent of deformation could be readily reproduced, and (c) the shape of specimens cut from the wire was convenient for tensile, magnetic, and electrical-resistivity measurements. Prior to the wire drawing, the stock had been reduced to 0.0751 inch in diameter. The wire drawing on the austenitic specimens was carried out at 2 inches/minute through six even steps of natural strain to a final diameter of 0.0382 inch, the total reduction by wire drawing then being approximately 75 percent.

To vary the ausforming temperature, the die and wire were heated in a specially designed hot-air furnace which enclosed the die and undrawn wire. Recrystallized specimens having the final diameter were obtained by first electropolishing the drawn wire, and then reaustenitizing for 1 hour at 1000°C in evacuated Vycor capsules.

Three and one-half-inch lengths were cut from the 0.0382 inch wire for the tensile tests. One-half inch was detached in each case for magnetic or metallographic studies, and a 1-3/4 inch reduced section was electromachined at the center of the remaining 3-inch tensile specimen. The final cross-sectional area of the gage section was about 10 percent less than that of the unmachined grip ends.

The magnetic specimens were prepared from pieces of the 0.0382 inch diameter wire by grinding the ends normal to the wire axis at a length of about 0.4 inch.

The resistivity specimens consisted of 3-1/2 inch lengths of the 0.0382 inch diameter wire. Potential leads of 30 gage copper wire were soldered about 2 inches apart to the specimens, requiring only a brief heating at 200°C. The prior ausforming temperature for these specimens was 225°C, and so the soldering operation had no material effect on the structure. Current leads in the form of heavy copper wire were soldered to the ends of the specimen.

To obtain desired amounts of martensitic transformation with or without ausforming, specimens were refrigerated to pre-selected temperatures below the M_s temperature by immersion in baths of petroleum ether and methylcyclohexane cooled with liquid nitrogen. Subsequent tempering of the transformed specimens was performed in salt or oil baths, or in water for the 25° and 30° treatments.

2. **Magnetic Measurements** - An apparatus for measuring spontaneous magnetization at 5000 oersteds was constructed along the lines suggested by Schaller and Zackay.[14] The magnetic readings (deflections on a ballistic galvanometer) were corrected for the specimen diameter, and were then normalized according to the reading obtained on a pure-iron standard. The purpose of these measurements was to determine the volume fraction of martensite. Suitable calibration was provided by a series of test specimens having different amounts of unausformed martensite up to about 85 percent, the maximum that could be generated by refrigeration alone. The martensite contents in this series were measured separately by quantitative metallography.[15] The magnetic deflection for 100 percent martensite was determined by tensile straining several specimens (ausformed and unausformed) to fracture at -195°C. Inasmuch as the normalized magnetic readings on such specimens all increased to nearly the same limiting value regardless of the initial amount of martensite, this value was taken to represent 100 percent martensite for the calibration.

A second apparatus for measuring the percentage of martensite

by magnetization at 580 oersteds was constructed in the general form of a small Fahy permeameter, as described by Bozorth.[16] As for the higher-field method, the deflections of a ballistic galvanometer were corrected for specimen diameter and normalized with reference to a pure-iron standard. The advantage of the permeameter configuration was that the electromagnet could be attached to the center of the reduced section of a tensile specimen for martensite determinations either before or during the tensile test. Calibration was carried out on specimens whose martensite contents were known from the high-field magnet. It was found that, because saturation was not attained at the low field, the calibration curves for the ausformed and nonausformed specimens were not the same.

Differences of 0.15 percent martensite could be detected by both the high-field and low-field methods.

3. Tensile Testing - The tensile tests were performed on a Tinius-Olsen machine, using special grips and a low-temperature extensometer for the wire specimens. The grips were of a modified Templin design in which spacers on either side of the wire specimen between the jaws insured that the axis of the specimen was well aligned with the direction of the applied load. The extensometer was similar to that suggested by Feltner for cryogenic testing,[17] but was redesigned to be self-aligning, and was suspended from a counterbalanced arm so that its weight did not bear upon the specimen. Spring-loaded knife edges were incorporated to attach the extensometer to the wire specimens.

For low-temperature tensile testing, the specimen was surrounded by a cylindrical cryostat insulated with styrofoam. Cooling was effected by means of vapor from a pressurized container of liquid nitrogen which was sprayed into the cryostat through holes in a spiral coil of copper tubing, deflecting against the walls to provide good mixing action. The temperature was measured with two copper-constantan thermocouples adjacent to the specimen at the extensometer knife-edges, and was manually controlled by adjusting the supply of nitrogen with a magnetic on-off valve.

The tensile tests were made at two temperatures, 30°C and -100°C. The specimen grips were connected to the pull rods of the tensile machine through spherical bearings. To enhance the alignment, a small preload was applied before attaching the extensometer to the specimen. If in-situ magnetic measurements were to be conducted, the low-field magnet was clamped to the specimen between the knife-edges of the extensometer (the search coil having been slipped over the specimen prior to attaching the grips).

For the testing of virgin martensite, the specimen was mounted in the tensile machine in the austenitic condition, but the grip-ends were previously converted to martensite for strengthening purposes. The desired initial martensite content was obtained by cooling to -100°C or below in the tensile machine, and then warming to -100°C for the testing.

All the tensile tests were performed at a constant cross-head speed of 0.015 inch per minute. The load and extension were auto-

graphically recorded. When magnetic readings of the instantaneous martensite percentages were taken during the test, they were located by tick-marks on the load-extension curve.

4. <u>Electrical-Resistivity Measurements</u> - The electrical resistivity of specimens in the austenitic state was measured at 0°C in an ice-water bath. The diameter of a specimen was measured with a micrometer to an accuracy of 0.0001 inch, which was about 0.26 percent of the diameter or 0.52 percent of the cross-sectional area. The specimen was inserted in a jig with spring-loaded knife-edges making the potential contacts at a spacing of 2.500 inches. The resistance was measured with a Rubicon 1622 Kelvin Bridge to four significant figures. The resistivity could then be computed to an accuracy of 0.5 percent as limited by the diameter measurements.

Following this, the specimen was removed from the jig and leads were soldered on, as described previously. Again the resistance was measured at 0°C, and by comparison to the previous value, the spacing of the soldered potential leads could be computed. This enabled conversion of subsequently measured resistances to resistivities.

Resistance changes caused by tempering were determined in the following way. The specimen was refrigerated in liquid nitrogen and its resistance was measured in the virgin condition. Then it was up-quenched into a silicone oil bath at the tempering temperature, controlled to within ± 0.1°C, and resistance measurements were begun at temperature after one minute of tempering. Occasionally, the tempering was interrupted for additional measurements at the liquid-nitrogen temperature.

C. <u>Experimental Results</u>

1. <u>Austenites</u> - In contrast to the annealed austenite which was paramagnetic, significant ferromagnetism was observed in the deformed austenites. The latter magnetization (measured in a field of 5000 oersteds) was converted to percent martensite and related to the deformation temperature, as in Figure IV-1.

The high martensite content of the austenite deformed[*] at room temperature was to be expected. Although the magnetization decreased substantially with increasing deformation temperature, it did not go all the way to zero. According to Kaufman and Cohen,[18] there is a temperature T_0 above which plastic deformation should not convert austenite of a given composition into martensite. Typically in iron-nickel alloys this temperature is 200°C above the M_s. If this correlation holds in the presence of carbon, then no martensite should be found in the austenite under consideration when it is deformed above 150°C. But here, ferromagnetism in the austenite was observed after deformations up to 325°C. It was concluded that some martensite did form under these conditions due to lowering of the effective carbon content. Whether this was caused

---

[*] All of the deformations in these experiments corresponded to 75 percent reduction in area by wire drawing.
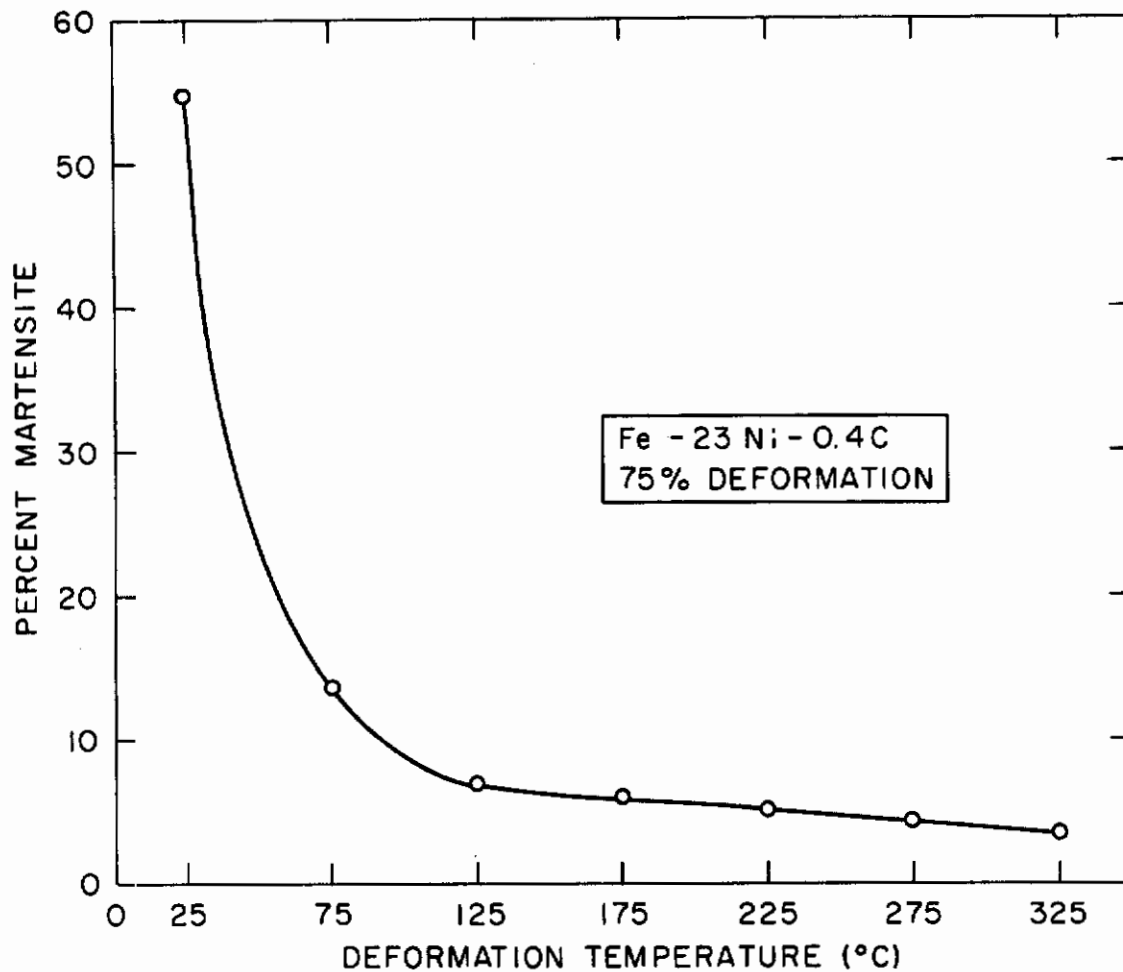
FIGURE IV-I FERROMAGNETISM IN AUSTENITE (CONVERTED TO PERCENT MARTENSITE) AS A FUNCTION OF DEFORMATION TEMPERATURE.

28

by a trapping of carbon atoms at lattice imperfections or by actual carbide precipitation will be considered later.

The M_s temperatures and transformation characteristics of the annealed and deformed* austenites were observed magnetically by immersing the specimen together with the 580-oersted magnet in a bath which could then be cooled progressively by additions of liquid nitrogen. The M_s is plotted as a function of deformation temperature in Figure IV-2. After each M_s measurement, the martensite content was monitored during further cooling down to -195°C. Curves of percent transformation vs cooling temperature are given in Figure IV-3.

The annealed austenite exhibited a large burst of transformation at the M_s temperature, but prior deformation at 75°C suppressed the burst and lowered the M_s slightly. The amount of martensite formed on cooling to -195°C was also diminished. With further raising of the deformation temperature, however, the burst phenomena reappeared, accompanied by an increase in M_s and in the extent of transformation achieved on cooling to -195°C. Nevertheless, the amount of martensite generated by refrigeration in liquid nitrogen remained less than was obtained from the undeformed austenite (75 vs 85 percent martensite). Evidently the transformation characteristics were being affected by the austenite deformation in a complex way, depending upon the structural changes produced and the extent of carbon trapping or depletion.

Back-reflection Laue x-ray photographs were made on the deformed austenites for determining preferred orientation. Wire specimens electropolished to about one-half their original diameter and unfiltered iron radiation were used for this purpose. In addition, x-ray patterns were obtained with the wire axis tipped 30° toward the film to bring more textural spots onto the diffraction rings. The annealed austenite produced spotty rings with no texture, whereas the deformed austenites had a duplex (111) and (100) fiber texture, typical of FCC materials.[19] By visual examination, no difference was noted in the relative strengths of these two textural components in austenite deformed at 75°C and at 325°C.

The tensile behavior of the austenites, with and without prior deformation, was investigated at 0°C. The stress-strain plots for the deformed austenites exhibited fairly abrupt yielding followed by very low work-hardening, as reported by Thomas et al.[6] In Figure IV-4, the 0.2 percent yield strength is plotted against deformation temperature, showing a monotonic decrease with increasing temperature. On the other hand, meaningful tensile strengths and ductility parameters could not be determined in these tests because in-situ magnetic measurements showed that strain-induced transformation to martensite set in after only a few percent of strain, and was accompanied by an enhancement in the rate of work hardening.

The high yield strength of the material deformed at 25°C resulted from the presence of deformation-induced martensite (see Figure IV-1). This was also true to a lesser extent for deformation

*See Footnote on Page 27.
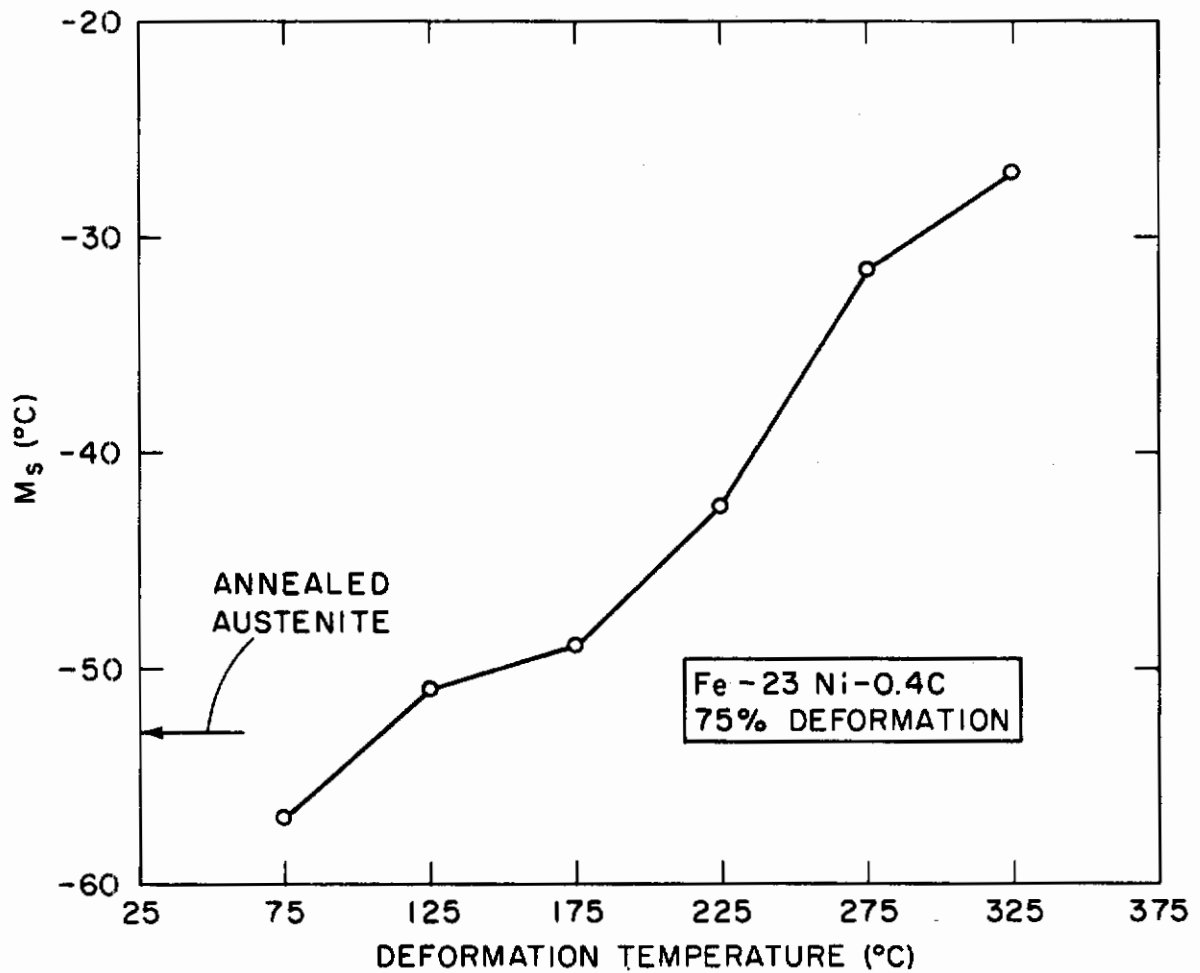
FIGURE IV-2 M_S TEMPERATURE VS. AUSFORMING TEMPERATURE.

30
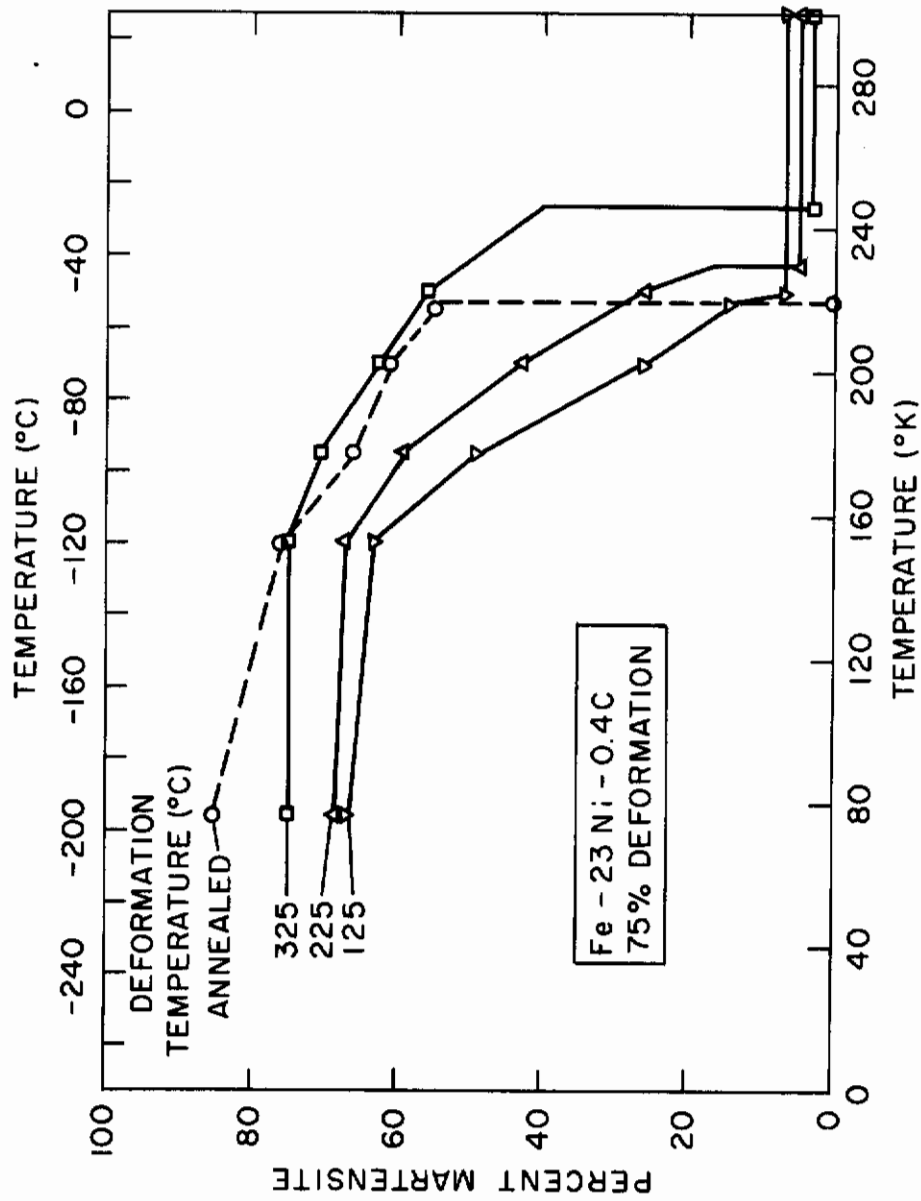
FIGURE IV-3 PERCENT MARTENSITE VS COOLING TEMPERATURE AFTER AUSFORMING AT VARIOUS TEMPERATURES.

31
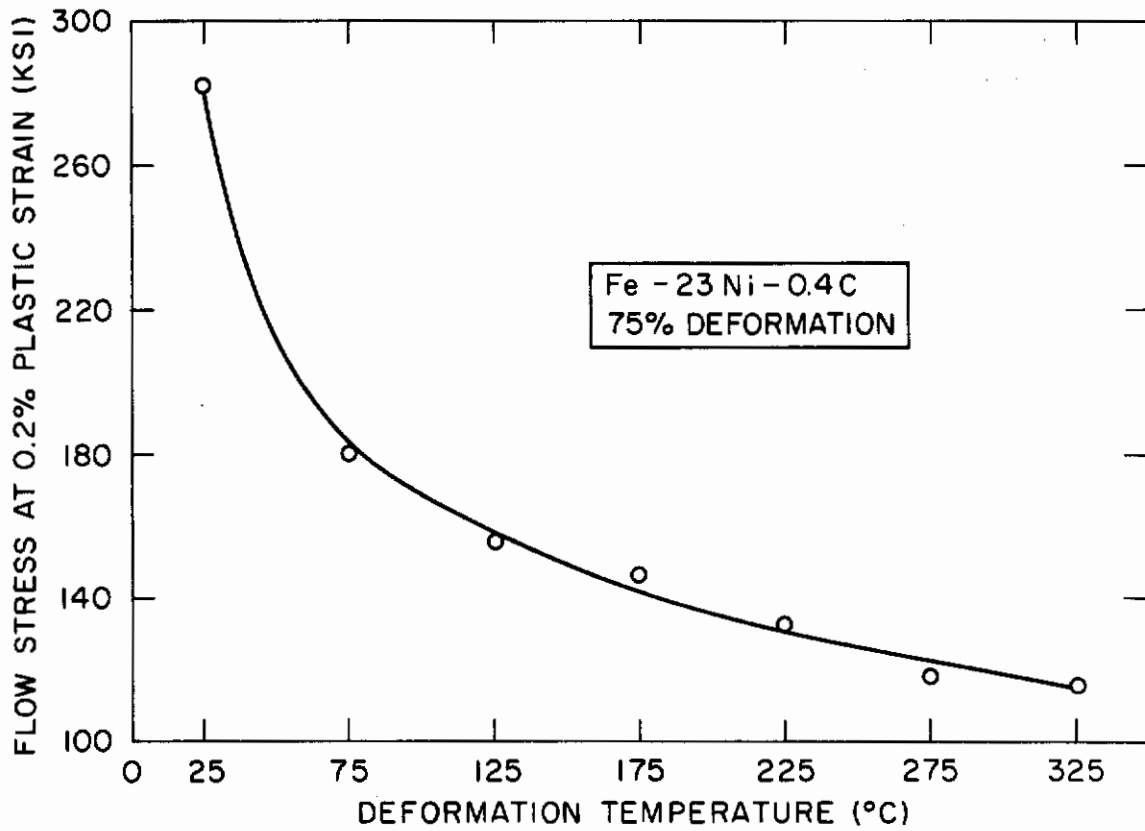
FIGURE IV-4 YIELD STRESS OF DEFORMED AUSTENITE AT 0°C VS. DEFORMATION TEMPERATURE.

temperatures up to 125°C.   Above 125°C, however, the amount of martensite caused by the deformation did not vary enough with deformation temperature to account for the observed change in strength.   Apparently, significant differences in substructure of the austenite were obtained, in addition to the production of some martensite, depending on the deformation temperature.

The annealed austenite had an equiaxed structure comprised of large grains and numerous twins.   The photomicrographs in Figure IV-5 show a selection of deformed austenites, with slip bands in elongated grains.   After the deformation at 125°C, the slip bands were heavily decorated with a fine constituent, but this delineation faded with increasing deformation temperature until, at 275°C and above, the bands etched out only as vaguely-defined stripes having little if any decoration.   In the light of these trends, it was concluded that the fine constituent was the deformation-induced martensite previously mentioned.

A patchy light-etching constituent was also detected in the austenites deformed at the higher temperatures, amounting to something less than five percent of the area under observation.   It was judged to be surface martensite, and was too small in quantity to account for the ferromagnetism found in the same austenites.

Electrical-resistivity measurements at 0°C were carried out on five wires each of annealed austenite and of austenite deformed 75 percent at 225°C.   The average values were 77.11 ± 0.15 and 76.39 ± 0.12 microhm-centimeters, respectively, the ± ranges representing the standard deviations.   Surprisingly, the resistivity of the deformed austenite was about one percent less than that of the annealed austenite.   This difference, opposite in sign to the effect of lattice imperfections per se, could be accounted for by the presence of martensite, the latter having about one-half the resistivity of austenite.   Moreover, the removal of carbon atoms from their random positions in the austenite during deformation could also lead to a decrease in resistivity.

The above resistivity difference was not attributable to the crystallographic texture of the deformed material, inasmuch as electrical resistivity is spherically symmetric in cubic crystals.

2. _Martensites_ – The tensile behavior of ausformed martensite was first investigated by testing specimens that had been ausformed (by 75 percent reduction) at 125°C.   Since retained austenite could not be entirely eliminated by refrigeration, extrapolations were made to ascertain the behavior of fully martensitic materials. The procedure was to refrigerate a series of tensile specimens to different temperatures, producing various martensite contents (see Figure IV-3).   These specimens were warmed to room temperature and held for twelve hours.   The respective martensite contents in the gage sections were then measured magnetically, using the low-field apparatus.   The specimens were tempered all together for three hours in an oil or salt pot at the desired tempering temperature, and tensile testing was then performed at 30°C.   From each autographically recorded load-elongation chart, the stresses corresponding to a pre-selected series of plastic strains were deter-

33
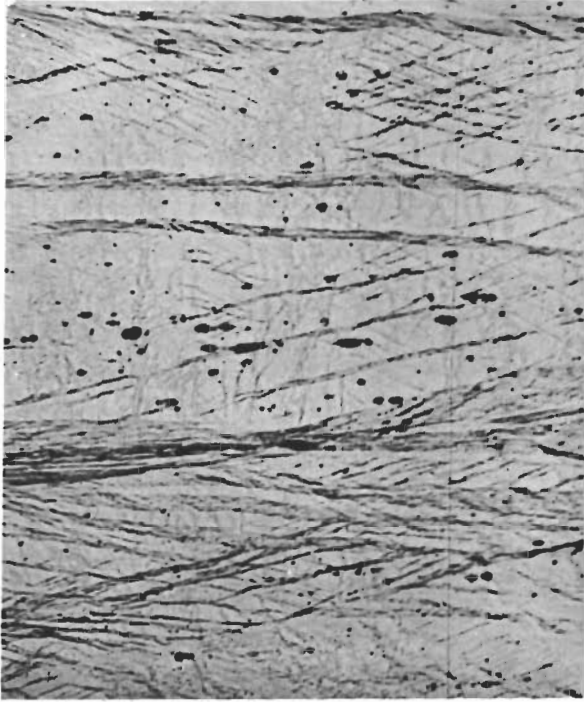
A. 125° C

B. 225° C
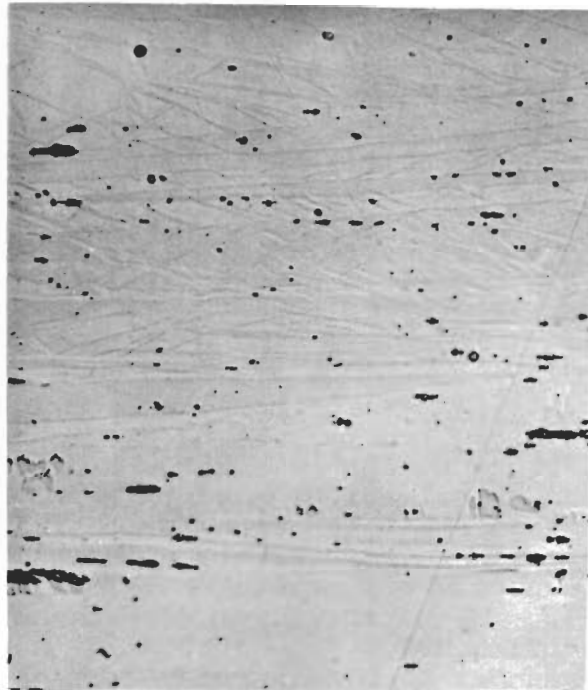
C. 325° C

FIGURE IV-5. Austenite Deformed 75 Percent at the Indicated
Temperatures. Longitudinal Section Etched with
Modified Aqua Regia. 500×.

34

mined.   Stress vs initial martensite content curves were drawn in order to extrapolate to the flow stress of 100 percent martensite at each of the selected tensile strains.

A set of such plots for regular martensite tempered at 30°C is shown in Figure IV-6.   Contrary to the findings of Winchell and Cohen,[20] the curves were found to be nonlinear, although the deviation from linearity was small.   The curvature decreased at higher tensile strains and higher martensite contents.   Extrapolation to 100 percent martensite was performed by extending the tangent to the experimental curve from the highest martensite point.   This is shown in Figure IV-6 for 0.4 percent plastic strain, the lowest strain for which this procedure appeared reliable in the worst case. However, the nonlinearity tended to vanish on tempering the regular martensite above 30°C, and except for the lowest strains, linear extrapolations could be made with confidence.

Corresponding curves for ausformed specimens tempered at 30°C are given in Figure IV-7. Here, the nonlinearity was quite pronounced, and the curves for the lower strains actually passed through a minimum.   This behavior reflected the change in shape of the stress-strain curves as the martensite content was increased.   Compared to the deformed austenite, the yielding became less abrupt with increasing amounts of ausformed martensite, but the strengthening due to the martensite did not show up at low strains until the martensite content approached some 60 percent.   Because of the nonlinearity and the longer required extrapolations (more retained austenite) in the ausformed series than in the nonausformed series, greater uncertainty was encountered in deducing the strength of the ausformed 100 percent martensites; the tangential extrapolation method adopted undoubtedly led to conservative values of the flow-stress properties after ausforming.   Here, again, tempering improved the reliability of the extrapolations, in that the strength became less sensitive to the amount of retained austenite and the dependence became more linear.

The flow strength at 0.4 percent plastic strain extrapolated to 100 percent martensite is plotted against tempering temperature in Figure IV-8 for both the regular and ausformed treatments.   The increment of ausform-strengthening present after tempering at 30°C and 100°C was found to increase upon tempering at 200°C and then decrease somewhat at still higher temperatures.   This trend was a consequence of the fact that the ausformed martensite maintained its enhanced strength on tempering at 200°C, whereas the regular martensite weakened appreciably.   Clearly, the tempering behavior was being altered by the ausforming, despite the absence of carbide-forming elements.   The ausform-strengthening was significant even after tempering at 400°C.   This was the highest tempering temperature investigated because reaustenization occurred at 500°C.

Noting that tempering produced an enhancement in the increment of ausform-strengthening, it was deemed important to know whether tempering played a role in the ausform-strengthening even when the tempering temperature was only 30°C.   Actually, iron-nickel-carbon martensites have been shown to undergo age-hardening at temperatures as low as -60°C.[20]   This raised the critical question as to wheth-

35
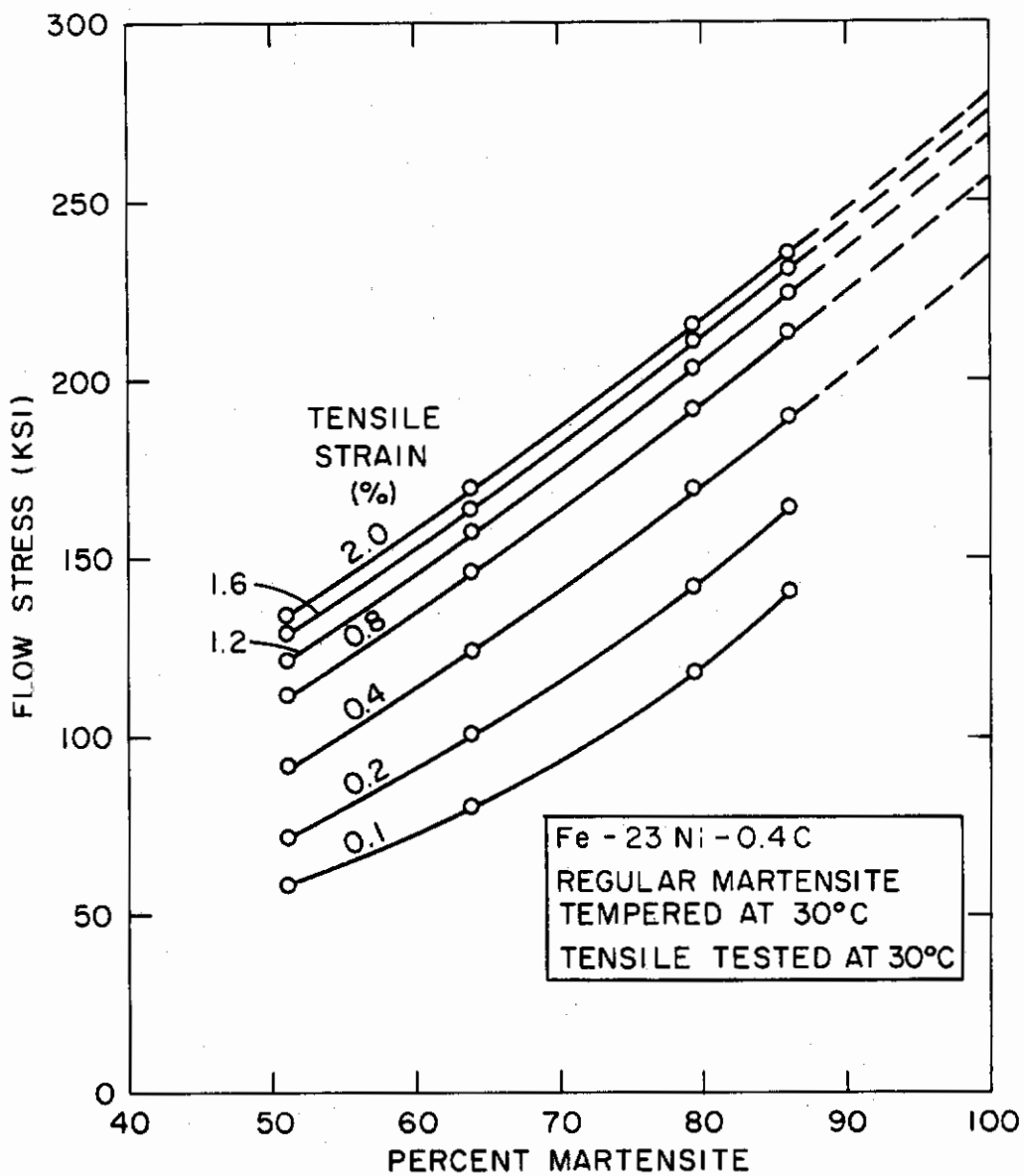
FIGURE IV-6 FLOW STRESS AT VARIOUS PLASTIC STRAINS
AS A FUNCTION OF THE AMOUNT OF REGULAR MARTENSITE PRESENT.
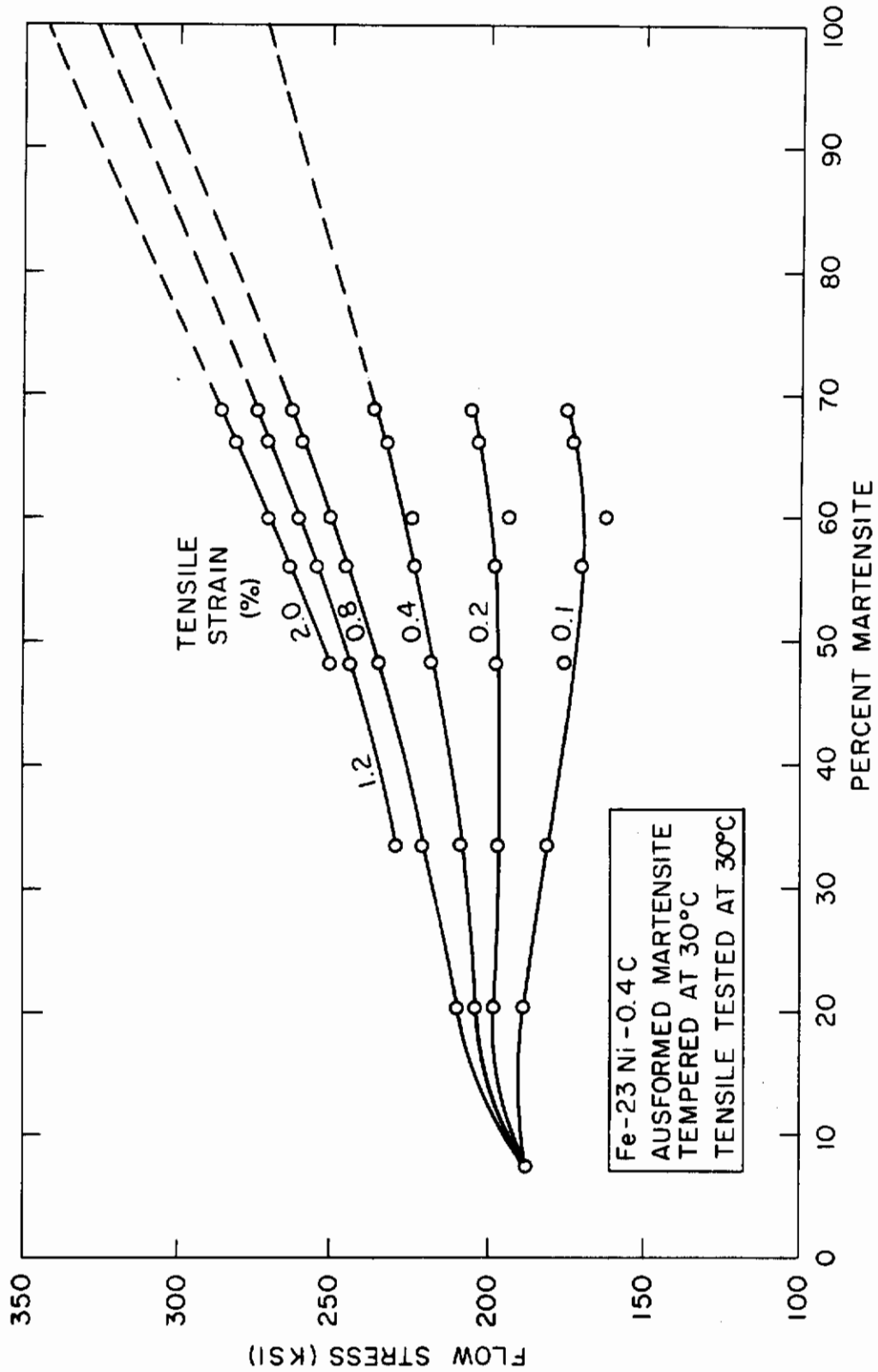
FIGURE IV-7 FLOW STRESS AT VARIOUS PLASTIC STRAINS AS A FUNCTION OF THE AMOUNT OF AUSFORMED MARTENSITE PRESENT. AUSFORMING TEMPERATURE = 125°C, AUSFORMING REDUCTION = 75 PERCENT.
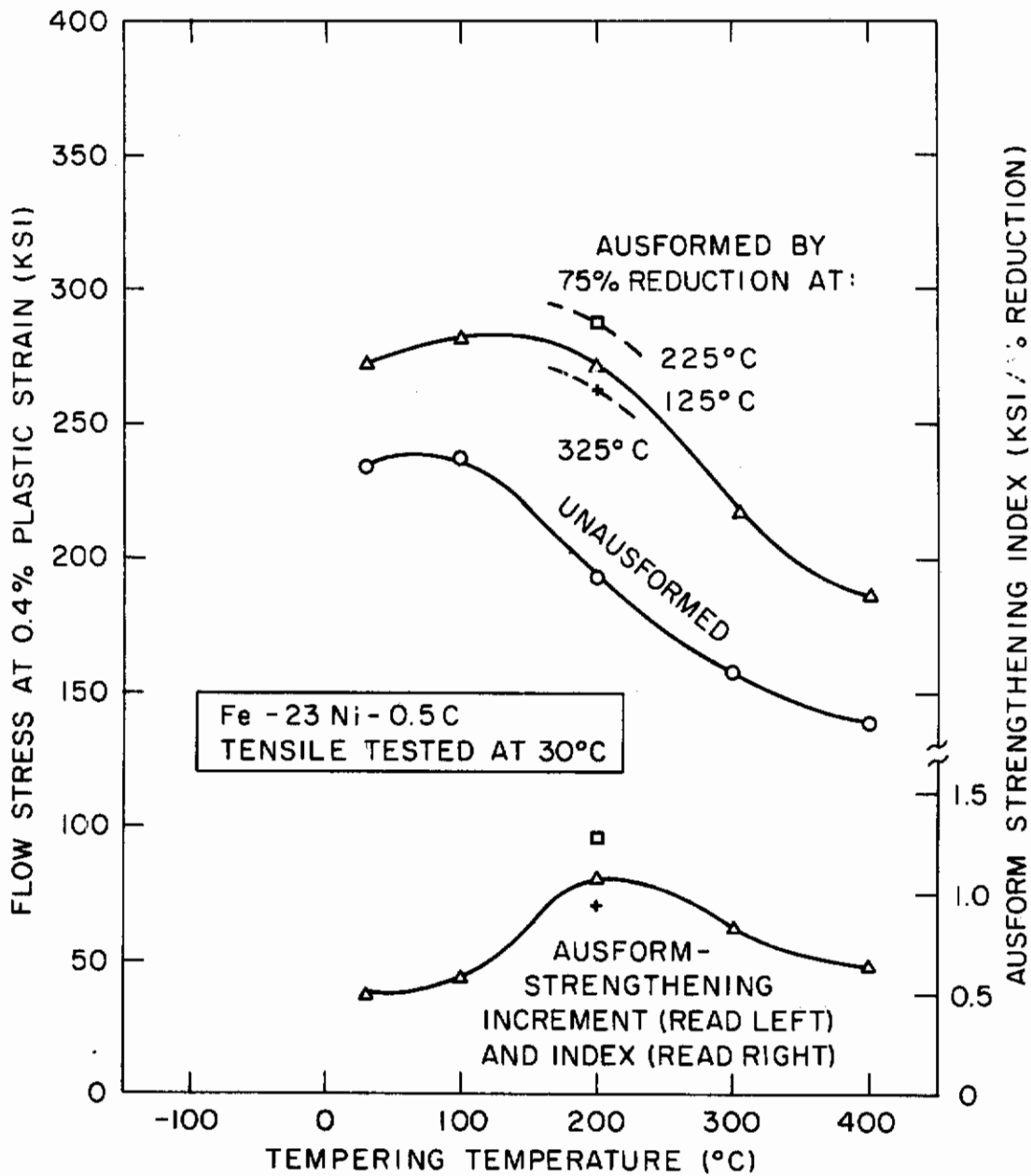
FIGURE IV-8 STRENGTH OF 100 PERCENT MARTENSITE VS. TEMPERING TEMPERATURE (3 HRS), WITH AND WITHOUT AUSFORMING.

er ausform-strengthening would be present in <u>virgin martensite</u>, i.e., in the absence of aging or tempering.

To settle this point, regular and ausformed martensites in the virgin condition were tested at -100°C. Specimens mounted in the tensile machine were cooled to temperatures below -100°C to generate various initial amounts of martensite, whereupon they were warmed to -100°C and tested. The retained austenite was subject to rapid conversion during these tensile tests, so that the martensite content was monitored by means of in-situ magnetic measurements with the low-field apparatus. After the tensile testing, the final martensite percentage was measured in the 5,000-oersted magnet. In all cases, the final martensite content was greater than 98 percent and usually greater than 99 percent. It was further found that the maximum flow stress attained by these almost fully martensitic specimens was nearly independent of the initial martensite content, although it did depend upon whether the martensite was ausformed or not. Thus, it was possible to conclude that the martensite arising from the retained austenite during the tensile testing behaved about the same as the martensite formed during the prior cooling treatment. In addition, the flow stresses at low strains (where the extrapolation to 100 percent martensite was important) were found to be quite consistent with the flow stress at higher strains (where the extrapolation was not necessary because of the virtually complete conversion of the retained austenite during the tensile test).

Representative stress-strain curves for 100 percent martensite are plotted in Figure IV-9. Evidently, ausform-strengthening was manifested even in the virgin martensite. The differences exhibited among the three ausforming temperatures were not regarded as significant.

The effects of subsequent tempering on the strength of 100 percent martensite tested at -100°C are summarized in Figure IV-10. Both the regular and ausformed martensite increased in strength during tempering up to 100°C for the former and 200°C for the latter. The increment of ausform-strengthening remained the same on tempering from subzero temperatures up to about 30° and then increased, in agreement with the previous findings (Figure IV-8).

An interesting feature of the flow curves obtained at -100°C (Figure IV-9) was the low strength level of both the unausformed and ausformed martensites at small tensile strains, and the rapid rate of strengthening during the first percent of plastic strain. Such behavior has been observed by McEvily and co-workers[21] in a series of unausformed iron-nickel-carbon martensites with 0.017 - 0.57 percent carbon. They made no correction for the presence of retained austenite, but concluded its transformation during testing did not account for the low initial strength levels. This conclusion was substantiated by the present results even after the retained austenite was taken into account by the extrapolation procedures.

Some electrical-resistivity measurements were made during the tempering of regular and ausformed martensites at 100°C. Retained austenite was present in these specimens but, as King and Glover have reported,[22] it did not transform during the tempering. These

39
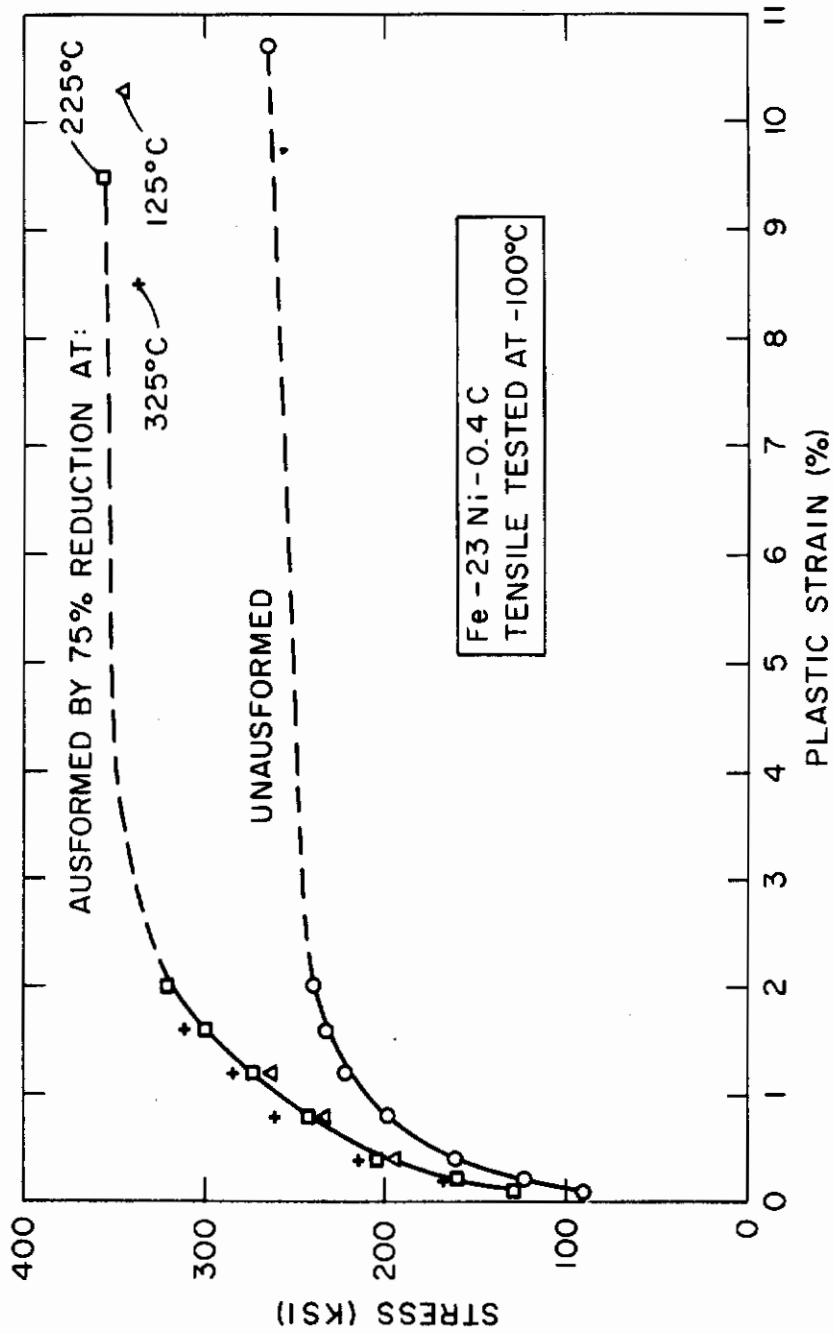
FIGURE IV-9 STRESS-STRAIN CURVES FOR 100 PERCENT VIRGIN MARTENSITE, WITH AND WITHOUT AUSFORMING.
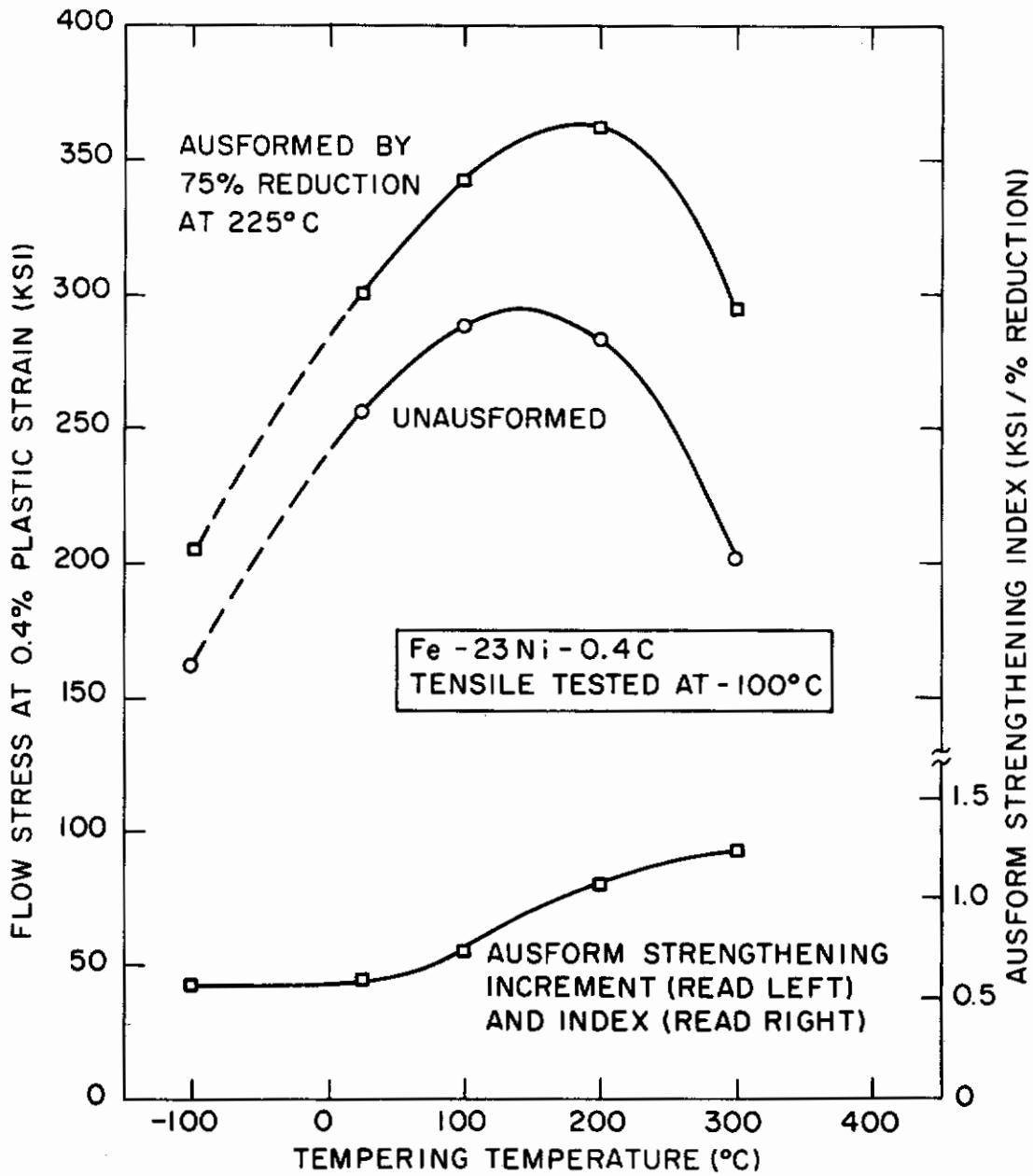
FIGURE IV-10 STRENGTH OF 100 PERCENT MARTENSITE VS. TEMPERING TEMPERATURE (3 HRS.) WITH AND WITHOUT AUSFORMING.

41
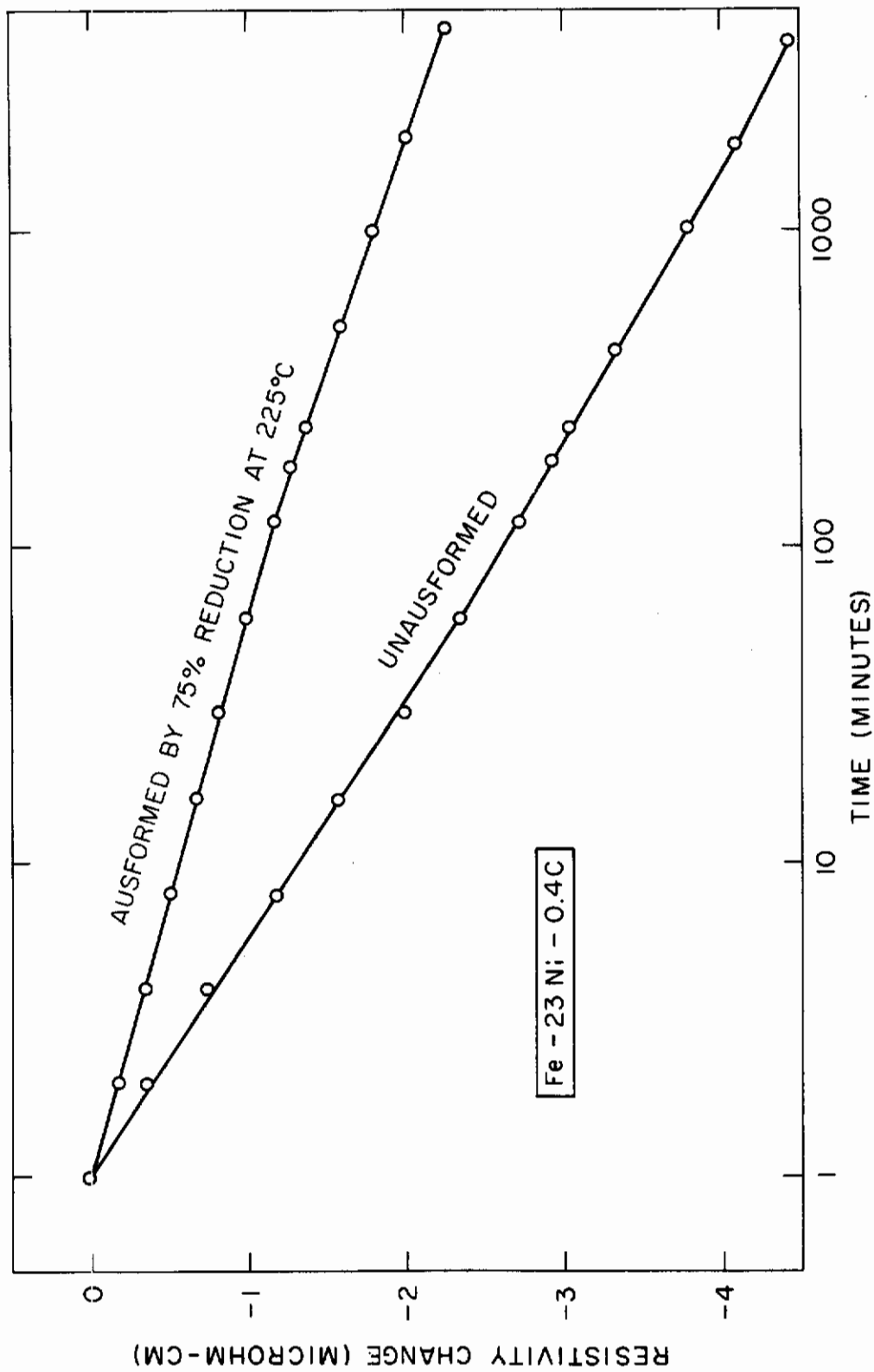
FIGURE IV-II RESISTIVITY CHANGES AFTER ONE MINUTE DURING TEMPERING OF 100 PERCENT MARTENSITE AT 100°C.

42

investigators also found that the resistivity changes on such tempering was directly proportional to the amount of martensite, thus making it possible to correct the measurements in Figure IV-11 to 100 percent martensite.

The ausformed martensite obviously tempered much more slowly than the regular martensite, as indicated by the retarded decrease in resistivity. This difference was also reflected by resistivity measurements at -195°C made before and during tempering. For example, the resistivity changes corresponding to 3 hours of tempering at 100°C, when corrected to 100 percent martensite, were 2.91 microhm-cm for the unausformed martensite and only 2.17 microhm-cm for the ausformed martensite. This suggests that the regular martensite precipitated 1.34 times as much carbon as did the ausformed martensite during the given tempering treatment, and that carbon removal from the martensitic solid solution, whether by clustering or precipitation, was being inhibited in the ausformed martensite. An alternate explanation based on the depletion of carbon from the parent austenite during the ausforming deformation (leaving less carbon available for the tempering process) was considered unlikely because no evidence of carbide precipitation in the austenite has been found with the electronmicroscope.[6]

Careful examination of the autographic load-elongation charts yielded some important observations on the strain-aging behavior of ausformed and unausformed martensite. During each tensile test at 30°C, the specimen was unloaded after about 1.7 percent plastic strain, and then reloaded for continuation of the test. Plastic flow did not resume until the load attained a higher value than the level at which unloading was begun, but there was no yield drop. The higher flow stress remained steady during further straining until it met the extension of the original flow curve, after which strain hardening set in once more. The aging time during the unloading cycle varied from two to eight minutes, but produced little effect on the strain-aging phenomenon. Evidently, the aging occurred very rapidly, within the first minute or two at 30°C.

The increment in flow stress caused by the aging was found to be an increasing function of the martensite content. In most instances, no detectable strain aging was observed in the austenite. The flow-stress increments for specimens containing 70 to 85 percent martensite and tested at 30°C are shown as a function of the prior tempering temperature in Figure IV-12. The difference in the behavior of the ausformed and unausformed martensites was striking. Considerably more strain aging occurred in the ausformed martensite after all tempering treatments, although tempering reduced the strain aging in both the ausformed and unausformed martensites. During the testing of one ausformed specimen tempered at 200°C, the straining was interrupted for only 15 seconds without removal of the load. The increase in stress observed when straining was resumed is also plotted in Figure IV-12; this strain aging had attained half of the increment observed after several minutes of aging in the unloaded condition.

Analogous strain aging was found by Stephenson and Cohen on unausformed 4340 steel,[23] the comparable tests being those in which retempering (aging) was limited to room temperature.
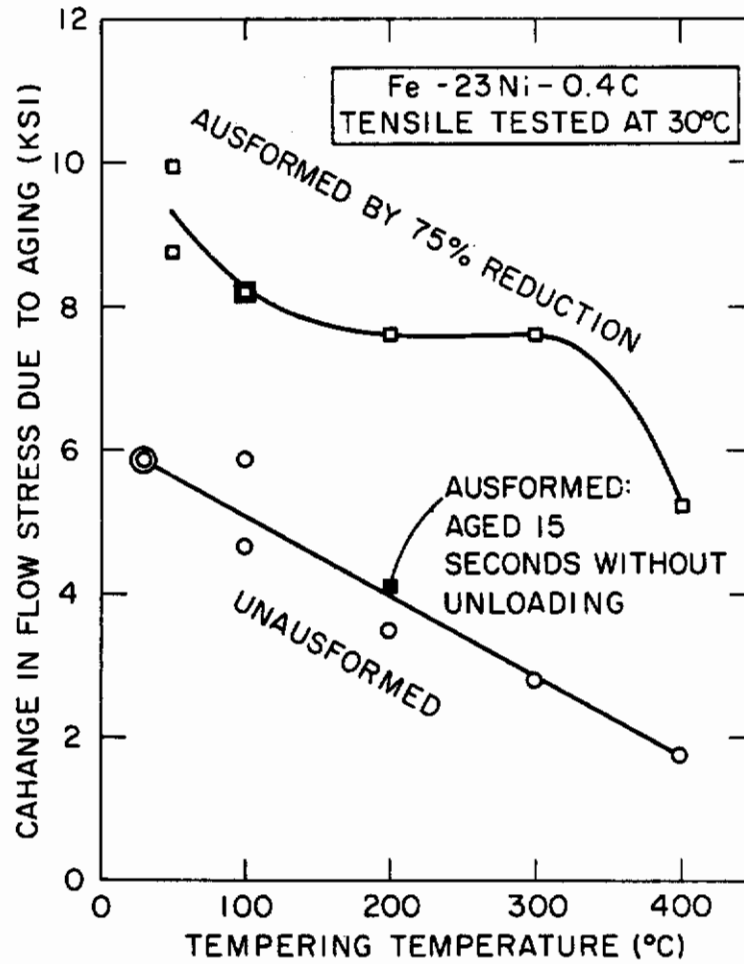
FIGURE IV-12 EFFECT OF TEMPERING ON THE INCREASE IN FLOW STRESS AT ~ 1.7 PERCENT STRAIN CAUSED BY AGING ~ 4 MINUTES IN UN-LOADED CONDITION AT 30°C. SPECIMENS 70-85 PERCENT MARTENSITIC.

44

The strain-aging results described here exhibited the characteristics of stress-induced ordering of interstitials, as discussed by Wilson and Russell for the case of ferrite.[14] Breyer and Polakowski have concluded that stress-induced ordering also occurs within the strain fields around dislocations in martensite.[25] The stress-induced ordering in ferrite takes place within a minute at room temperature; in contrast, aging by the segregation of carbon to dislocations proceeds more slowly by a factor of several thousand. Because the aging observed in the present investigation was so rapid it was probably caused by the stress-induced ordering of the interstitial carbon atoms near dislocations in the martensite.

According to Wilson and Russell,[24] the increase in yield stress of ferrite caused by stress-induced ordering is directly proportional to the dissolved interstitial content, with a proportionality constant of 18 KSI per atomic percent carbon (and nitrogen) when aged in the unloaded condition. This figure leads to a predicted stress increase of 34.8 KSI by stress-induced ordering in a 0.4 weight percent martensite. If the strain-aging increments reported in Figure IV-12 for tempering at 100°C are linearly corrected to 100 percent martensite, they become 12.1 KSI for the ausformed martensite and 6.2 KSI for the unausformed martensite. Comparing these figures to 34.8 KSI provides a measure of the fraction of the initial 0.4 percent carbon remaining in solution after the tempering treatment. This simple proportionality gives 0.14 percent carbon still in solution in the tempered ausformed martensite and 0.07 percent in solution in the tempered regular martensite.

There are so many differences in substructure between ferrite and martensite that the extension of Wilson and Russell's data to martensite can only be regarded as a very rough approximation. Nonetheless, the strain-aging measurements in Figure IV-12 now offer strong evidence that more carbon was retained in solid solution to higher tempering temperatures in the ausformed martensite than in the regular martensite.

D. Discussion of Results

It is evident from Figure IV-10 that ausform-strengthening occurs even in virgin martensite, and that the strengthening increment remains the same on aging or tempering at least up to 30°C. At the same time, the strength of both regular and ausformed martensite increases remarkably with the tempering temperature in this range.

Because the strengthening response to tempering at higher tempering temperatures is not the same in regular and ausformed martensite, the ausform-strengthening increment is approximately doubled by tempering at 200°C compared to tempering at 30°C or below. This phenomenon results from the more rapid weakening of the unausformed martensite on tempering beyond 100°C.

Referring to the 30°C tests, the ausform-strengthening index can be obtained by dividing the increment in strength by the 75 percent reduction in area used for the ausforming. The index is 525 psi/% for a tempering temperature of 30°C, and this represents

45

the response of untempered martensite as well.   Cohen has reported
an index of 300 psi/% for a low-carbon iron-nickel alloy.[4]   Tempering the present 0.4 percent carbon iron-nickel alloy at 200°C
raises the index to 1080 for an ausforming temperature of 125°C
and to 1280 when the ausforming is performed at 225°C.   The latter
value compares favorably with the ausforming response of high-strength steels such as 4340 and H11.[7,26]

Justusson and Schmatz have found somewhat similar results on
an iron-4 percent nickel - 12 percent chromium - 0.35 percent carbon steel having an M_s of 100°C.[5]   The strengthening index was
about the same as for the present iron-nickel-carbon alloy, when
tempered at room temperature and at 260°C.   However, their ausforming was performed at 510°C, and the ausformed martensite did
not soften even when tempered at 430°C.   This greater resistance
to softening seems to be related to the presence of chromium.

Although the results assembled here do not point unequivocally
to a complete interpretation of the strengthening of ausformed martensite, they do indicate what may be the dominant strengthening
mechanisms in the iron-nickel-carbon alloy at hand.   Perhaps the
pivotal data are the strain-aging effects (Figure IV-12) which
strongly suggest that more carbon remains in solution when the ausformed martensite is tempered than when the regular martensite is
tempered, although some carbide precipitation takes place in both
cases.   The resistivity changes on tempering (Figure IV-11) also
support this conclusion.   If the resistivity changes during tempering are assumed to be proportional to the carbon removed from
solution in the martensite, the regular and ausformed martensite
can be readily compared on this basis.   As previously mentioned,
after tempering for 3 hours at 100°C, the regular martensite precipitates 1.34 times more carbon than does the ausformed martensite.   A similar calculation for the strain-aging changes shows
this factor to be 1.27, which is in good agreement considering the
widely different nature of the two sets of measurements.

From these figures we may infer that within the usual first
stage of tempering, a larger proportion of the strength of ausformed martensite is due to solid-solution hardening than is the
case with regular martensite.   On tempering at 100°C, the ausform-strengthening increment is only slightly enlarged over that
produced without tempering.   This behavior can be attributed to
the precipitation hardening which occurs in the early stages of
tempering[20] and which more than makes up for the reduced solid-solution hardening, thereby raising the strength level of both
types of martensite a little.   However, as the tempering process
proceeds at 200°C and the dispersion of epsilon carbide in the un-ausformed martensite coarsens beyond the optimum for precipitation
hardening, the difference in solid-solution strengthening in the
two types of martensite becomes more evident.   In the prevailing
carbon range, the work of Winchell and Cohen[20] has shown that
small differences in solid-solution carbon make relatively large
differences in the flow stress.

Of course, if less carbon precipitates in the ausformed martensite, one would expect a difference in the carbide morphology.

Investigations by electron microscopy on this point have been some-
what conflicting.(5,27,28,29)   Some alteration of the carbide dis-
persion is usually noted, but in two instances, reduced amounts of
carbide were observed in the tempered ausformed martensite.(5,27)
The electron micrographs in Figure IV-13 show less precipitated
carbide in the ausformed martensite than in the regular martensite,
although a quantitative estimate cannot be made by this approach.
Rather, the resistivity and strain-aging measurements, indicating
the amount of carbon remaining in solution, are more capable of di-
rect interpretation.   From these findings it is concluded that re-
tention of carbon in solution and the accompanying resistance to
carbide coalescence account for the enhanced stability of the
strength of ausformed martensite during tempering.

While the effect of ausforming on the tempering kinetics has
not been investigated in detail, the indications are that the driv-
ing force for the precipitation of epsilon carbide is diminished.
This could be a consequence of the trapping of carbon atoms at the
extra dislocations or even in lattice vacancies, as proposed for the
more severe case of strain-tempered martensite in Section V; these
traps constitute more stable positions for the carbon atoms than do
the interstitial sites in the martensite.   At the same time, the
"stabilized" carbon atoms can contribute to both the general strength-
ening and the strain-aging phenomenon, because these atoms will have
to be forced into the high-energy interstitial sites in order to
move the dislocations.

Having rationalized the effect of ausforming on tempering we
now consider the ausform-strengthening of the untempered martensite.
Thomas et al,(6) have reported that the presence of dissolved car-
bide-forming elements in the austenite greatly increases the strain-
hardening response of the austenite, and that the strength of the
resulting ausformed martensite is also benefited.(6)   This suggests
that one might gage the strengthening obtainable from ausforming by
noting the strain-hardening of the austenite.   For example, Cohen
found that 75 percent reduction of iron - 31.9 percent nickel,
0.017 percent carbon austenite at 300°C raised the flow stress by
50 KSI,(4) whereas with the present 0.4 percent carbon alloy, the
same reduction in area at 275°C raised the austenite to flow stress
by 90 KSI.   The difference is undoubtedly the result of carbon-
dislocation interactions in the austenite, inasmuch as there is no
evidence that carbides precipitate from the austenite under these
conditions.   Thomas et al(6) have examined an iron - 28 percent
nickel - 0.3 percent carbon austenite deformed 30 percent at 510°C
by transmission electron microscopy.   In contrast to similar al-
loys containing carbide-forming solutes, they were not able to de-
tect any carbide in the deformed iron-nickel-carbon austenite.   As-
suming that this observation also applies after deformation at the
lower temperatures studied here, the interaction responsible for
the increased strain hardening of austenite in the presence of car-
bon must be one that retains the carbon in solution.

A simple explanation can be offered for the effect of carbon
on the strain hardening of austenite.   It is known that the rapid
work hardening of FCC single crystals in stage II is prolonged by

A. Unausformed

⊢———⊣
1μ

B. Ausformed

⊢———⊣
1μ
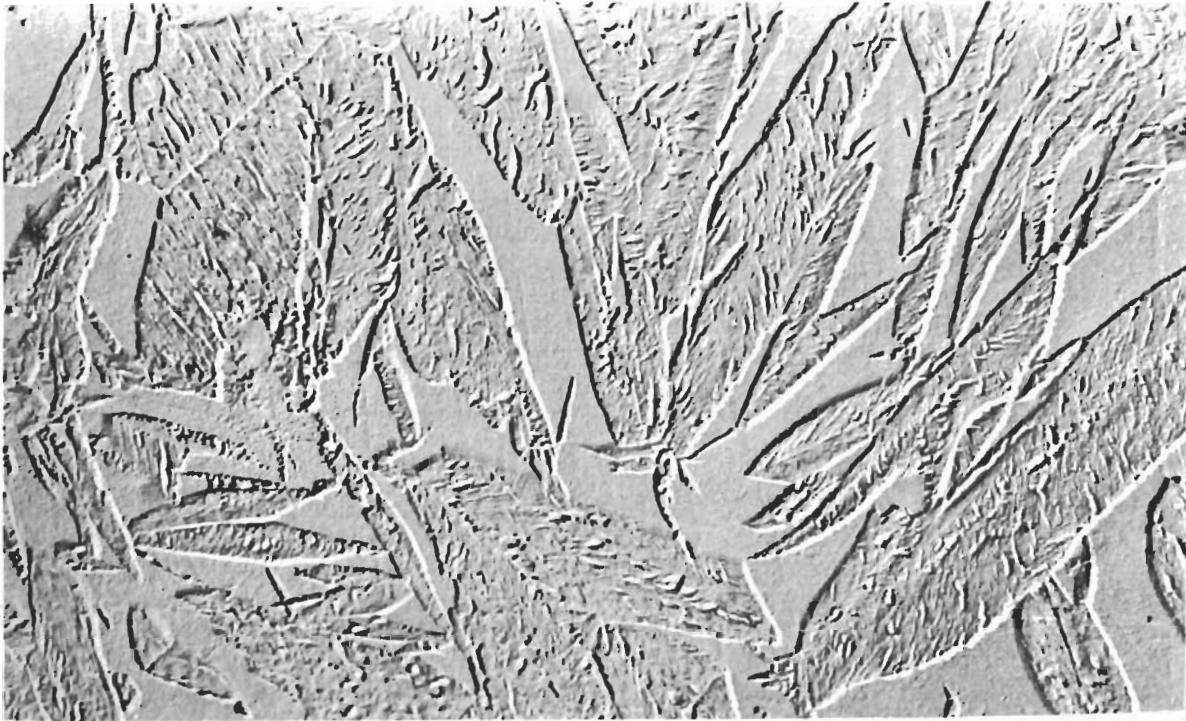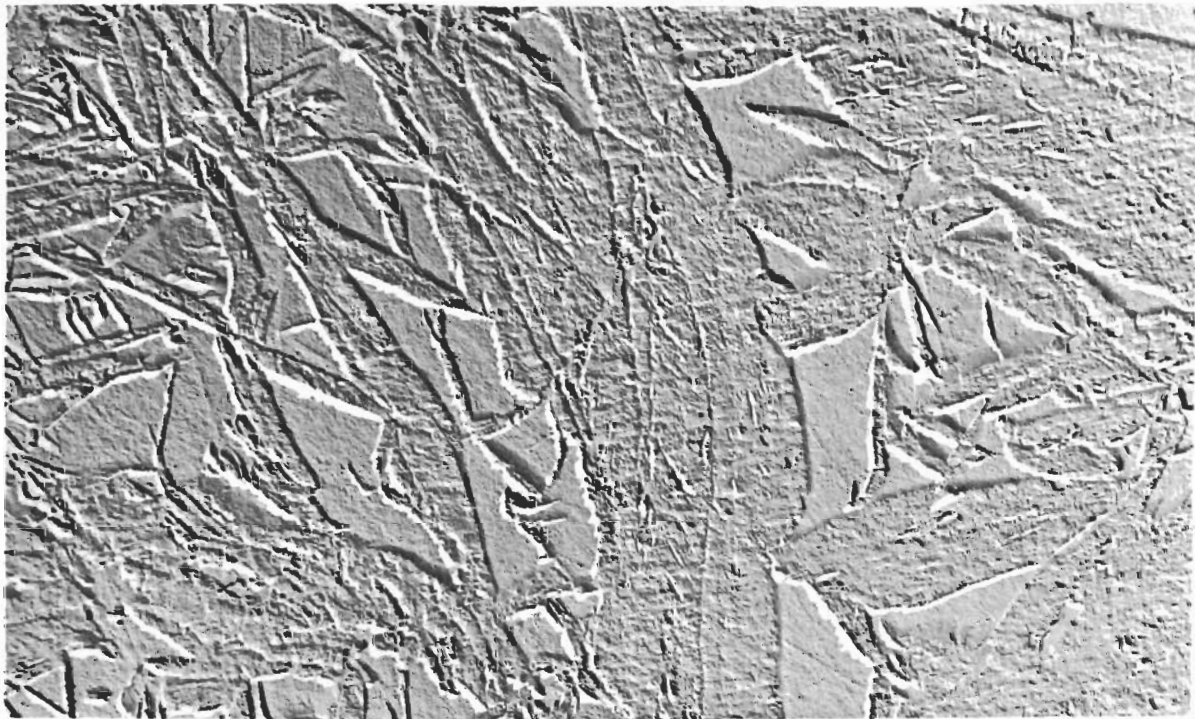
FIGURE IV-13. Electron-Replica Micrographs of Regular and Ausformed
(75 Percent Reduction at 225° C) Martensites, Subsequently
Tempered at 200° C.   Static Shadowed with Chromium.
Nital Etch.   10,000×.

48

the presence of solute atoms.[30] Cross slip and dynamic recovery which give rise to the decreasing rate of strain hardening denoted by stage III are hindered. Thus, the dislocation density rises more rapidly in the presence of solutes, in that concurrent recovery does not set in so soon. Most of the available data along these lines are for substitutional solutes, but Fleischer and Hibbard[31] point out that the important distinction between substitutional and interstitial solutes depends mainly upon whether the distortion produced by the solute atom is symmetrical or tetragonal. The interstitial sites occupied by carbon atoms in austenite are symmetrical, so that the effect of carbon on the strain hardening of austenite can be explained in the same way as for substitutional solutes in FCC materials.

Because of the diffusionless nature of the martensitic transformation, the dislocation substructure in the strain-hardened austenite is carried over into the martensite. Consequently, the resulting dislocation density is higher in ausformed martensite than in regular martensite, and is further increased by the presence of carbon. This inherited dislocation substructure is believed to be the principal cause of the ausform-strengthening observed in virgin martensite.* However, part of this strengthening may also be attributable to the reduced plate size of the ausformed-martensite, a factor which can operate even in the absence of carbon.[4]

It is recognized that the changes in magnetization and M_s temperature resulting from the deformation of austenite could be construed as evidence of iron-carbide precipitation. In fact, a similar raising of M_s in an ausformed alloy containing strong carbide-forming solutes (H-11) has been interpreted in just this way by Raymond and Reuter.[32] We have not adopted that viewpoint for the iron - 23 percent nickel - 0.4 percent carbon alloy primarily because (a) the strain-aging behavior indicates that more carbon is in solution in the ausformed martensite than in the unausformed martensite, and (b) no carbides have been observed by electron microscopy in the deformed iron-nickel-carbon austenites.

Moreover, although cementite is ferromagnetic, a simple calculation will show that its precipitation could not account for the observed increase in magnetization in the deformed austenite. Based on the specific magnetization of iron (182 erg/gm-gauss) and of cementite (103.5 erg/gm gauss) in a field of 5000 oersteds,[33] it would require the precipitation of three-fourths of the carbon in the austenite to cementite to explain the change in magnetization at 325°C, which is the deformation temperature where the change is the smallest. Precipitation of this magnitude should be readily detectable by electron microscopy.

---

* Previous studies on the internal twinning in iron-nickel-carbon[6] martensites have disclosed no definite change in this structural feature as a result of ausforming. Hence, the presence or absence of internal twinning is not regarded as an important factor in the ausform-strengthening.

We have concluded that the increase in magnetization arises
from the formation of a minor quantity of finely-dispersed mar-
tensite due to a lowering of the effective carbon content by trap-
ping of the interstitial atoms in lattice imperfections. Most
likely the imperfections active in this respect are the disloca-
tions generated during the plastic deformation of the austenite,
but vacancies are also a possibility for carbon trapping, as dis-
cussed in Section V of this report. The postulated formation of
martensite is consistent with the decrease in electrical resisti-
vity that attends the deformation process.

When the virgin martensite (whether ausformed or unausformed)
is heated from subzero temperatures to room temperature and some-
what above, substantial strengthening takes place in both types of
martensite. Considering the low temperature range involved, it
is not likely that enough epsilon carbide could precipitate to ac-
count for the strengthening. Instead, this interesting phenome-
non undoubtedly reflects the very low flow stress exhibited by vir-
gin martensite at low strains. As McEvily et al[21] have found,
tempering even at room temperature removes this anomalous behavior,
and the strength level at low strains rises rapidly. On the other
hand, the increment of ausform-strengthening is not affected by
these interesting changes, and so their origin will not be exam-
ined here.

All of the strengthening mechanisms dealt with in this inves-
tigation relate to slip, rather than mechanical twinning, as the
prevailing mode of deformation. Richman[34] has reported that me-
chanical twinning becomes important in iron-nickel-carbon marten-
sites when the carbon content is above 0.4 percent. However, in
the present alloy, optical microscopy revealed very few mechanical
twins in the tensile-tested martensite, and it may be safely pre-
sumed that the operative strengthening processes are controlled by
slip-interference mechanisms.

E. Conclusions

1. The strength of iron - 23 percent nickel - 0.4 percent
carbon martensite in the virgin (unaged or untempered) condition,
tested at -100°C, is substantially enhanced by ausforming. How-
ever, the yield strengths of both ausformed and unausformed mar-
tensites are very low in the virgin state, even after correction
for the retained austenite by extrapolation to 100 percent marten-
site. The ausform-strengthening in virgin martensite is thought
to result mainly from the lattice imperfections introduced into the
parent austenite by the prior plastic deformation.

2. The extrapolation to 100 percent martensite requires par-
ticular care because the flow stress at any given strain is not al-
ways a linear function of the retained-austenite content. The
linearity becomes more definite the higher the tempering tempera-
ture and the higher the strain at which the flow stress is taken.

3. The yield strength of virgin martensite, whether ausformed
or not, rises rapidly on tempering from -100°C to slightly above
room temperature, but the increment of ausform-strengthening re-
mains the same. With further tempering up to about 200°C the in-

50

crement of ausform strengthening increases to a level comparable
to that observed in the more complex steels containing carbide-
forming elements.   This change comes about because the ausformed
martensite resists weakening on tempering more effectively than
does the regular martensite.

4.   Strain-aging and electrical-resistivity measurements indi-
cate that the rate of carbide precipitation on tempering is appre-
ciably retarded in the ausformed martensite.   Electron microscopy
seems to confirm this in the appearance of fewer carbides during
tempering.   Consequently, it is proposed that the greater reten-
tion of strength by the ausformed martensite on tempering results
from a larger component of interstitial solid-solution hardening
than is the case during the tempering of regular martensite. This
difference in tempering kinetics is ascribed to the trapping or
stabilization of carbon atoms at lattice imperfections in the aus-
formed martensite.

F. References

1. C.W.Marschall, "Hot-Cold Working of Steel to Improve Strength," DMIC Report 192, Battelle Memorial Institute, Columbus, Ohio (October 11, 1963).

2. S.V.Radcliffe and E.B.Kula, "Deformation, Transformation and Strength," Fundamentals of Deformation Processing, Edited by W.A.Backofen et al., Syracuse University Press (1964) 321.

3. J.J.Harwood and R.Clark, "Thermomechanical Treatment of Steel," DMIC Report 210 Problems in the Load-Carrying Application of High-Strength Steels, Battelle Memorial Institute, Columbus, Ohio (October 26, 1964) 201.

4. M.Cohen, "On the Development of High Strength in Steel," JISI 201 (1963) 833.

5. W.M.Justusson and D.J.Schmatz, "Some Observations on the Strength of Martensite Formed from Cold-Worked Austenite," Trans.ASM 55 (1962) 640.

6. G.Thomas,D.Schmatz and W.Gerberich, "Structure and Strength of Some Ausformed Steels," Proc.of 2nd International Symposium on High Strength Materials, Berkeley, California (1964), to be published.

7. E.B.Kula and J.M.Doshi, "Effect of Deformation Prior to Transformation on the Mechanical Properties of 4340 Steel," Trans. ASM 52 (1960) 346.

8. D.J.Schmatz, F.W.Schaller and V.F.Zackay, "Structural Aspects and Properties of Martensite of High Strength," The Relation Between the Structure and Mechanical Properties of Metals, National Physical Laboratory Symposium 15, London (January 1963).

9. A.J.McEvily,Jr.,R.H.Bush,F.W.Schaller and D.J.Schmatz, "On the Formation of Alloy Carbides During Ausforming," Trans.ASM 56 (1963) 753.

10. J.C.Shyne, V.F.Zackay and D.J.Schmatz, "The Strength of Martensite Formed from Cold-Worked Austenite," Trans.ASM 52 (1960) 346.

11. F.W.Schaller and D.J.Schmatz, "The Inheritance of Defects by Martensite," Acta Met. 11 (1963).

12. G.S.Ansell and A.Arrott, "The Strengthening Mechanism of Ferrous Martensite," Trans.AIME 227 (1963) 1080.

13. J.C.Shyne and W.D.Nix, "Dislocations in Martensite Inherited from Austenite," Acta Met.13 (1965) 869.

14. F.W.Schaller and V.F.Zackay, "Low Temperature Embrittlement of Austenitic Cr-Mn-N-Fe Alloys," Trans.ASM 51 (1959) 609.

15. R.T.Howard and M.Cohen, "Quantitative Metallography by Point Counting and Lineal Analysis," Trans. AIME 172 (1947) 413.

16. R.M.Bozworth, Ferromagnetism, Van Nostrand, New York (1951) 850.

17. C.E.Feltner, "An Extensometer for Use at Low Temperatures," Publication Preprint from Ford Scientific Laboratory, Dearborn, Michigan.

18. L.Kaufman and M.Cohen, "Thermodynamics and Kinetics of Martensitic Transformations," Progress in Metal Physics 7 (1958) 165.

19. C.S.Barrett, Structure of Metals, McGraw-Hill, New York (1952) 443.

20. P.G.Winchell and M.Cohen, "The Strength of Martensite," Trans.ASM 55 (1962) 347.

21. A.J.McEvily, R.C.Ku and T.L.Johnston, "The Source of Martensite Strength," Publication Preprint from the Ford Scientific Laboratory, Dearborn, Michigan.

22. H.W.King and S.G.Glover, "A Resistometric Study of the First stage of tempering in Plain Carbon Steels," JISI 193 (1959) 123.

23. E.T.Stephenson and M.Cohen, "The Effect of Prestraining and Retempering on AISI Type 4340," Trans.ASM 54 (1961) 72.

24. D.V.Wilson and B.Russell, "Stress Induced Ordering and Strain-Aging in Low Carbon Steels," Acta Met. 7 (1959) 628.

25. N.N.Breyer and N.H.Polakowski, "Cold Drawing of Martensitic Steels up to 400,000 psi Tensile Strength," Trans. ASM 55 (1962) 667.

26. L.Raymond, W.W.Gerberich and C.F.Martin, "Effect of Carbon on the Strength, Ductility, and Fracture Toughness of Ausformed H11 Steel," Trans.ASM 58 (1965) 95.

27. I.Tamura, H.Yoshimura, M.Ibaraki and M.Tagaya, "On the Tempering Behavior of Martensite in an Ausformed Fe-Ni-C Alloy," Trans.Jap.Inst.Met. 5 (1964) 97.

28. B.R.Banerjee, R.C.Westgren, J.M.Capenos and E.J.Dulis, "Ausworking Type 422 Stainless Steel," Trans.ASM 56 (1963) 1629.

29. M.G.H.Wells, Discussion of Reference 5, Trans.ASM 55 (1962) 1088.

30. D.McLean, Mechanical Properties of Metals, Wiley, New York (1963) 170.

31. R.L.Fleischer and W.R.Hibbard,Jr., "Solution Hardening,"
    The Relation Between the Structure and Mechanical Proper-
    ties of Metals, National Physical Laboratory Symposium 15,
    London (January 1963).

32. L.Raymond and W.G.Reuter, "The Role of Carbides in Aus-
    forming," Acta Met. 12 (1964) 949.

33. M.Mentser, "Magnetic Analysis of Phase Changes Produced
    in Tempering a High Carbon Steel," Trans.ASM 51 (1959)
    517.

34. R.H.Richman, "Plastic Deformation Modes in Fe-Ni-C Mar-
    tensites," Trans.AIME 159 (1963) 159.

V. STRAIN TEMPERING OF IRON-CARBON MARTENSITES

B. A. MacDonald[*]

A. Introduction

Untempered or tempered martensite can be further strengthened by plastic deformation and subsequent tempering. Such strain tempering involves an interaction between the normal stages of tempering and the imperfections generated by the deformation. Under some conditions the resultant enhancement in strength is striking.

Several studies have shown that the yield and tensile strengths of martensitic steels can be increased significantly through a combination of plastic straining and retempering (1-5). A systematic investigation of strain tempering was conducted by Stephenson and Cohen,[1] encompassing a wide range of pretempering, straining, and retempering treatments on AISI 4340 steel. Pretempered specimens were deformed to 0, 1 and 3 percent tensile strain, and the tensile properties measured after retempering. The greatest strengthening due to this process was found when the martensite was pretempered at relatively low temperatures (~200°C), strained 3 percent, and retempered at about the same temperature. Retempering treatments above the pretempering temperature caused a progressive loss of the strengthening increment due to strain tempering.

Breyer and Polakowski[2] have since studied AISI 4340 steel, cold drawn to reductions in area of 3-9 percent. With deformations over 4 percent, strain tempering was found to result in light-etching martensite. This effect was attributed to reduced amounts of epsilon carbide precipitating in the martensite. To account for this phenomenon it was proposed that carbon atoms may prefer to reside in the tensile-stressed regions around dislocations rather than occupy positions in the epsilon-carbide lattice.

This light-etching characteristic of strain-tempered martensite was reported earlier for plain-carbon steels by Wilson[3] who used a Vickers-type pyramid indenter to deform the martensite. He concluded that, when as-quenched or low-tempered martensite is deformed and retempered, the precipitation of epsilon carbide is inhibited at temperatures up to about 200°C, whereas the precipitation of cementite is little affected at higher tempering temperatures. The dislocations introduced by the plastic straining were considered to provide sufficiently stable sites for the carbon atoms in the martensite to retard the kinetics of epsilon-carbide precipitation.

In the present investigation the hardness-indentation method of deforming the martensite was adopted in order to examine the effect of large plastic strains and to accentuate the phenomena that are operative in strain tempering. A Rockwell diamond conical brale was employed for this purpose. Both the pretempering and retempering temperatures were varied systematically for three plain-carbon steels. The hardening response was determined by micro-

---

[*] Now at Ingersoll-Rand Company, Princeton, New Jersey.

hardness tests in the deformed regions, and the structural changes were studied by light and electron microscopy. Special attention was given to the roles of epsilon carbide and cementite in the pretempered martensite, and to the imperfection/carbon interactions during the retempering stage.

B. Experimental Details

1. **Materials and Heat Treatment** - Table V-1 lists the steel compositions investigated in this part of the program. The specimens were in the form of 1/8-inch thick discs cut from 5/8-inch diameter rod in the annealed condition. The end faces were surface ground to a disc thickness of 0.09 inch, wet ground on 240-grit paper, and the edges beveled to reduce quench-cracking tendencies during the subsequent hardening.

The discs were austenitized for one hour at 805 $\pm$ 5°C (0.80 percent carbon steel) or 1000 $\pm$ 5°C (0.18 and 0.38 percent carbon steels) under an argon atmosphere in Vycor tubing, and then quenched into iced brine. The pretempering, if any, was carried out for one hour in an oil or salt bath, followed by water quenching to room temperature. Retempering after the plastic straining was conducted in a similar way. The retained austenite was always less than 10 percent.

2. **Brale Indentation and Microhardness Tests** - A standard Rockwell diamond indenter (with a conical apex angle of 120° rounded to a radius of 0.20 mm) was used for imparting plastic deformation to the martensites. From previous studies of plastic flow under such conditions,[6,7] it appears that the maximum plastic strain occurs at the tip of the indentation and varies inversely as a function of the cube of the radial distance. However, this relationship also depends on the size of the indentation; hence, the latter was standardized in the present work by adjusting the applied load in the Rockwell hardness machine to give impressions of 0.40 $\pm$ 0.2 mm diameter for the 0.80 carbon steel, and 0.48+0.02 mm for the 0.18 and 0.38 carbon steels. These indentation sizes were chosen to correspond to those obtained with the conventional Rockwell C test for the as-hardened 0.80 and 0.38 carbon steels, respectively.

Vickers microhardness tests (DPH) were carried out on polished and etched sections along traverses leading radially away from the brale indentations. Inasmuch as the maximum hardness invariably occurred near the indentation apex, most of the hardness readings were taken on surfaces carefully ground to a depth (below the original surface) where the indentation diameter tapered down to 0.10 - 0.14 mm. Unless otherwise specified, the microhardness readings reported in the following figures and tables were taken at this level below the original surface. Figure V-1 illustrates how the microhardness decreases with distance from the indentation edge, when measured at two levels below the original surface. Microhardness determinations on sections passing through the axis of the indentation indicated similar trends.

It was found that the Vickers hardness measurements were not sensitive to the state of residual stress around the brale indenta-

56

TABLE V-1

Composition of Steels

(Weight Percent)

Steel No.	C	Mn	Si	S	P
1	0.18	0.85	0.19	0.037	0.009
2	0.38	0.75	0.23	0.024	0.014
3	0.80	0.81	0.17	0.025	0.014
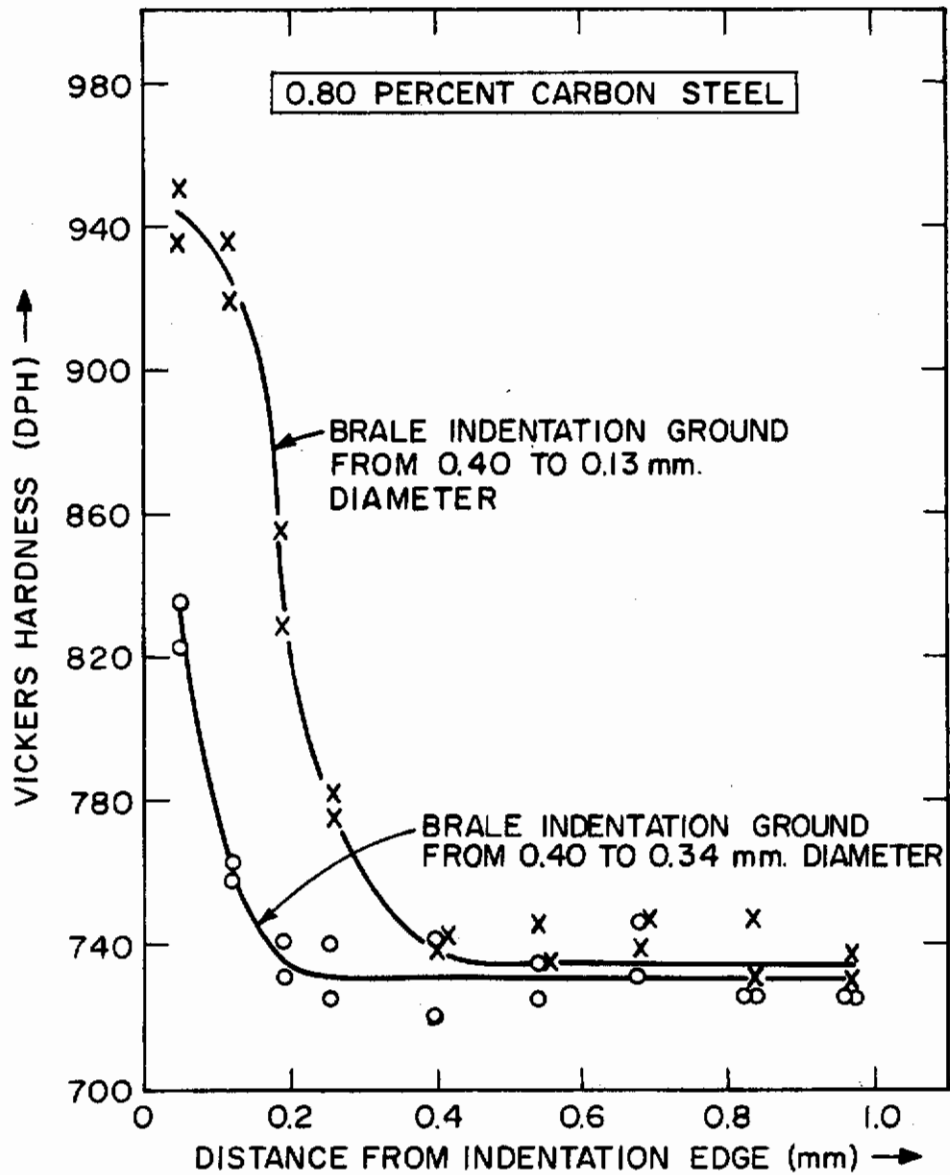
FIGURE V-I. VICKERS HARDNESS AT TWO LEVELS BELOW
THE ORIGINAL SURFACE IN STRAINED REGION NEAR BRALE
INDENTATION. QUENCHED MARTENSITE, INDENTED, THEN
TEMPERED AT 200°C FOR 1 HOUR.

tion, in contrast to Knoop hardness measurements.[8] Hence, the Vickers readings were relied on for the present purposes. In some instances, it was only necessary to deal with the maximum effects occurring near the apex of the indentation; in such cases, at least four Vickers hardness readings were averaged at 0.05 mm from the indentation edge.

3. <u>Electron Microscopy</u> - The electron microscopy involved rotary-shadowed replicas, carbide-extraction replicas, and thin-foil transmission specimens. Areas adjacent to, and far away from, the brale indentations were compared in this way. The rotary shadowing was deposited on collodion replicas stripped from specimens that had been etched with 2 percent nital containing zephiran chloride. Good results were obtained with chromium shadowing at an angle of 30°, and with silicon monoxide at 90°.

Carbide-extraction techniques for electron microscopy are well-known,[9-11] but the procedure described here proved to be especially appropriate for the extraction of epsilon carbide under the conditions at hand. After metallographic polishing, light etching, and repolishing with diamond paste, the specimen was heavily etched with 2 percent nital, rinsed in alcohol, and dried in a hot-air stream. The surface was then moistened with methyl acetate, and a strip of acetyl cellulose plastic applied. After drying, the strip, together with the adhering carbides, was removed and coated with a thin layer of evaporated carbon. The plastic strip was then dissolved away by the method of Jaffe.[12]

The Glenn- Raley technique[13] of electrothinning was used for preparing the transmission foils. Disc specimens 5/8-inch thick in diameter were wet ground to 3 - 4 mils thickness, the edges were lacquered, and the electrothinning was carried out in a chromic-acetic acid electrolyte until several holes appeared. The holes were allowed to grow until the remaining bridges between adjacent holes could be cut out for electron microscopy. These pieces were cleaned in ethyl alcohol, and examined at 100 kilovolts in a Siemens Elmiskop I.

C. <u>Experimental Results</u>

1. <u>Undeformed Martensites</u> - The tempering behavior of the 0.18, 0.38, and 0.80 percent carbon martensites was first studied in the undeformed condition to provide a basis for later comparisons with the strain-tempered martensites. The as-quenched structures exhibited twinning (Figure V-2) in some of the martensitic plates of the 0.38 and 0.80 carbon steels in agreement with previous work.[14] However, the 0.18 carbon martensite contained only dislocation networks.

Figure V-3 shows the hardness variation with tempering temperature for these materials. As expected, increasing the carbon content raised the as-quenched and tempered hardness. At 100°C, the hardness of the 0.80 carbon steel increased slightly due to precipitation of epsilon carbide during the first stage of tempering.[15] Although epsilon carbide could not be extracted at this low temperature, this was possible after tempering at 150, 200, and 250°C. The

0.5 μ

FIGURE V-2.   Internally Twinned Martensite in 0.38 Percent
Carbon Steel.   40,000X
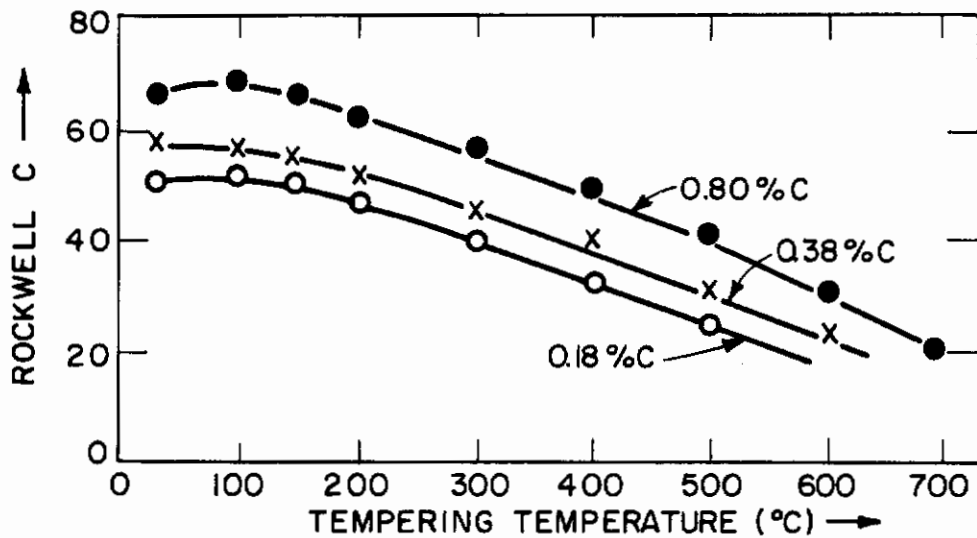
FIGURE V-3 HARDNESS OF THREE CARBON STEELS AS A
FUNCTION OF TEMPERING FOR I HOUR AT INDICATED TEMPERATURES.

TABLE V-2

Electron Diffraction of Epsilon Carbide Extracted from Martensite in 0.80 Percent Carbon Steel*

Indices	Present Results		Results of Jack(16)		Results of Hofer(18)	
	Observed Spacings** kX	Intensity***	Observed Spacings kX	Intensity	Observed Spacings kX	Intensity
10.0	2.39	w	2.40	m	2.38	w
00.2	not observed		2.15	vw	2.16	m
10.1	2.08	vs	masked by α and γ reflections		2.08	vs
10.2	1.60	s	1.60	ms	1.60	m
11.0	1.38	s	1.36	w	1.37	m
10.3	1.23	s	1.23	m	1.24	m
20.1	1.16	s				
20.2	1.05	w				
21.0	0.92	w				

* Tempered at 200°C for one hour. Epsilon carbide extracted from the 0.38 carbon steel gave similar results. This carbide could also be extracted from the 0.18 carbon steel, but the electron-diffraction lines were faint and indistinct.

** The spacings observed here agree closely with those calculated from a hexagonal close-packed unit cell of dimensions a = 2.729 kX and c = 4.326 kX, as given by Jack(16).

*** vw = very weak, w = weak, m = moderate, ms = moderately strong, s = strong, and vs = very strong.

$\overline{\text{0. 25}\mu}$
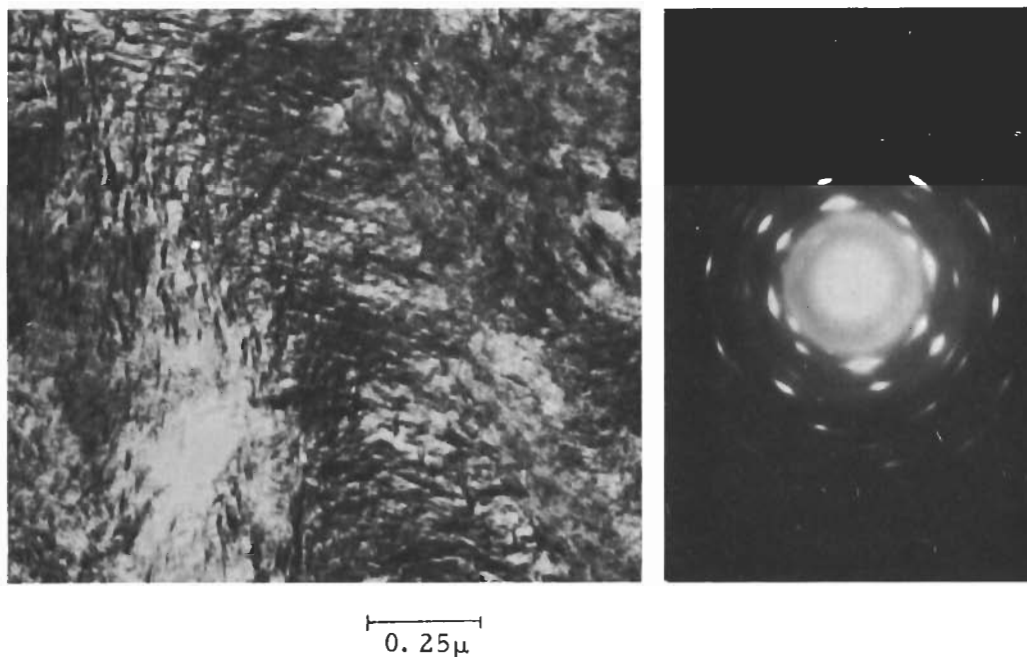
FIGURE V-4. Replica-Extraction of Epsilon Carbide from
0. 80 Percent Carbon Martensite, Tempered
at 200° C for One Hour.   60, 000X

63

Epsilon Carbide   0.5 μ

FIGURE V-5.   Replica-Extraction of Epsilon Carbide and
Cementite from 0.80 Percent Carbon Martensite,
Tempered at 250° C for One Hour.   40,000X

64

TABLE V-3

Diffraction of Cementite in Tempered Martensite

Present Results (Electron Diffraction on Extracted Carbides)		Jack's [16] Results (X-ray Diffraction Without Extraction of Carbides)	
Observed Spacings kX	Intensity*	Observed Spacings kX	Intensity*
2.50	w	2.51	m
2.38	m	2.38	m
		2.26	m
2.21	m	2.20	m
2.09	s	2.10	w
		2.06	ms
2.03	vs	2.04 - 2.00	$(110_{\alpha Fe})$
		1.97	m
1.68	w	1.68	vw
1.59	ms	1.57	s
1.53	m	1.53 - 1.52	vw
1.40	m	1.44 - 1.42	$(200_{\alpha Fe})$
1.36	w	1.34 - 1.32	m
1.23	s	1.22 - 1.21	vs
1.17	ms	1.18 - 1.16	$(211_{\alpha Fe})$
1.13	m	1.13 - 1.12	vs
1.11	ms	1.11 - 1.10	s
		1.09	mw
1.05	w	1.02 - 1.01	$(220_{\alpha Fe})$
0.994	m		

* vw = very weak, w = weak, m = moderate, ms = moderately strong, s = strong, vs = very strong

epsilon-carbide diffraction spacings are listed in Table V-2, and agree closely with existing data.[16-18] After tempering for 1 hour at 150°C, the extracted epsilon carbide was rather dendritic in form, but holding for 10 hours at 150°C or 1 hour at 200°C produced platelike epsilon carbide with moderately sharp diffraction spots (Figure V-4). The fourfold symmetry of the spots will be discussed later.

On further tempering these steels to 250°C, the drop in hardness corresponded with the formation of cementite. This phase gave many more diffraction spots than the epsilon carbide, and was easily recognized in the carbide-extraction replicas. An example of the two types of carbide coexisting in the 0.80 carbon steel tempered for 1 hour at 250°C is shown in Figure V-5. The electron-diffraction lines obtained from cementite are listed in Table V-3 along with Jack's x-ray results[16] on cementite in tempered steel.

The structural changes in the 0.80 carbon steel due to tempering between 200° and 700°C are illustrated in Figure V-6. Thin, irregular plates of epsilon carbide emerged after tempering for 1 hour at 200°C, intersecting the surface at many angles. Considerable pitting of the carbide was noted at this stage. On tempering at 300°C, cementite became the dominant carbide at the expense of the epsilon carbide, and took the form of platelets lying both along martensitic boundaries and within the martensitic grains. After tempering at 500°C, thick cementite plates were found preferentially at the prior martensitic boundaries, most of the cementite particles within the martensitic grains having dissolved. Upon tempering at 700°C, this process of cementite coalescence developed further, leaving massive oval-shaped particles along the ferritic boundaries. At this point, the ferritic grains were still elongated in configuration, although somewhat coarsened compared to the acicular structure of the original martensite.

Among the three steels studied, there were two notable differences in the structural changes on tempering. The amount of epsilon carbide in the 0.18 percent carbon steel appeared to be quite minor compared to that in the two higher-carbon martensites, and spherodization of the cementite occurred more slowly (maintaining an elongated form) in the 0.80 carbon steel than in the two lower-carbon materials.

2. <u>Deformed Martensites</u> – The brale-indentation method adopted here for deforming the martensite made it possible to impose large plastic strains despite the attendant brittleness. The resulting strainhardening of the 0.80 carbon martensite, pretempered at various temperatures before the indentation straining, is summarized in Figure V-7. For all such pretempers, the hardness was highest near the indentation edge,* and decreased with increasing radial distance until the hardness level of the undeformed matrix was reached. The greatest degree of strain hardening was noted in the as-quenched martensite.

---

* Note that the microhardness data given in this and subsequent figures were taken on sections ground below the original specimen surface, as described in the section on Experimental Details.

20,000×   A.   200° C   1μ   20,000×   B.   300° C   1μ

20,000×   C.   500° C   1μ   10,000×   D.   700° C   2μ
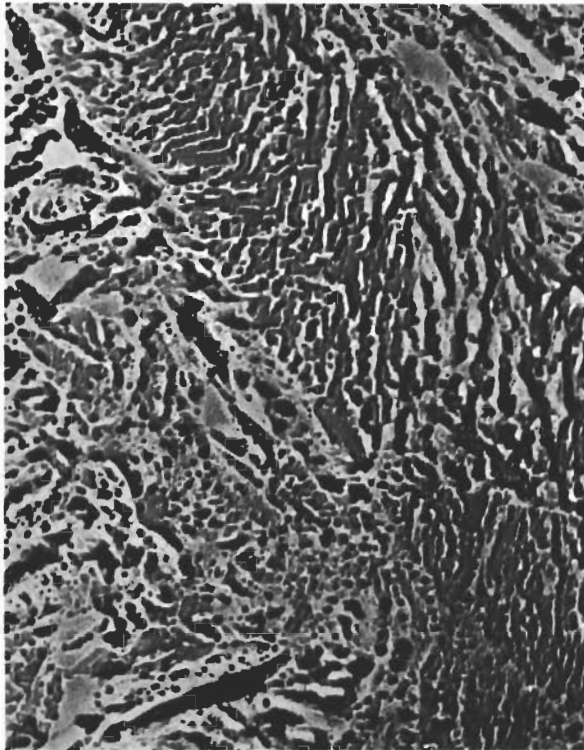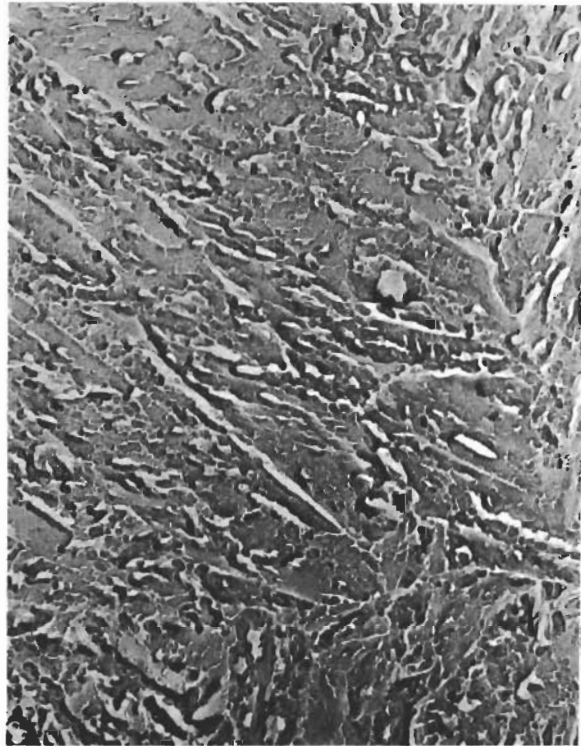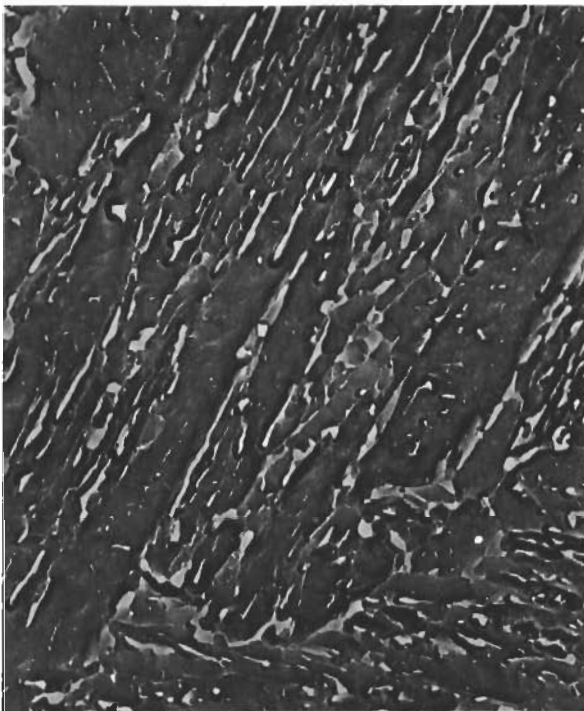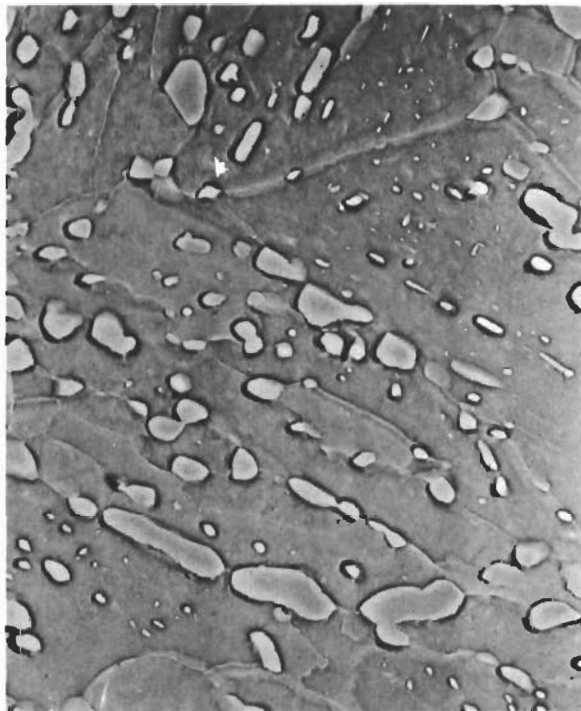
FIGURE V-6.   Electron-Replica Micrographs of 0.80 Percent Carbon
               Martensite, Tempered at Indicated Temperatures for
               One Hour.   Rotary Shadowed.   Modified Nital Etch.

67
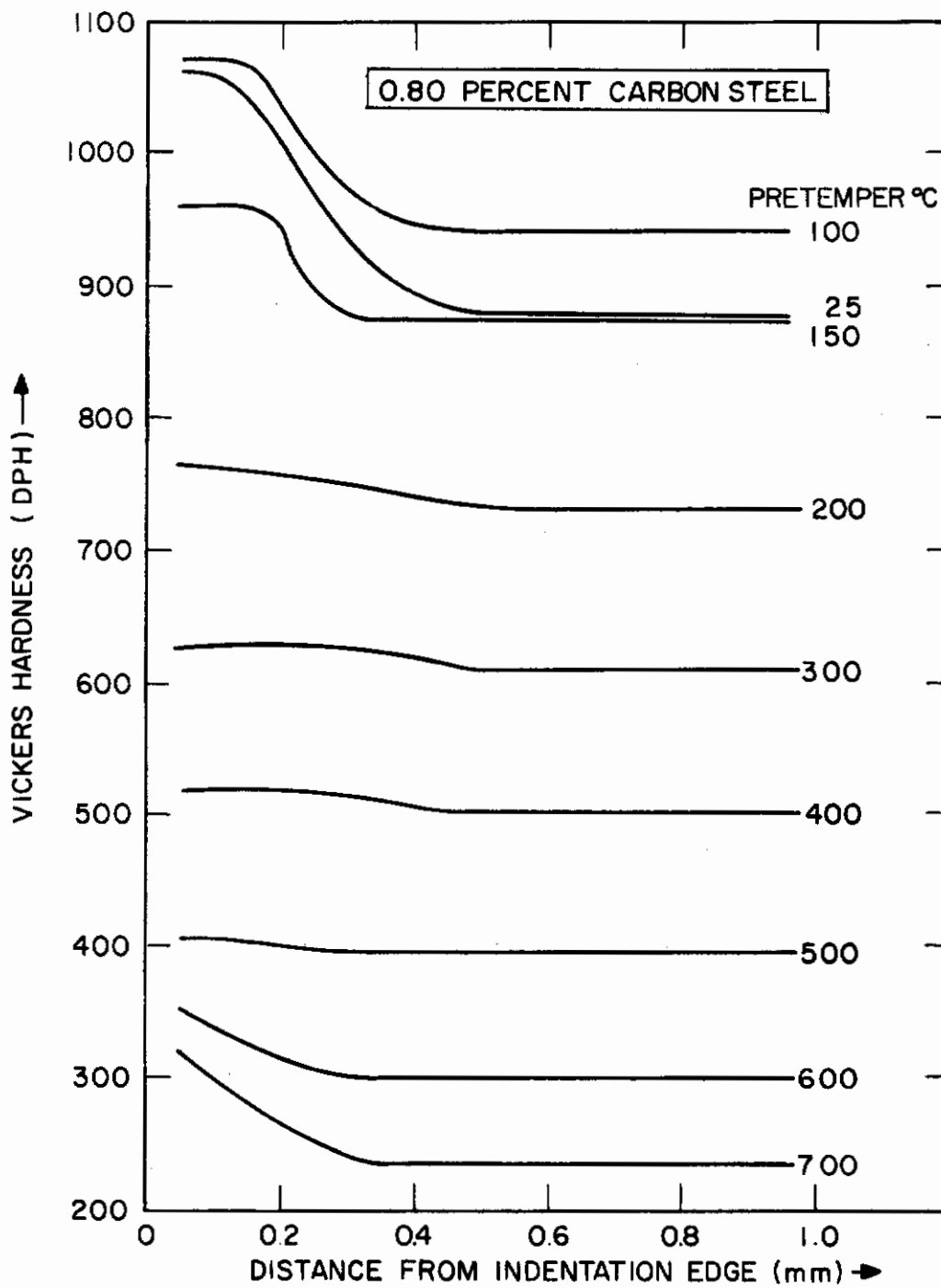
FIGURE V-7. EFFECT OF STRAIN HARDENING BY BRALE INDENTATION
OF 0.80 PERCENT CARBON MARTENSITE, TEMPERED FOR 1 HOUR AT
INDICATED TEMPERATURES PRIOR TO INDENTATION.
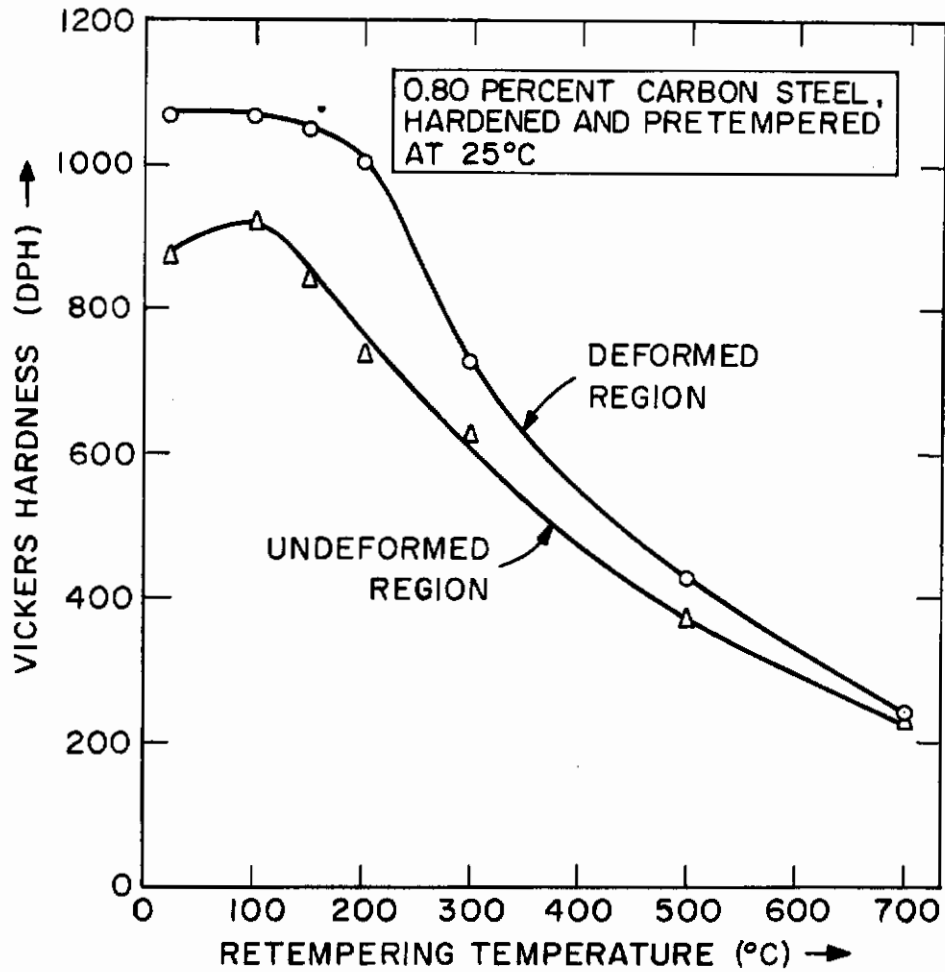
FIGURE V-8. HARDNESS OF DEFORMED (AT 0.05 mm FROM BRALE INDENTATION EDGE) AND UNDEFORMED REGIONS IN 0.80 PERCENT CARBON STEEL AS A FUNCTION OF RETEMPERING FOR I HOUR AT INDICATED TEMPERATURES.
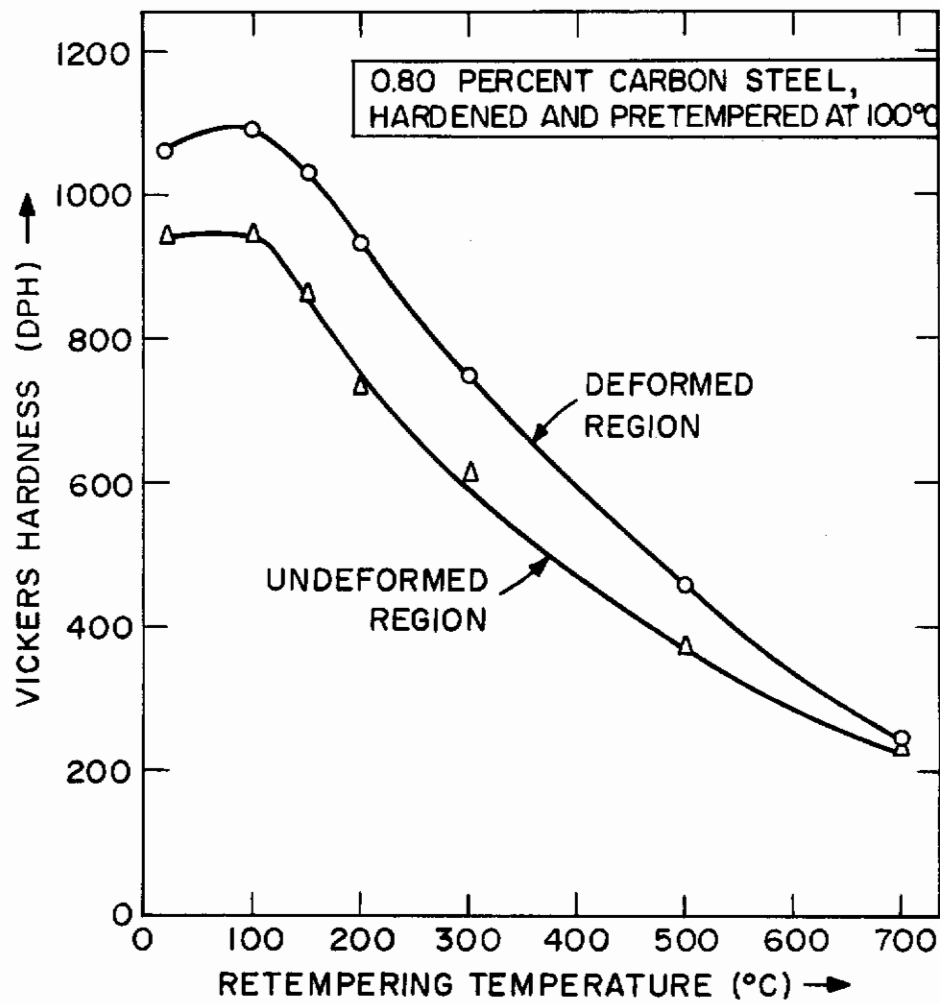
FIGURE Ⅴ-9   HARDNESS OF DEFORMED (AT 0.05 mm FROM BRALE INDENTATION EDGE) AND UNDEFORMED REGIONS IN 0.80 PERCENT CARBON STEEL AS A FUNCTION OF RETEMPERING FOR I HOUR AT INDICATED TEMPERATURES.
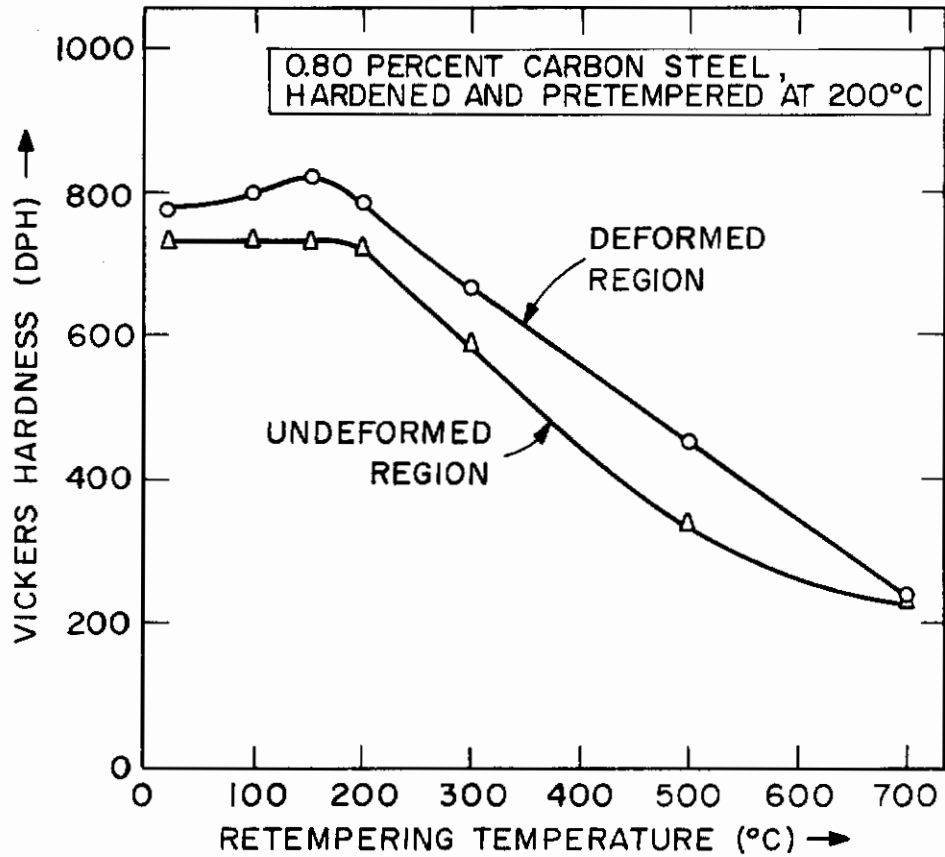
FIGURE Ⅴ-10. HARDNESS OF DEFORMED (AT 0.05 mm FROM BRALE INDENTATION EDGE) AND UNDEFORMED REGIONS IN 0.80 PERCENT CARBON STEEL AS A FUNCTION OF RETEMPERING FOR 1 HOUR AT INDICATED TEMPERATURES.

71

Remarkably little strain hardening was observed after pretempering in the range of 200 - 500°C. Yet, after pretempering at 600°C and 700°C, the strain hardening became appreciable again.

To describe the hardness change taking place on retempering *after* the above plastic straining (this combined process being the same as strain tempering), it is convenient to divide the pretempering into two temperature ranges according to whether epsilon or cementite is the predominant carbide formed prior to the strain tempering. Also, to emphasize the underlying phenomena, only the regions of maximum deformation near the rim of the brale indentations have to be compared with the unformed regions farther away, as is done in Figures V-8 to 10. This short-cut makes it unnecessary to plot the type of hardness-gradient curves shown in Figure V-7.

For *pretempering* temperatures up to 200°C (see Figures V-8 to 10 for the 0.80 carbon steel), the deformed martensites generally maintained their increments of strain hardening on *retempering* up to 150° - 200°C. In fact, some further hardening often occurred within this low retempering range. Upon retempering above 200°C, the extra hardness of the deformed martensites diminished progressively, and vanished at about 700°C for the 0.80 carbon steel, at 600°C for the 0.38 carbon steel, and at 550°C for the 0.18 carbon steel. Hardness data for the latter two materials are listed in Table V-4. After tempering at 700°C, the deformed martensite in the lower-carbon steels actually became softer than the undeformed martensite.

In these strain-tempering experiments on martensites as-quenched or pretempered up to 200°C, important differences in the carbide-precipitation morphology took place, as compared to the normal tempering processes in undeformed martensites. The electron micrograph in Figure V-11 illustrates how the martensitic plates were distorted by the plastic straining near the brale indentations. Upon retempering, the martensite in such deformed regions tended to resist etching, in contrast with the regular dark-etching of the undeformed regions. This light-etching effect around the indentations, previously observed by Wilson,[3] was brought into highest contrast by tempering at 200°C after the plastic straining (Figure V-12). This phenomenon was noted to varying degrees in all three steels, but it was most conspicuous in the 0.80 carbon steel.

As mentioned earlier, epsilon carbide could be detected in the replica extractions after tempering the undeformed martensites at 150° - 250°C. Yet, when the martensites were pretempered at 100°C or below, and then indented and retempered at 200°C, practically no epsilon carbide could be found in the replica extractions of the light-etching regions. In another series of extractions, the specimens were pretempered at 150°C to produce epsilon carbide in appreciable amounts prior to the plastic straining; after retempering at 200°C, much less epsilon-carbide was detected in the light-etching zones than in the undeformed regions. Moreover, the diffraction patterns of the epsilon carbide were more diffuse in the deformed zones.

It was also found that the epsilon carbide generated during the pretempering operation could be made to disappear progressively by strain tempering. Several 0.80 carbon steel specimens were pretempered for 5 hours at 150°C, indented, and retempered for periods

72

TABLE V-4

Hardness of Strain-Tempered 0.18 and 0.38 Percent Carbon Martensites

Vickers Hardness, DPH

Retempering Temperature °C	As-quenched Prior to Brale Indentation				Pretempered at 700°C Prior to Brale Indentation			
	0.18 C Steel		0.38 C Steel		0.18 C Steel		0.38 C Steel	
	Undeformed	Deformed*	Undeformed	Deformed*	Undeformed	Deformed*	Undeformed	Deformed*
25	494	586	660	780	190	278	214	290
100	495	625	649	769	190	286	206	320
150	490	605	577	698	-	-	204	315
200	464	592	536	695	180	305	212	310
300	415	528	465	620	185	312	202	312
400	330	410	396	488	178	294	200	303
500	270	350	306	385	180	255	204	290
600	230	165	255	260	181	161	204	204
700	185	164	206	176	199	160	204	166

* Hardness of deformed martensites measured at 0.05 mm from the brale indentation edge.

73
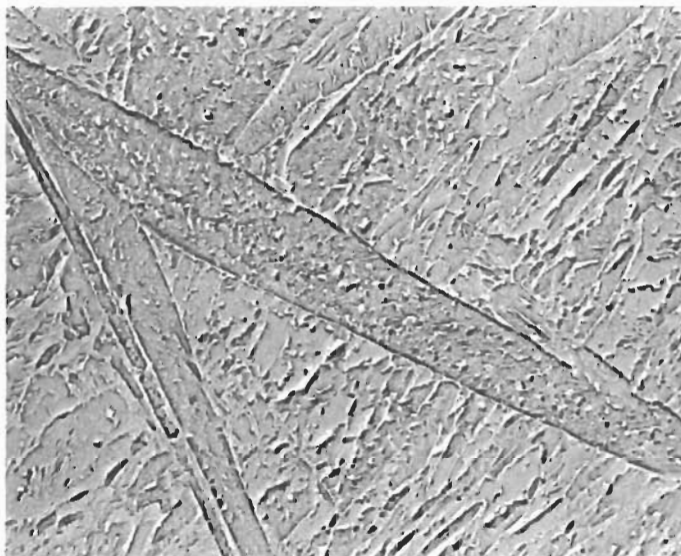
10,000×   A.   Undeformed |———| 1μ
                 Region

10,000×   B.   Deformed |———| 1μ
                 Region

FIGURE V-11.   Electron-Replica Micrographs of   0.38 Percent
               Carbon Martensite, Indented and Tempered at
               200° C for One Hour.   Rotary Shadowed.   Modified
               Nital Etch.
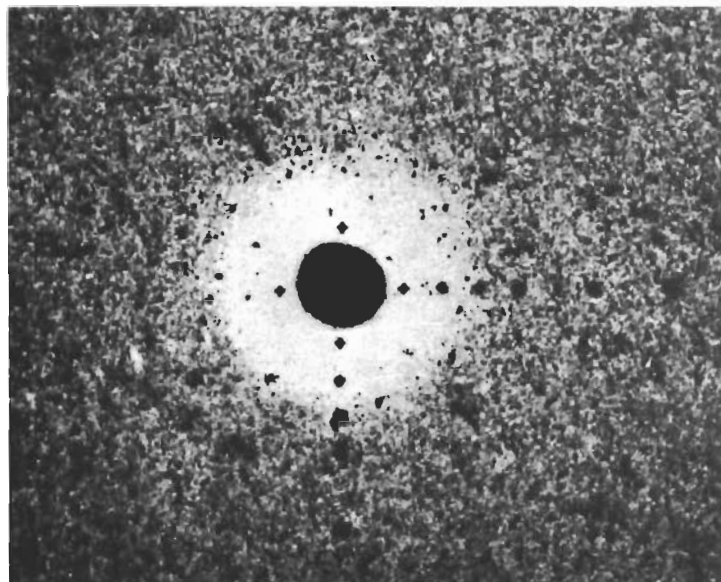
FIGURE V-12.   Light-Etching Region Around a Brale
Indentation in 0. 80 Percent Carbon Martensite,
Tempered at 200° C for One Hour after Indentation.
Modified Nital Etch.   75×

20,000×   A. 200° C   1μ   20,000×   B. 300° C   1μ

20,000×   C. 500° C   1μ   10,000×   D. 700° C   2μ
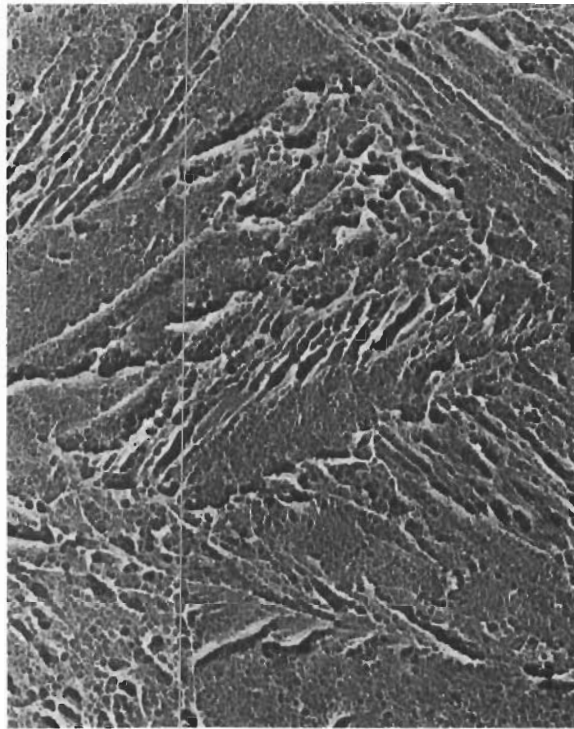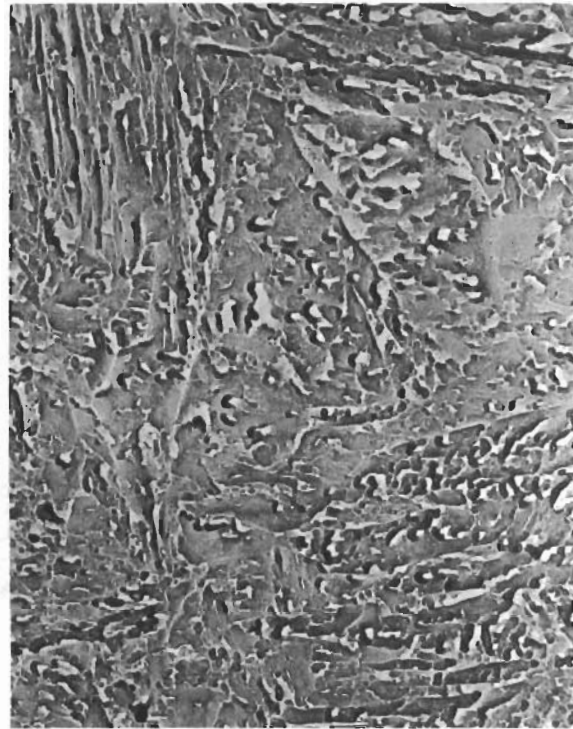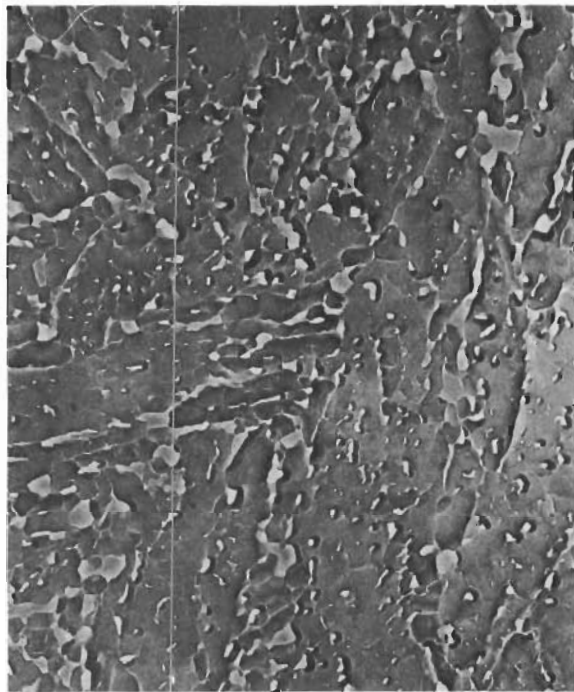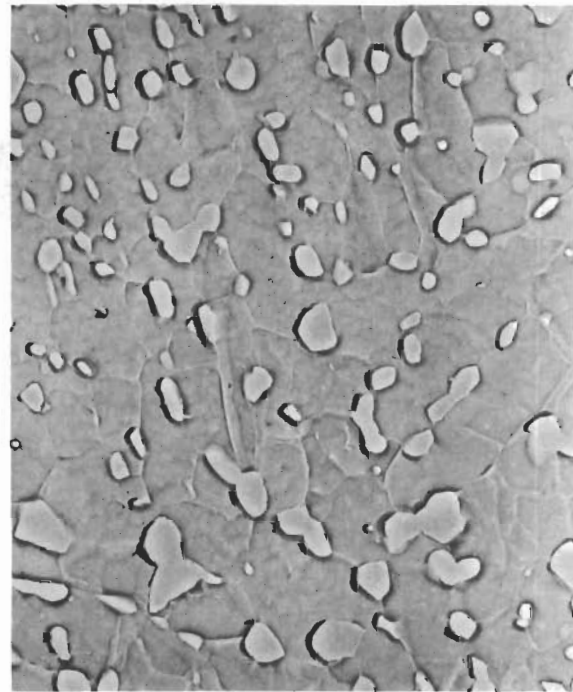
FIGURE V-13.   Electron-Replica Micrographs of 0.80 Carbon Martensite,
                Plastically Deformed by Brale Indentation, and Retempered
                at Indicated Temperatures for One Hour.   Rotary Shadowed.
                Modified Nital Etch.

76

up to 20 hours at 150°C. The light-etching zones were not initial-
ly present after the deformation, but developed as a function of
time during the retempering at 150°C. As before, virtually no epsi-
lon carbide could then be detected in the deformed and retempered
regions by the replica-extraction method.

On the other hand, when the pretempering was raised to 200°C,
the light-etching effect after subsequent deformation and retemper-
ing was less marked, and the corresponding reduction in epsilon car-
bide was smaller. Evidently the epsilon carbide formed during the
pretempering at 200°C became more stable than that formed at 150°C.

After pretempering in the first stage of tempering and then
plastic straining, as in the foregoing experiments, the first ex-
traction evidence of <u>cementite</u> precipitation during retempering was
obtained at 300°C, although the electron microscopy suggested ce-
mentite formation at 250°C. Figure V-13 presents a series of ro-
tary-shadowed electron micrographs of the 0.80 carbon steels after
such strain tempering, whereas Figure V-6 shows the corresponding
structures without the plastic straining, i.e., after regular tem-
pering. On strain tempering up to 200°C, the structures were es-
pecially pitted, giving the impression of carbide films, but as pre-
viously emphasized, no carbides could then be detected by extrac-
tion and diffraction methods. After retempering at 300°C, however,
cementite became clearly visible and identifiable, and there was rel-
atively little difference in the replica micrographs between the de-
formed and the undeformed regions (Figure V-13B vs V-6B). How-
ever, it was surprising to find that retempering at 500°C and 700°C
<u>did</u> cause a difference in structure between the deformed and unde-
formed regions. After the 500°C retemper, the cementite particles
were finely spheroidized in the deformed zones, but maintained an
elongated shape in the undeformed regions. In both cases, coales-
cence occurred on tempering at 700°C, but some difference in particle
shape persisted (Figure V-13D vs V-6D). At the same time, recrys-
tallization of the ferritic matrix took place in the deformed zones,
leading to equiaxed ferritic grains as compared to the acicular fer-
rite inherited from the martensite on regular tempering.

Unlike the 0.80 carbon steel, the 0.18 and 0.38 carbon steels
exhibited definitely less cementite in the deformed zones on strain
tempering at 300°C than during ordinary tempering. An example is
given in Figure V-14. However, the cementite particles were coarser
in the deformed zones than in the undeformed regions, and they sphe-
roidized more rapidly on further tempering.

We now consider further strain-tempering experiments in which
the pretempering was conducted at 300°, 500°, and 700° in order to
have cementite present <u>before</u> the plastic straining and subsequent
retempering. The associated hardness changes for the 0.80 carbon
steel are plotted in Figures V-15 to 17. While the general hard-
ness level decreased with increasing pretempering temperature in
this series, the degree of strain tempering became more pronounced
and resulted in an extended hardness plateau after the 500° and 700°C
pretempers. Data showing similar trends for the 0.18 and 0.38 car-
bon steels are given in Table V-4.

This hardening due to strain tempering when cementite was al-
ready present in the pretempered martensite took place at retemper-

A. Undeformed Region   B. Slightly Deformed   C. Highly Deformed
                             Region   Region
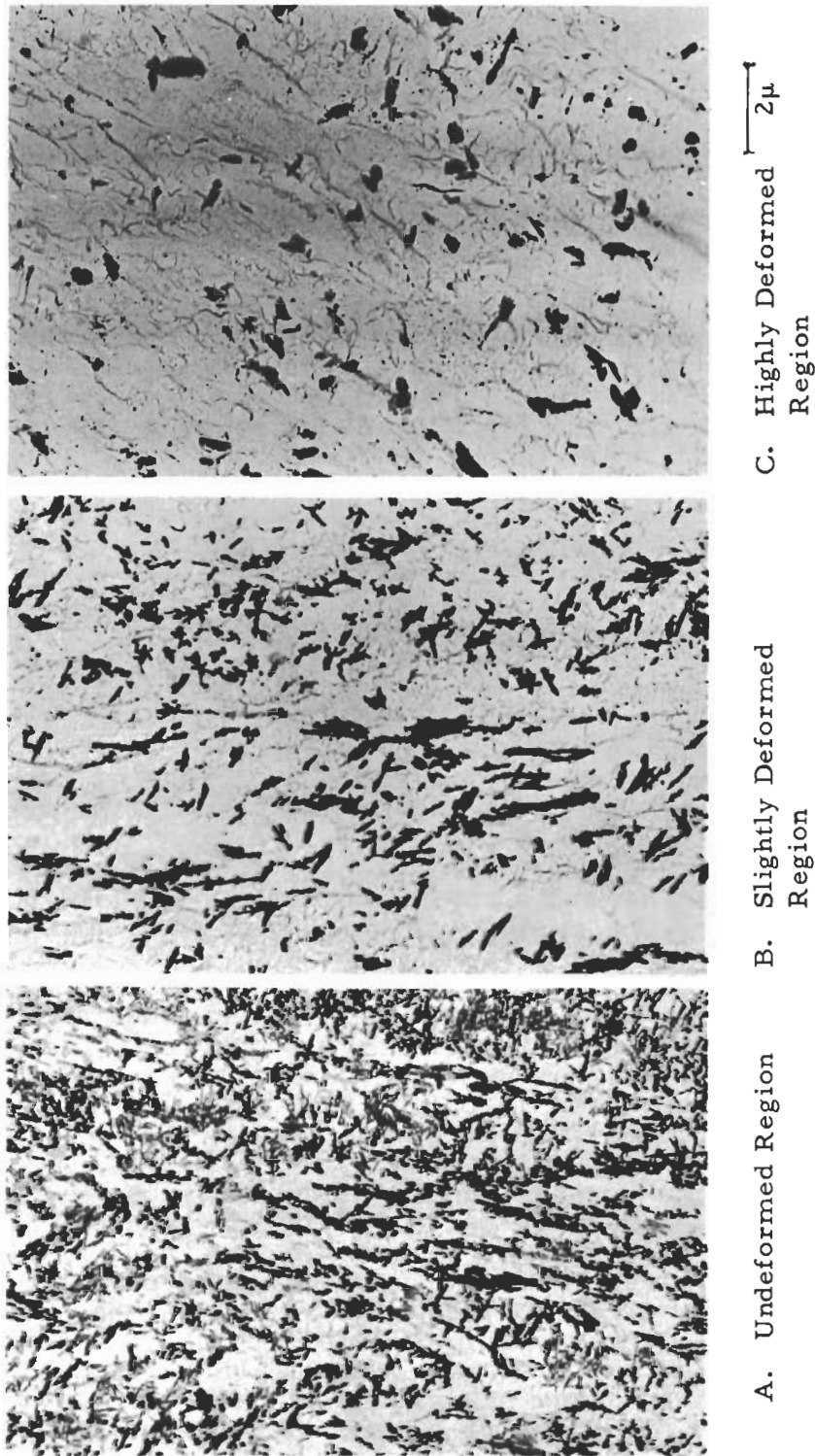
FIGURE V-14.   Cementite Particles in Carbide-Extraction Replicas of 0.18 Percent Carbon
Martensite, Plastically Strained by Brale Indentation, and Tempered at 300° C
for One Hour. 6,000X

78
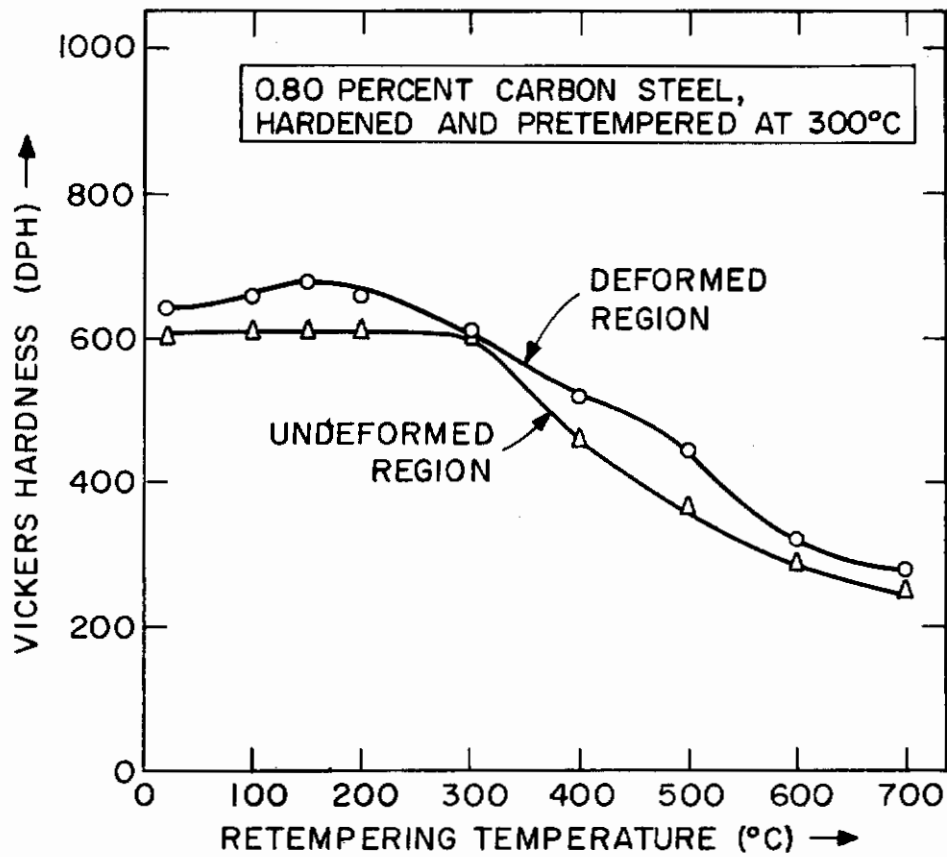
FIGURE V-15. HARDNESS OF DEFORMED (AT 0.05 mm FROM BRALE INDENTATION EDGE) AND UNDEFORMED REGIONS IN 0.80 PERCENT CARBON STEEL AS A FUNCTION OF RETEMPERING FOR 1 HOUR AT INDICATED TEMPERATURES.
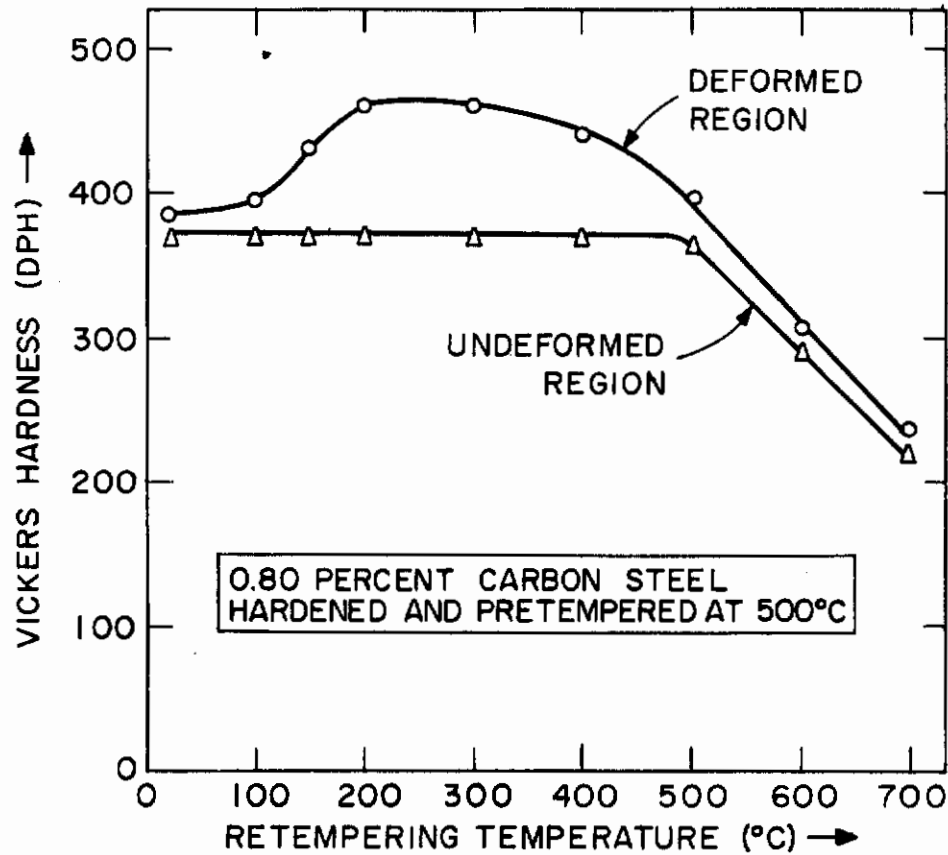
FIGURE V-16. HARDNESS OF DEFORMED (AT 0.05 mm
FROM BRALE INDENTATION EDGE) AND UNDEFORMED REGIONS
IN 0.80 PERCENT CARBON STEEL AS A FUNCTION OF
RETEMPERING FOR 1 HOUR AT INDICATED TEMPERATURES.
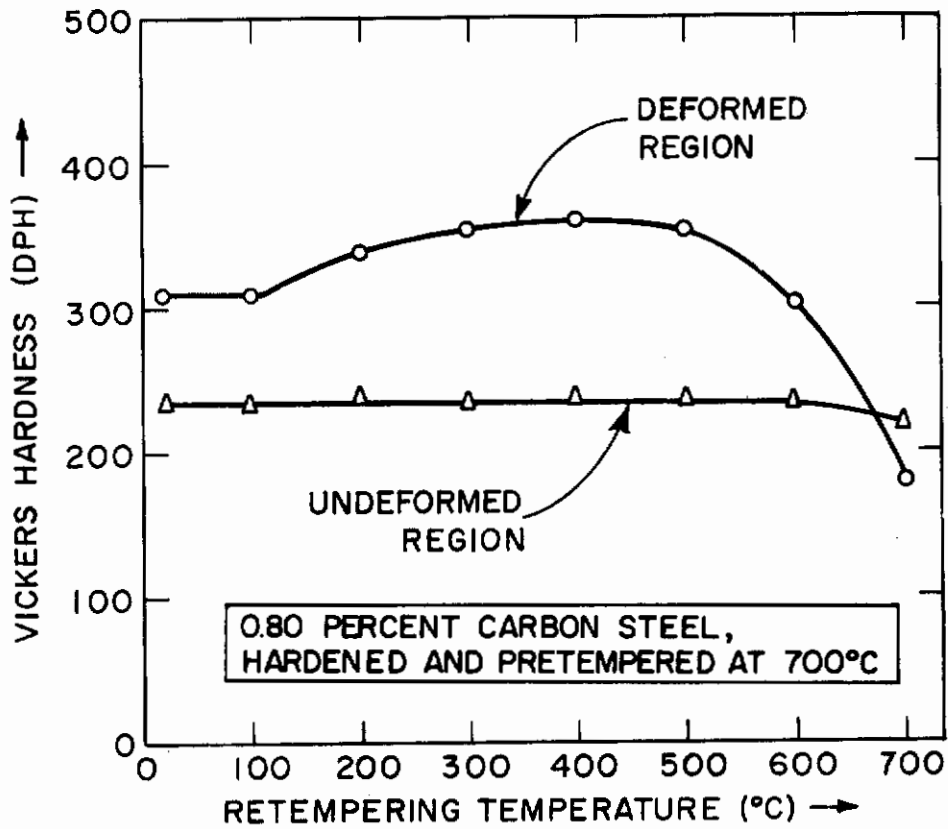
FIGURE V-17. HARDNESS OF DEFORMED (AT 0.05 mm FROM BRALE INDENTATION EDGE) AND UNDEFORMED REGIONS IN 0.80 PERCENT CARBON STEEL AS A FUNCTION OF RETEMPERING FOR I HOUR AT INDICATED TEMPERATURES.

81

A. Pretempered at 700° C.

0.5µ
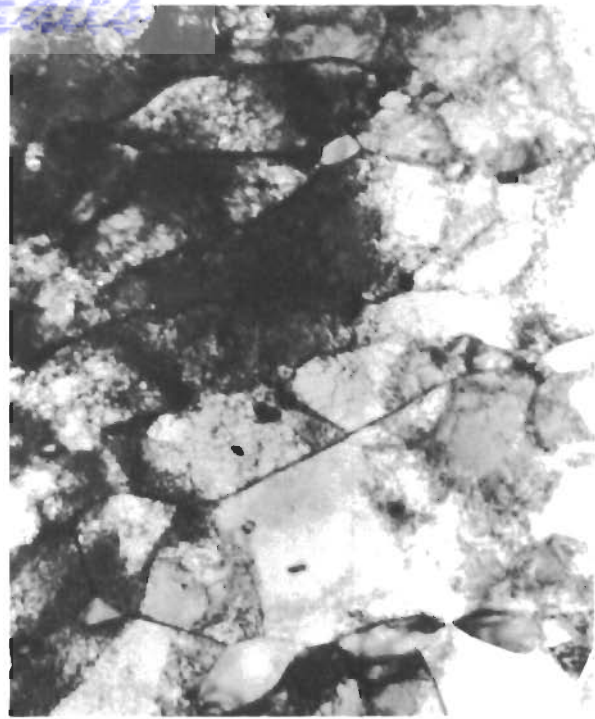
B. Pretempered and Deformed.

0.5µ
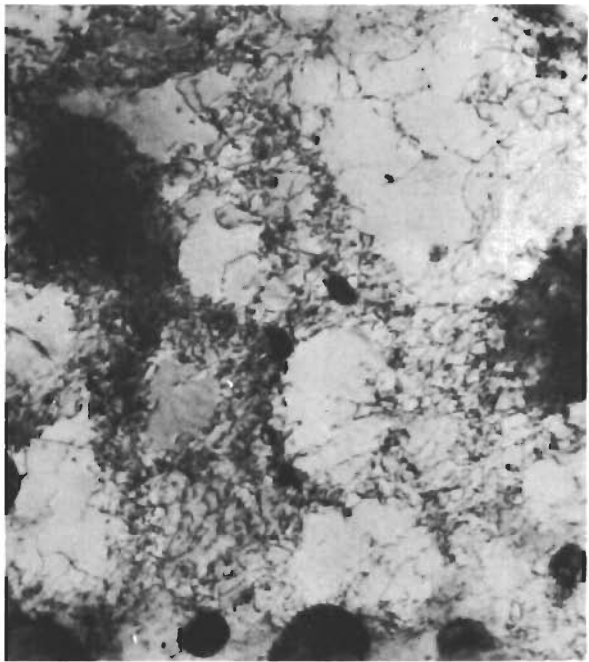
C. Pretempered, Deformed, and Retempered at 300° C.

0.25µ
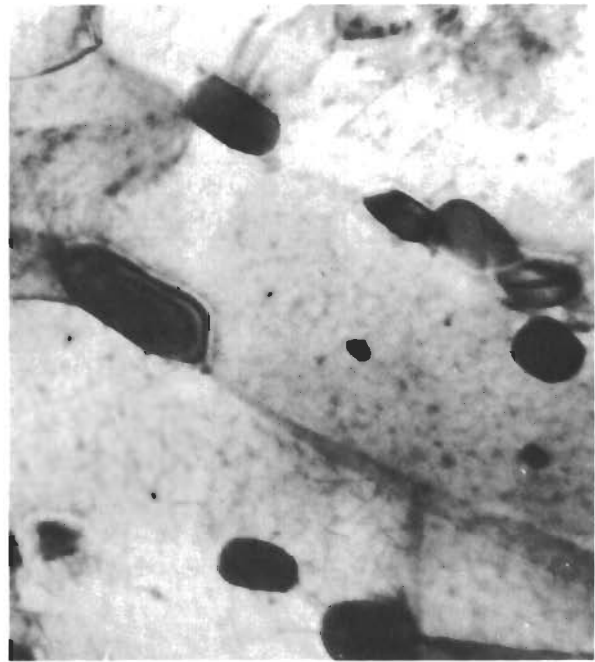
D. Pretempered, Deformed and Retempered at 700° C.

0.5µ

FIGURE V-18. Electron Transmission Micrographs of 0.38 Percent Carbon Steel, Hardened and Pretempered at 700° C before Plastic Straining and Retempering at Indicated Temperatures for One Hour.

82

ing temperatures <u>below</u> the pretempering temperature. An attempt was made to reveal the corresponding changes in microstructure. The replica-extraction technique showed only the cementite existing before the strain tempering. Also, point-counting[19] on replica electron micrographs disclosed no consistent change in the volume percent of cementite due to such strain tempering. Electron transmission metallography was then applied to the 0.38 carbon steel pretempered at 700°C. In this instance the plastic straining was accomplished by overlapping indentations of a Brinell ball before the retempering and electrothinning; this method of deformation was adopted to provide larger regions for electron transmission microscopy than could be obtained in the deformed rim around a brale indentation.

The results are shown in Figure V-18. The as-pretempered (700°C) structure (Figure V-18A) contained cementite particles lying mainly at grain boundaries; the ferritic grains were acicular in shape, and in some cases were separated from each other by low-angle dislocation-type boundaries. After the plastic deformation (Figure V-18B), dense arrays of dislocations appeared in the ferritic matrix, producing subgrains outlined by entangled dislocation networks and attended by the strain hardening indicated in Figure V-17. The further hardening caused by retempering at 300°C was accompanied (Figure V-18C) by some decrease in dislocation density and the precipitation of small particles along the remaining dislocations. In line with the strain-aging studies of Keh and Leslie,[20] this precipitate was judged to be cementite, but it could not be properly identified here because of the coarse cementite already present.

It appears that the carbon for this fine carbide precipitation resided in supersaturated solution in the ferritic matrix after the pretempering at 700°C, and that nucleation was promoted by the extra dislocations introduced in the plastic straining. Yet, the hardness increment due to the retempering at 300°C was independent of whether brine quenching or furnace cooling was employed after the 700°C pretemper. This signified that the degree of supersaturation required for the strain-tempering phenomenon was relatively small.

On raising the retempering temperature to 700°C in this series (Figure V-18D), the small carbides redissolved, the dislocation networks disappeared, and recrystallization of the ferrite matrix took place. In the 0.18 carbon steel, the recrystallization around the brale impression could be seen even at low magnifications (Figure V-19). Such recrystallization caused the hardness in the deformed regions to drop below that of the undeformed regions on retempering at 700°C, as shown by the cross-over in Figure V-17.

D. Discussion of Results

1. <u>Tempering Behavior of Undeformed Martensites</u> - The three stages of tempering in plain-carbon steels have received the attention of many investigators.[21-23] The present work is directed primarily to the formation of epsilon carbide and cementite, the maximum amount of retained austenite being always less than 10 percent. Thus, the second stage of tempering (involving the conver-
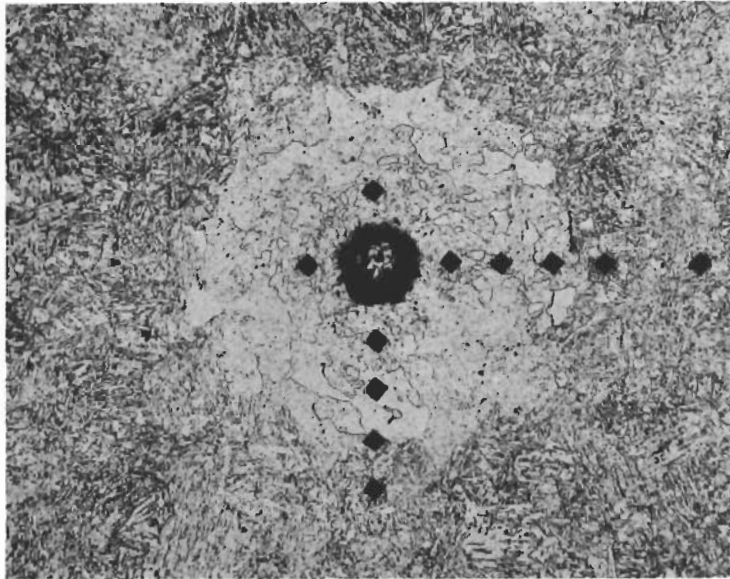
FIGURE V-19.   Recrystallization in the Strained Region Around
a Brale Indentation in 0. 18 Percent Carbon
Martensite Pretempered at 700° C, Indented,
and Retempered at 700° C for One Hour.
Modified Nital Etch.   100×

84

sion of retained austenite to bainite) is not an important factor here.

Epsilon carbide precipitates from the as-quenched martensite on tempering up to 200°C (1 hour), but the replica extraction of this carbide was successful only at 150°C and above. Notwithstanding the recognized difficulties in this technique, the following observations seem pertinent. (a) The structure of epsilon carbide precipitated at low-tempering temperatures appears to be dendritic with interlocking arms. (b) Additional tempering converts this carbide into a platelike structure. (c) The electron diffraction patterns for such plates are sharp, and are consistent with the known orientation relationship of $(10.1)_\epsilon \| (101)_M$, $(00.1)_\epsilon \| (011)_M$ [16] and $\{100\}_M$ as the habit plane. [24,25] Fisher[9] has interpreted the previously mentioned four-fold symmetry as an indication that epsilon carbide lies with its (10.0) planes parallel to the four (101) planes of the parent martensite.

Although the precipitation of epsilon carbide is basically a strengthening process, softening sets in toward the end of the first stage of tempering because of carbide coalescence. This softening continues with the formation of cementite in the third stage of tempering. At tempering temperatures above 300°C, the cementite becomes coarse enough for some quantitative electron microscopy on the intercarbide spacings, whereas this approach was not at all feasible with the epsilon-carbide structures. On the assumption that hardness and yield strength reflect approximately the same dependence on the microstructural parameters, [26] Orowan's model [27] of dispersion strengthening gives:

$$H = H_{matrix} + \frac{cGb}{\lambda} \qquad\qquad (V-1)$$

where H = hardness of steel

H_{matrix} = hardness of matrix

c = a constant

G = shear modulus

b = Burgers vector of a glide dislocation

λ is often regarded as the mean free distance between particles, [28] but Tyson[29] has suggested that λ is more properly defined as the mean distance between nearest-neighbor particles in a slip plane because this is the spacing parameter that a moving dislocation "sees." Measurements of λ were carried out for the 0.8 percent carbon steel, according to the method of Tyson, [29] and the results are plotted in Figure V-20 as a function of $1/\lambda$. The straightline relationship observed for the hardness data corresponds to a tempering range of 300° to 600°C. Over this range, the slope is about the same as that found by Tyson for the yield-strength variation with $1/\lambda$.
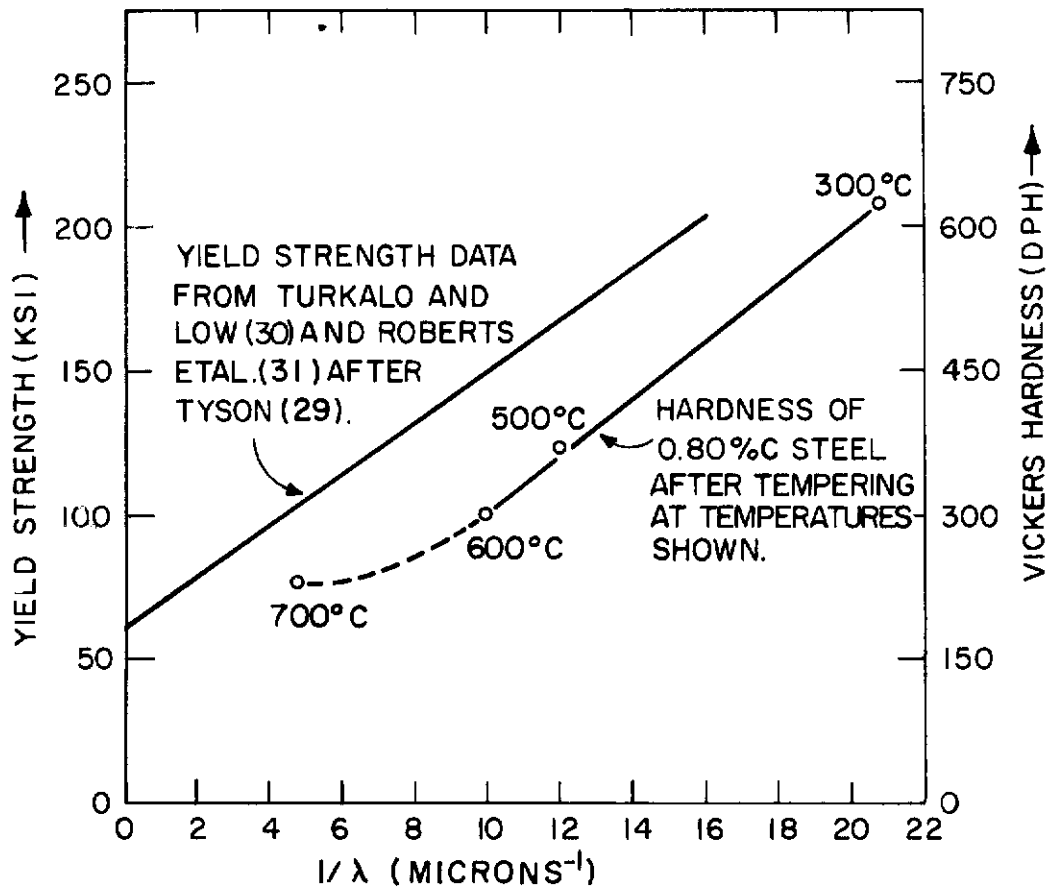
FIGURE V-20 VARIATION OF HARDNESS WITH INVERSE OF MEAN DISTANCE BETWEEN NEAREST-NEIGHBOR CARBIDES IN 0.80 PERCENT CARBON STEEL. YIELD STRENGTH DATA FOR TEMPERED STEELS ARE INCLUDED (AFTER TYSON).

86

Despite this correlation which seems to support a simple dispersion-strengthening hypothesis for the highly tempered steels, it should be emphasized that carbon-depletion of the matrix occurs as the tempering proceeds, and hence the matrix hardness is not held constant while the carbide distribution is changing. This may explain why the 700°C hardness point in Figure V-20 lies above the linear trend displayed between 300° and 600°C. Furthermore, the cementite distribution is by no means random, as called for by the simple theory. And, finally, in the strain-tempered martensites, correlations with the carbide spacings of the type shown in Figure V-20 are not obtained because of the concommitant changes in dislocation density as the intercarbide spacings are varied.

2. <u>Tempering Behavior of Deformed Martensites</u> - It is evident that significant increments of hardening can be developed by the strain tempering of as-quenched or low-tempered martensites. The resulting hardness gain may be reflected either by an increase in hardness on retempering, over that contributed by the deformation process itself, or by retarded softening on retempering compared to that shown by undeformed martensite during tempering. The maximum degree of strain tempering takes place when the retempering temperature is no higher than about 200°C, and is not sensitive to the carbon content. At higher temperatures the hardness increment of the strain-tempered material above that achieved by regular tempering decreases gradually, and actually becomes negative when recrystallization of the deformed matrix occurs.

As proposed by Wilson,[3] the most striking hardness changes associated with the strain-tempering process are related to the light-etching phenomenon observed after the plastic straining of as-quenched or low-tempered martensites and retempering at about 200°C. The fact that epsilon-carbide precipitation is inhibited, or that particles of this carbide may even be dissolved if already present, indicates strongly that the plastic straining provides relatively stable traps for the carbon atoms. Indeed, these traps must constitute higher-affinity sites for the carbon than does the epsilon-carbide structure. It is likely that both dislocations and lattice vacancies are important in this respect, as will now be discussed.

The interaction of carbon atoms with dislocations in ferrite has received much attention.[2,32-34] It is generally agreed that the stress fields around edge or screw dislocations can accommodate the carbon atoms in preferred interstitial sites in the BCC[34] or BCT[2] unit cell. For example, an edge dislocation on a (110) slip plane with the half-plane extending in the [001] direction has associated tensile stresses which favor the location of carbon atoms in interstitial sites between the [010] or [100] cube edges.[2]

There are two obvious conditions which must be fulfilled to account for the presence of carbon atoms at dislocations instead of in the epsilon-carbide structure. First, a sufficient number of dislocations must be available, and second, the binding energy of the carbon atoms to dislocations must be greater than to the epsilon carbide. There are 3.1×10^{21} carbon atoms in one cubic centimeter of the 0.8 carbon steel. Making allowance for the low-carbon martensite (~ 0.2 percent carbon) which can normally coexist with epsilon carbide, this means that up to 2.5×10^{21} carbon atoms/cm^3 must be trapped by dislocations if epsilon carbide is to be inhibited

from precipitating. Even for an extremely high dislocation density of $10^{12}/cm^2$, there would have to be some 70 carbon atoms trapped per atomic plane of iron.

If the carbon atoms could arrange themselves in such atmospheres around the dislocations, the strength of the martensite would be substantially raised because of dislocation locking, and the extra hardness on strain tempering could be accounted for. However, it is not likely that the precipitation of epsilon carbon would be greatly retarded thereby. The binding energy between a carbon atom and a dislocation is about 0.5 eV[35] but this applies only when the carbon atom is very close to the dislocation core; all the other carbon atoms in the atmosphere experience much weaker interactions[36] which are probably smaller than the binding energy of carbon in epsilon carbide (~ 0.27 eV). The latter value was obtained by Arndt and Damask[37] for the low-temperature carbide which precipitates from supersaturated ferrite.

Perhaps a more realistic picture is one in which the carbon atoms migrate along dislocations and cluster at special sites, such as jogs or kinks. In fact, Phillips[34] has found evidence of carbon clusters on aging an 0.015 percent carbon ferrite. This configuration could also lock dislocations quite effectively for strengthening purposes but there would then be not nearly enough of such carbon traps to explain the inhibition or absence of epsilon-carbide formation during the first stage of strain tempering.

An alternate viewpoint is that carbon atoms may be trapped in lattice vacancies produced by the plastic straining of the martensite. This situation would be rather analogous to the vacancy production in supersaturated ferrite (0.015 percent carbon) by neutron irradiation, as described by Damask et al.[37-39] In the latter work it was concluded that carbon atoms are trapped in the (iron-atom) vacancies with a binding energy of 0.41 eV, which represents a more stable state for the carbon than does the first carbide (binding energy = 0.27 eV) that precipitates during ordinary aging. On the other hand, the carbon is still more stable in cementite, the binding energy then being (according to various investigators) 0.42 eV[40], 0.52 eV[41] or 0.89 eV[42]. Thus, the existence of carbon-atom/vacancy complexes in deformed martensite is a real possibility, and their relative stability could nicely explain the reduced tendency for epsilon-carbide formation during strain tempering.

Due to the lack of experimental data on vacancy generation by plastic deformation, it is difficult to estimate the number of vacancies that might be expected in deformed martensite. Seitz[43] and Cottrell[44] have proposed deformation mechanisms of vacancy production, and van Bueren[45] has used Seitz's model to compute the number of vacancies in deformed copper, as follows: for 1 percent plastic strain, $10^{19}/cm^3$; for 10 percent, $10^{20}/cm^3$; and for 100 percent, $10^{21}/cm^3$. With the brale indentation used here, perhaps 10-50 percent plastic strain is a reasonable range in the light-etching rim. Consequently, $10^{20} - 10^{21}/cm^3$ vacancies may be present if the numbers can be carried over to martensite. A different approach to such es-

timates is to assume that some fraction (~ 2 percent) of the mechanical work expended in the indentation process remains stored in the martensite as vacancies. This calculation gives 3×10^{20} vacancies/cm^3. Such values are within an order of magnitude of the 2.5×10^{21}/cm^3 carbon atoms which must be trapped to suppress epsilon-carbide formation.

From geometrical considerations of this problem it is possible to fill the iron-atom vacancy with not one but two carbon atoms and still obtain a reduction in strain energy relative to the as-quenched interstitial state of the carbon atoms. Figure V-21 illustrates the trapping of two carbon atoms in an iron vacancy in BCT martensite. Considering the carbon and iron atoms to be hard spheres of 2.478 and 1.410 kX[46] respectively, the lattice parameters of the resulting cell can be calculated by minimizing strain energy in terms of the angle θ. This gives the parameters of the hypothetical cell as c = 2.718 and a = 2.589 kX, compared to a_o = 2.861 kX for the lattice parameter of BCC iron. Although this hard-sphere approximation is quite crude, it does indicate that two carbon atoms can reside in an iron-atom vacancy without requiring severe distortion of the iron unit cell, and the tetragonal symmetry of the as-quenched martensite is still preserved. If such a model is operative in the 0.8 carbon steel, about 6×10^{20}/cm^3 carbon atoms can be trapped by vacancies, which is within a factor of four of that required. The balance of the carbon atoms could certainly be accommodated as clusters around dislocations. In fact, the latter traps could more than make up for any overestimates in the vacancy concentrations deduced here.

As suggested earlier, the existence of carbon-atom/vacancy complexes offers a possible explanation for the inhibition of epsilon-carbide precipitation on strain-tempering. In the extreme case, there would then be no driving force for the precipitation of epsilon carbide because the lattice vacancies, once produced by external means, would provide more stable sites for the carbon atoms than does the epsilon carbide. However, such trapping should result in lower strain fields around the complexes than around the original interstitial carbon atoms in the as-quenched martensite, and consequently, any such change in carbon position during strain tempering could not be regarded as a strengthening mechanism. The strengthening would seem to arise mainly from dislocation arrays generated by the plastic deformation, and their subsequent locking at strategic points by carbon clusters. This state of affairs could persist on retempering to 200°C because carbon-depletion is retarded through the suppression of epsilon-carbide formation.

When the strain tempering is carried to 250°C or above, cementite precipitates, the carbon now being more stable in this carbide than in the vacancy traps. Nevertheless, the driving force for cementite nucleation is now smaller than in the case of normal tempering where the epsilon carbide of the first stage is converted into cementite during the third stage. This explains why, at least in the 0.18 and 0.38 carbon steels, fewer cementite particles nucleate (at 300°C) in the deformed martensite than in the undeformed martensite. In addition, spheroidization of the cementite proceeds more rapidly in the deformed than in the undeformed regions; this could

BCT UNIT CELL   (110) PLANE
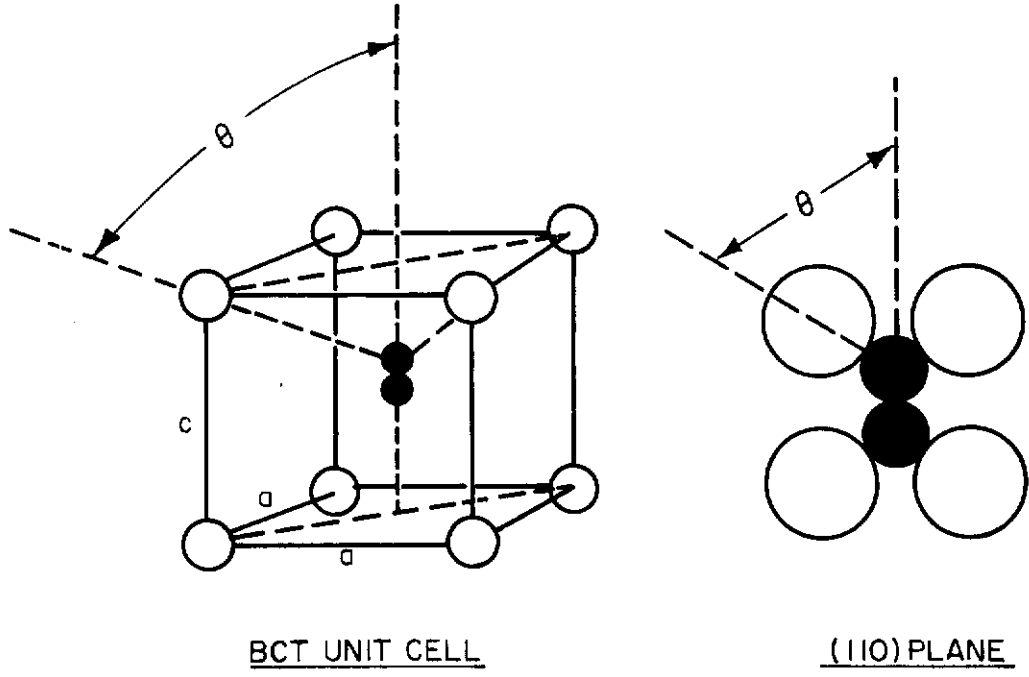
FIGURE V-21 TWO CARBON ATOMS TRAPPED
IN A VACANCY IN MARTENSITE

90

be a consequence of the vacancies released when the carbon atoms pass from the vacancy traps to the cementite. During this higher-temperature tempering, the hardness increment of the strain-tempered martensite over that of straight-tempered martensite gradually vanishes as the dislocation densities converge on each other. Still, the difference in hardness is not entirely wiped out until a relatively high tempering temperature is reached, because the removal of the extra dislocations in the deformed material is impeded by the cementite particles.

When the strain tempering is carried out after pretempering to produce cementite instead of epsilon carbide, strain hardening associated high dislocation densities is again observed, but there is no indication that the existing cementite is appreciably dissolved in this process. If the dislocations or lattice vacancies provide traps for carbon atoms in this instance, the carbon involved must come principally from the ferritic matrix, as in the case of strain aging or quench aging of low-carbon ferrites. Yet, the further hardening and retention of the strain hardening on retempering to rather high temperatures suggests that such small carbon contents are important in the locking of the extra dislocations. In fact, tiny carbide particles, presumably cementite, are found to precipitate on the dislocations during retempering, and they undoubtedly help impede the annealing-out of the dislocations. Accordingly, the hardness changes during strain tempering of this sort seem to depend on the locking and stabilization of high dislocation densities generated by the plastic deformation, rather than on dispersion hardening due to the cementite particles per se. This is probably why the strain-tempered materials do not exhibit a close relationship between the hardness achieved and the intercarbide spacings, such as is observed for the regularly tempered martensites in the cementite-precipitation range.

E. Conclusions

1. Martensites in the range of 0.18 - 0.80 percent carbon studied here follow the normal stages of tempering. The initial form of epsilon carbide is dendritic, while further tempering coarsens it into plates. With the subsequent precipitation and growth of cementite, the steel hardness varies as the inverse of the mean distance between nearest-neighbor particles.

2. Plastic straining of martensite develops substantial increases in hardness with combinations of low pretempering and retempering temperatures. However, the hardening increment thus derived is insensitive to the carbon content, at least between 0.18 and 0.80 percent.

3. Plastic straining and retempering of martensites pretempered below 200°C tends to suppress the formation of epsilon carbide during the retempering or even to dissolve it if already present. Evidently the trapping of carbon atoms by dislocations and lattice vacancies is sufficient to inhibit the first stage of tempering. A model of two carbon atoms per iron vacancy is suggested for the carbon-atom/vacancy complex.

4. The increased hardness of strain-tempered steels stems

91

primarily from the dislocation structure introduced by the plastic deformation. Additional strengthening and the retention of the strain hardening through the first stage of tempering can be accounted for by persistent clusters of carbon atoms which lock these dislocations.

5. Cementite nucleation in the third stage of tempering is retarded by prior deformation of the martensite; this phenomenon is attributed to the trapping of carbon atoms in lattice defects, thereby reducing the driving force for cementite precipitation. However, spheroidization of the cementite is accelerated under such conditions, and it is suggested that the vacancies released from the carbon-atom/vacancy complexes are responsible.

6. The hardness of strain-tempered martensites pretempered to form cementite follows the characteristic strain-aging behavior of low-carbon ferrites. The hardness increase and its retention on retempering probably result from the atmosphere-locking of dense dislocation arrays and their subsequent pinning by actual carbide precipitation. The latter process is believed to contribute its main effect by stabilizing the dislocations against annealing-out processes, rather than through dispersion hardening as such.

F. References

1. E.T.Stephenson and M.Cohen, "Effect of Prestraining and Retempering on AISI Type 4340," Trans.ASM 54 (1961) 72.

2. N.N.Breyer and N.H.Polakowski, "Cold Drawing of Martensitic Steels to 400,000 Psi Tensile Strength," Trans.ASM 55 (1962) 667.

3. D.V.Wilson, "Effects of Plastic Deformation on Carbide Precipitation in Steel," Acta Met.5 (1957) 293.

4. C.C.Busby, M.F.Hawkes and H.W.Paxton, "Tensile and Impact Properties of Low Carbon Martensites," Trans.ASM 47 (1955) 135.

5. H.W.Paxton and C.C.Busby, "Strain Aging of AISI 4340," Trans.AIME 206 (1956) 788.

6. G.H.Williams and H.O'Neill, "The Straining of Metals by Indentation, Including Work-Softening Effects," J.Iron and Steel Inst. 182 (1956) 266.

7. T.O.Mulhearn, "The Deformation of Metals by Vickers-Type Pyramidal Indenters," J.Mech.Phys.Solids 7 (1958-1959) 85.

8. B.A.MacDonald, "Strain Tempering of Iron-Carbon Martensites," Ph.D.Thesis (1964) Department of Metallurgy, MIT.

9. R.M.Fisher, "Electron Microstructure of Steel by Extraction Replica Technique," Symposium on Techniques for Electron Metallography, ASTM Special Technical Publication, No.155 (1953) 49.

10. E.Smith and J.Nutting, "Direct Carbon Replicas from Metal Surfaces," British J. of App.Phys.7 (1956) 214.

11. R.H.Munson and D.J.Schmatz, "A Modified Carbide Extraction Replica Technique," Trans.ASM 56 (1963) 788.

12. E.F.Fullam,"Replica Washing Methods," Symposium on Techniques for Electron Metallography, ASTM Special Technical Publication No. 155 (1953) 101.

13. R.C.Glenn and J.C.Raley, "An Improved Procedure for Thinning Metallic Specimens for Transmission Electron Microscopy," Symposium on Techniques in Electron Metallography, ASTM Special Technical Publication No.339 (1962) 60.

14. P.M.Kelly and J.Nutting, "The Martensitic Transformation in Carbon Steels," Proc.Roy.Soc.A259 (1960) 45.

15. S.G.Fletcher and M.Cohen, "The Effect of Carbon on the Tempering of Steel," Trans.ASM 32 (1944) 333.

16. K.H.Jack, "Structural Transformations in the Tempering of High-Carbon Martensitic Steels," JISI 169 (1951) 26.

17. R.D.Heidenreich,L.Sturkey and H.L.Woods, "Investigation of Secondary Phases in Alloys by Electron Diffraction and the Electron Microscope," J.App.Phys. 17 (1946) 127.

18. L.E.Hofer, E.M.Cohn and W.C.Peebles, "The Modifications of the Carbide, Fe_2C; Their Properties and Identification," J.Amer.Chem.Soc. 71 (1949) 189.

19. R.T.Howard and M.Cohen, "Quantitative Metallography by Point-Counting and Lineal Analysis," Trans.AIME 172 (1947) 413.

20. A.S.Keh and W.C.Leslie, "Recent Observations on Quench-Aging and Strain-Aging of Iron and Steel," Materials Science Research, Plenum Press, New York 1 (1963) 247.

21. B.S.Lement,B.L.Averbach and M.Cohen, "Microstructural Changes on Tempering Iron-Carbon Alloys," Trans.ASM 46 (1954) 851.

22. J.Trotter and D.McLean, "Electron Microscope Study of Quenched and Tempered Steel," J.Iron and Steel Inst. 163 (1949) 9.

23. O.Bannyh, H.Modin and S.Modin, "An Electron Microscopic Study of a Eutectoid Carbon Steel After Quenching and Tempering," Jerkontorets Annaler 146 (1962) 774.

24. M.G.H.Wells, "An Electron Transmission Study of the Tempering of Martensite in an Fe-Ni-C Alloy," Acta Met.12 (1964) 389.

93

25. E.Tekin and P.M.Kelly, "A Study of the Tempering of Steel Using Transmission Electron Microscopy," Department of Metallurgy, The University of Leeds, Leeds, England.

26. D.Tabor, "The Hardness of Metals, Oxford-Clarendon Press, London (1951) 105.

27. E.Orowan, Discussion on "Effects Associated with Internal Stresses," Symposium on Internal Stresses in Metals and Alloys, Institute of Metals (1948) 451.

28. R.L.Fullman, "Measurement of Particle Sizes in Opaque Bodies," Journal of Metals (March 1953) 447.

29. W.R.Tyson, "Yield Strength of Spheroidite," Acta Met. 11 (1963) 61.

30. A.M.Turkalo and J.R.Low, "The Effect of Carbide Dispersion on the Strength of Tempered Martensite," Trans.AIME 212 (1958) 750.

31. C.S.Roberts, R.C.Carruthers and B.L.Averbach, "The Initiation of Plastic Strain in Plain Carbon Steels," Trans.ASM 44 (1952) 1150.

32. A.H.Cottrell and B.A.Bilby, "Dislocation Theory of Yielding and Strain Aging of Iron," Proc.Phys.Soc.Lond. A62 (1949) 49.

33. J.D.Eshelby, Appendix to "Strain-Aging in Low Carbon Steels," Acta Met. 7 (1959) 631.

34. V.A.Phillips, "An Electron Microscopic Study of Quench-Aging and Strain-Aging in a Dilute Fe-C-N Alloy," Trans. ASM 56 (1963) 600.

35. J.Friedel, Dislocations, Addison-Wesley Publishing Co., Reading, Mass. (1964) 356.

36. M.L.Rudee and R.A.Huggins, "The Temperature and Composition Dependence of the Segregation of Interstitial Impurity Atoms to Dislocations," Acta Met. 12 (1964) 501.

37. R.A.Arndt and A.C.Damask, "Kinetics of Carbon Precipitation in Irradiated Iron - III. Calorimetry," Acta Met. 12 (1964) 341.

38. F.E.Fujita and A.C.Damask, "Kinetics of Carbon Precipitation in Irradiated Iron - II. Electrical Resistivity Measurements," Acta Met. 12 (1964) 331.

39. H.Wagenblast, F.E.Fujita and A.C.Damask, "Kinetics of Carbon Precipitation in Irradiated Iron - IV. Electron Microscope Observations," Acta Met. 12 (1964) 347.

40. L.Darken and R.Gurry, Physical Chemistry of Metals, McGraw-Hill Book Company, New York (1953) Ch.16.

41. G.Borelius and S.Berglund, "Calorimetric Study of the Precipitation of Carbon Dissolved in Alpha Iron," Arkiv.f. Fysik $\underline{4}$ (1952) 173.

42. R.Smith, "The Diffusivity and Solubility of Carbon in Alpha Iron," Trans. AIME $\underline{224}$ (1962) 105.

43. F.Seitz, "On the Generation of Vacancies by Moving Dislocations," Advan.Phys. $\underline{1}$ (1952) 43.

44. A.H.Cottrell, "Point Defects and the Mechanical Properties of Metals and Alloys at Low Temperatures," A Symposium on Vacancies and Other Point Defects in Metals and Alloys, The Institute of Metals, London (1958) 1.

45. H.G.van Beueren, Imperfections in Crystals, North-Holland Publishing Company, Amsterdam (1960) 159.

46. M.Cohen, "The Strengthening of Steel," Trans.AIME $\underline{224}$ (1962) 638.

VI. STRAIN HARDENING OF BODY-CENTERED CUBIC VS. FACE-CENTERED CUBIC METALS AT VERY HIGH STRAINS

G. Langford

A. Introduction

The ausforming experiments in Section IV and the strain-tempering experiments in Section V have demonstrated that the dislocation substructure in virgin martensite contributes to the strengthening, although in a secondary way compared to the role of carbon in solid solution. In this section we have attempted to intensify the strengthening effect of the fine structure by wire drawing low-carbon iron-nickel martensite to very large strains, well beyond those achieved in an ordinary tensile test. For comparison purposes, low-carbon ferrite and low-carbon iron-nickel austenite were studied in a similar manner.

Body-centered cubic metals are known to strain harden markedly at very high strains, whereas face-centered cubic metals strain harden at a diminishing rate approaching zero. Peck[1] has measured the microhardness of drawn columbium and nickel wires, and observed an increase in the hardening rate of columbium at natural strains from 1 to 3 (depending on purity), but found no further hardening of nickel beyond a strain of about 2. Using tensile tests, Cohen and Taranto[2] noted a linear strain-hardening rate in rolled BCC martensite (iron - 31.9 percent nickel - 0.017 percent carbon), but the corresponding FCC austenite rolled at 300°C displayed a decreasing rate of hardening up to a strain of 2, the highest strain examined.

The iron-nickel alloy selected for the present investigation had an M_s temperature of -50°C, which made it possible to study the strain hardening of both FCC austenite and BCC martensite of the same composition. Vacuum-melted electrolytic iron (Ferrovac E) served as the comparison ferritic material, without having the initial complication of the martensitic substructure.

Large amounts of plastic deformation for the strain-hardening studies were achieved by wire drawing, affording natural strains up to about 7. Stress-strain curves were determined at various degrees of strain hardening, and the corresponding substructures were examined by transmission electron microscopy.

B. Experimental Procedures

1. Wire-Drawing Dies: Design and Testing - In order (a) to attain the high strains desired in this program, (b) to achieve the necessary close control over the conditions of deformation, and (c) to enable convenient testing of the deformed material, wire drawing was chosen as the means of deformation. The drawing dies were designed to minimize the inhomogeneous or redundant deformation normally occurring in wire drawing, so as to render the drawing strain more-or-less equivalent to a pure tensile strain.

According to Wistreich,[3] the redundant deformation per pass can be minimized by minimizing the parameter:

96

$$R = (\frac{1 - q}{q}) \sin \alpha \qquad\qquad (VI-1)$$

where q is the fractional reduction in cross-sectional area in the die, and α is the die semi-angle in radians. From a practical standpoint, the extent to which R can be reduced is limited by the maximum value of q, at which the drawing force exceeds the breaking load of the exit wire. In turn, q_{max} depends on the coefficient of friction (μ) and the die angle in the following way.

The drawing stress (σ_d) can be expressed approximately as:[3]

$$\frac{\sigma_d}{\sigma_m} = (1 + \mu \cot \alpha) \ln (\frac{1}{1 - q}) \qquad\qquad (VI-2)$$

where σ_m is the mean flow stress of the wire in the die. If the strain-hardening rate of the drawn wire is negligible, q will have its maximum, for given values of μ and α, when $\sigma_d = \sigma_m$. Then,

$$q_{max} = 1 - \exp[\frac{-1}{1 + \mu \cot \alpha}] \qquad\qquad (VI-3)$$

If the strain-hardening rate is appreciable, then the assumption that $\sigma_d = \sigma_m$ will cause an under-estimation of q_{max}, which is acceptable here.

In the light of these equations, the least redundant deformation is obtained, for a given coefficient of friction, when α is small and q_{max} is as large as possible for that α, since α and q_{max} are interrelated through Equation VI-3. Another factor to be taken into account is that, if α is made quite small, many dies will be needed to obtain large total reductions.

Equation VI-2 was used to determine the effective coefficient of friction with molybdenum disulphide as the lubricant by observing the drawing stress on pulling wire through a single die of known geometry. μ was found to equal 0.09 under the conditions at hand. Then a wire with stepped diameters was drawn through the same die, and q_{max} was noted as the maximum fractional reduction that could be obtained without breaking. q_{max} was also calculated independently from Equation VI-3, and the agreement was good.

Based on the foregoing considerations, the die geometry selected was $\alpha = 1.5°$ and q = 0.2. To achieve the desired over-all strains, a set of 35 sintered carbide dies was made, to take starting rods 0.400 inches in diameter down to wires 0.008 inch in diameter.

The dies were tested for inhomogeneous deformation by comparing the stress-strain curves* of tough-pitch copper in the annealed and

*Unless otherwise indicated in this section, the stress-strain curves are true stress-true strain curves containing the Bridgman correction for necking.(4) See following section.

wire-drawn conditions, as shown in Figure VI-1. The fitting-together of these curves indicates that the strain produced by the wire-drawing operation was reasonably homogeneous, and that the die design could be regarded as adequate for the purpose at hand.

For lubrication, molybdenum-disulphide powder was sprayed onto the clean wire surface and from an aerosol can. This was followed by burnishing lightly with the disulphide powder and a superficial coating of grease.

All the wire drawing was carried out with a Tinius Olsen tensile testing machine at a crosshead speed of 2 inches/minute. For elevated-temperature drawing the die was heated in a small box with forced hot air, and the wire was led to the die through an open-ended glass tube in order to preheat the wire as it approached the die.

2. <u>Tensile Testing</u> - The tensile testing of heavily drawn wires in this program posed several problems: (a) The tensile specimens had to have a reduced section of simple shape to minimize the preparation effort. (b) The gripping method had to accommodate a wide range of specimen diameters. (c) Most of the specimens underwent necking with virtually no uniform elongation in the tensile test; hence, true stress-true strain curves were required.

For the most part, the tensile-specimen gage sections were electro-machined in a jet of 5 percent perchloric acid (72 percent grade) in glacial acetic acid. During the electrolysis, while the specimen was being rotated horizontally, it was also oscillated axially by a cam to generate a slight hourglass shape along the gage length. The minimum section was only a few percent smaller in area than the grip ends.

The tensile grips consisted of two sets (maximum loads of 3500 and 600 pounds) of three-jaw drill chucks with the following two modifications: (a) Closely spaced teeth were ground into the jaws, and (b) the bodies of the chucks were relieved to permit enough jaw movement so that the teeth could sink into the grip ends of the specimen.

In the tensile testing the gage section was photographed frequently in order to establish the natural strain all along the stress-strain curve, while the crosshead speed was gradually reduced to achieve a constant strain rate. The minimum diameter, a reference diameter (taken where no plastic deformation had occurred), and the radius of curvature of the neck profile were measured from the enlarged photographs. The resulting data, together with the load corresponding to each photograph, were fed into a computer program to obtain both the true strain as well as the true stress corrected for necking.[4]

3. <u>Materials and Heat Treatment</u> - The iron-nickel alloy contained 31.9 percent nickel and 0.008 percent carbon. It was homogenized at 1150°C for 100 hours in vacuum, and was eventually recrystallized and austenitized at 900°C for 2 hours after cold-working to a strain of 0.45. In this condition the M_s temperature was -50°C, and the A_s temperature (start of the martensite-to-aus-
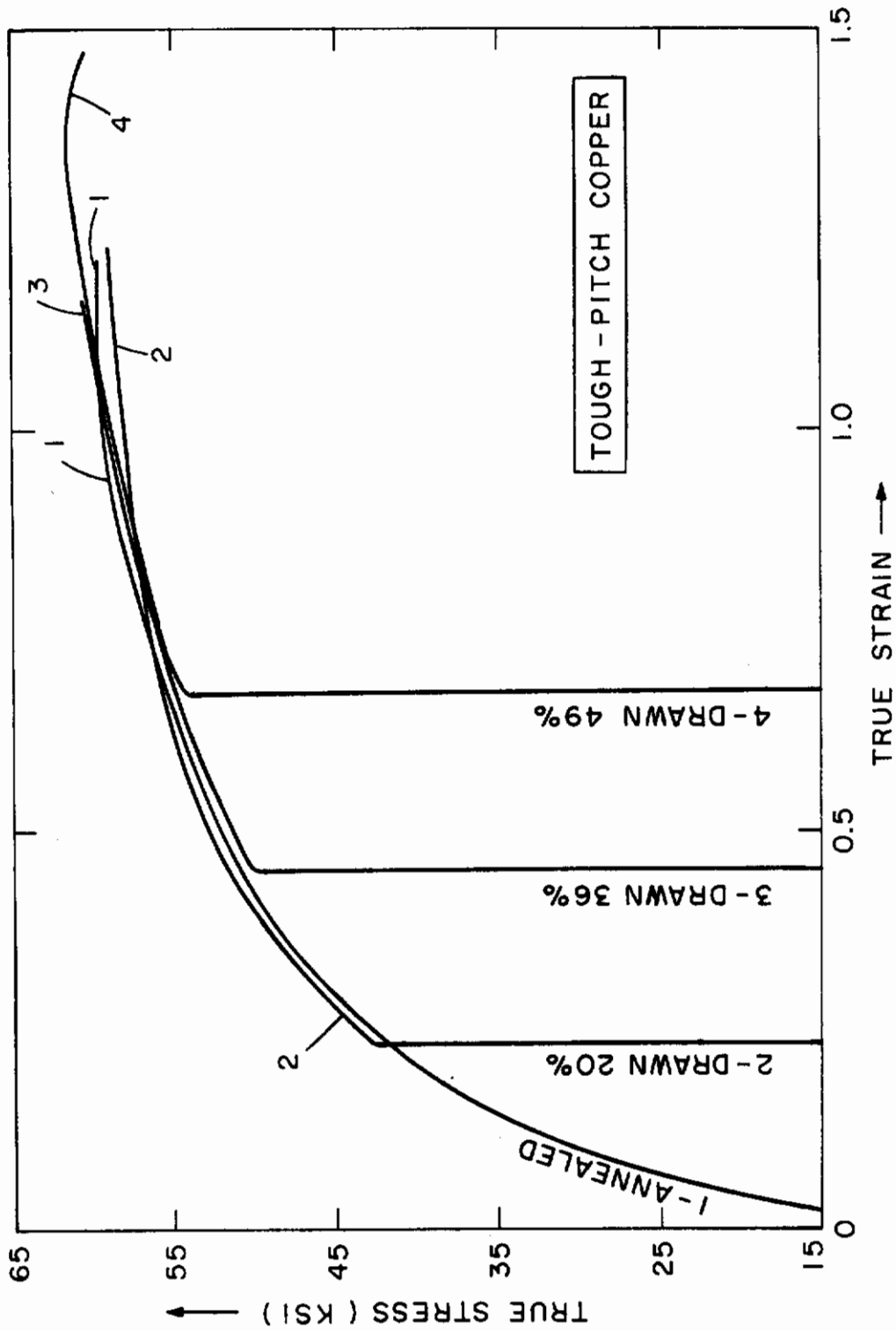
FIGURE VI-1. STRESS-STRAIN CURVES FOR ANNEALED AND WIRE-DRAWN TOUGH-PITCH COPPER. THE STRESS VALUES HAVE BEEN CORRECTED FOR NECKING.

tenite reversion on heating) was 310°C, giving an estimated equilibrium temperature of $T_o = 1/2 (M_s + A_s) = 130°C$. To produce martensite the austenite was water quenched from 900°C to room temperature and refrigerated in liquid nitrogen. The amount of retained austenite was then about 15 percent.

The Ferrovac E iron typically contained 0.006 percent carbon, 0.0020 percent oxygen and 0.0002 percent nitrogen, with other elements totaling less than 0.082 percent. The starting condition of this material for the wire-drawing experiments was a recrystallized and annealed state, obtained by cold drawing to a strain of 0.32, heating at 630°C for 3 hours, and cooling to room temperature over a period of 3 days to minimize the carbon retained in solution.

Both the iron and martensitic wires were always held in liquid nitrogen, except during the actual wire drawing or specimen preparation, in order to inhibit possible aging effects. The austenitic specimens were also kept refrigerated, but above the M_s temperature.

C. Discussion of Results

1. General - The tensile properties of the drawn wires are summarized in Figures VI-2, 3, and 4. The solid points represent the ultimate tensile strengths, while the curves are the Bridgman-corrected true stress - true strain relationships after selected amounts of plastic strain by wire drawing. In each instance, except for the undrawn and lightly drawn specimens, the uniform elongation was negligible, and so the indicated tensile strength is also the yield stress as well as a true stress. Consequently, the envelope generated by plotting the tensile strengths of the drawn wires against the prior plastic strain should provide a representation of the true stress-true strain properties of the material over the wide range of strains obtained here. This conclusion is supported by the individual stress-strain curves in Figures VI-2 and 4, where the curves nearly superimpose on one another, and the tensile strengths of all the specimens (even for those whose actual stress-strain curves are not shown) fall generally along the composite stress-strain curves.

The strain-hardening rate of the FCC iron-nickel austenite in Figure VI-2 drops off progressively to nearly zero with increasing strain, whereas the strain-hardening rate of the BCC ferrite in Figure VI-3 remains high even up to the highest strain reached. The BCC iron-nickel martensite in Figure VI-4 exhibits a high but somewhat decreasing strain-hardening rate up to the maximum strain investigated.

2. Strain Hardening of FCC Austenite - Figure VI-5 shows a series of transmission electron micrographs* of the drawn austenite

---

* The electron micrographs in Section VI of this report were prepared at the Edgar C. Bain Laboratory for Fundamental Research of the U.S.Steel Corporation, through the courtesy of Doctors R.M.Fisher and J.D.Embury.
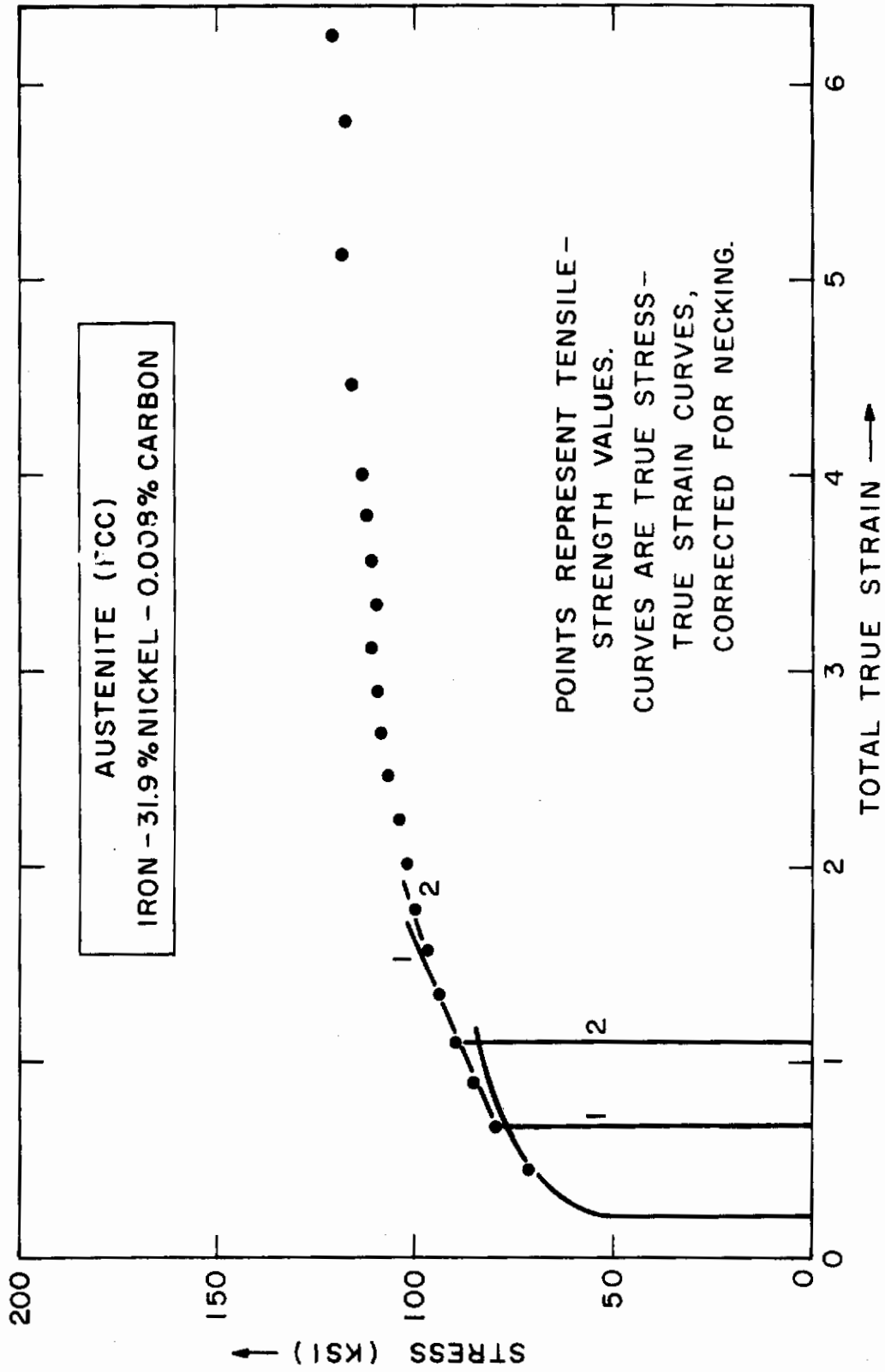
FIGURE VI-2. STRAIN HARDENING OF FCC AUSTENITE, WIRE DRAWN AND TESTED AT 130°C.
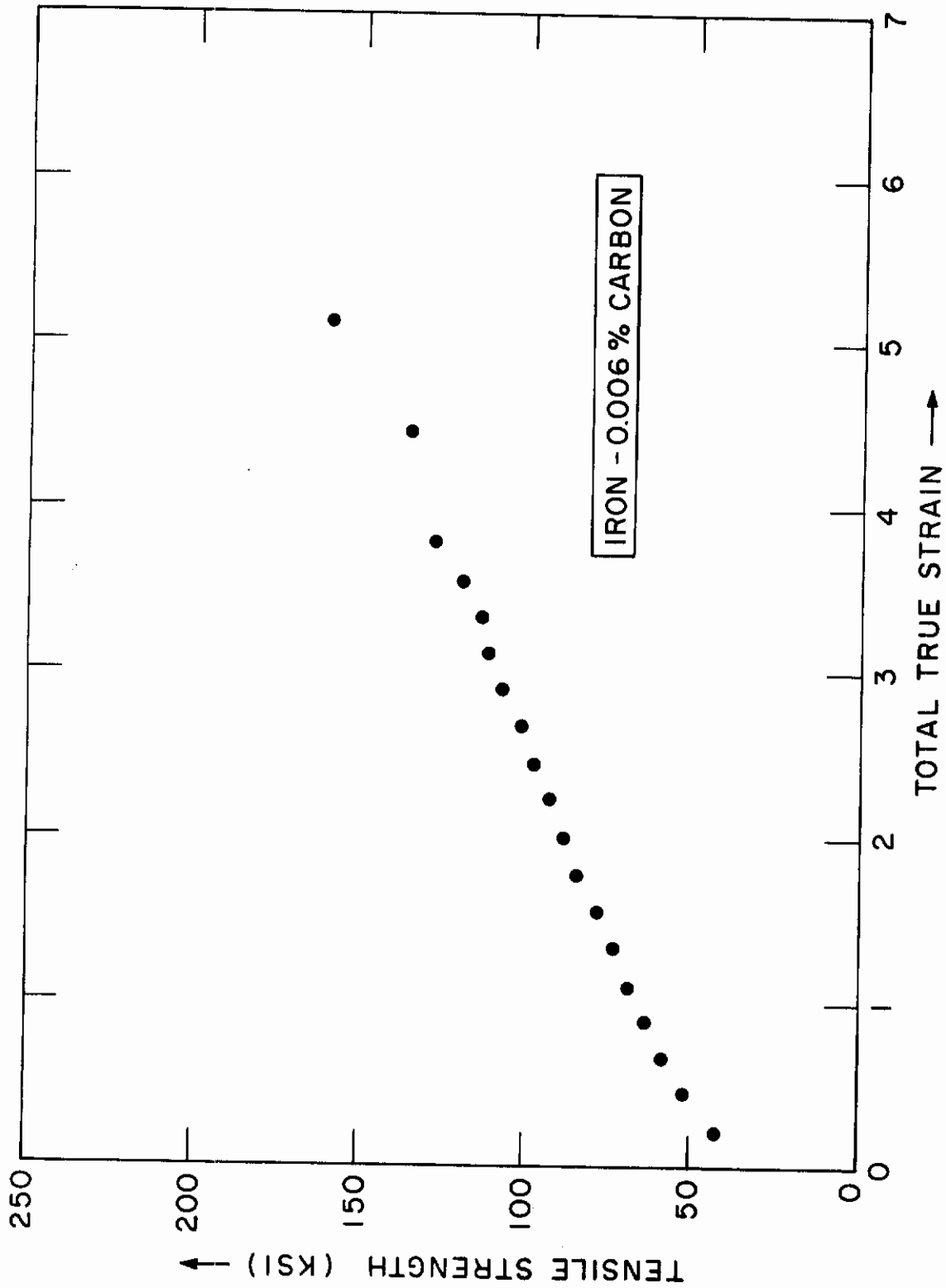
FIGURE VI-3. TENSILE STRENGTH OF BCC IRON, WIRE DRAWN AND TESTED AT ROOM TEMPERATURE.

IRON – 0.006 % CARBON

TOTAL TRUE STRAIN →

TENSILE STRENGTH (KSI) →
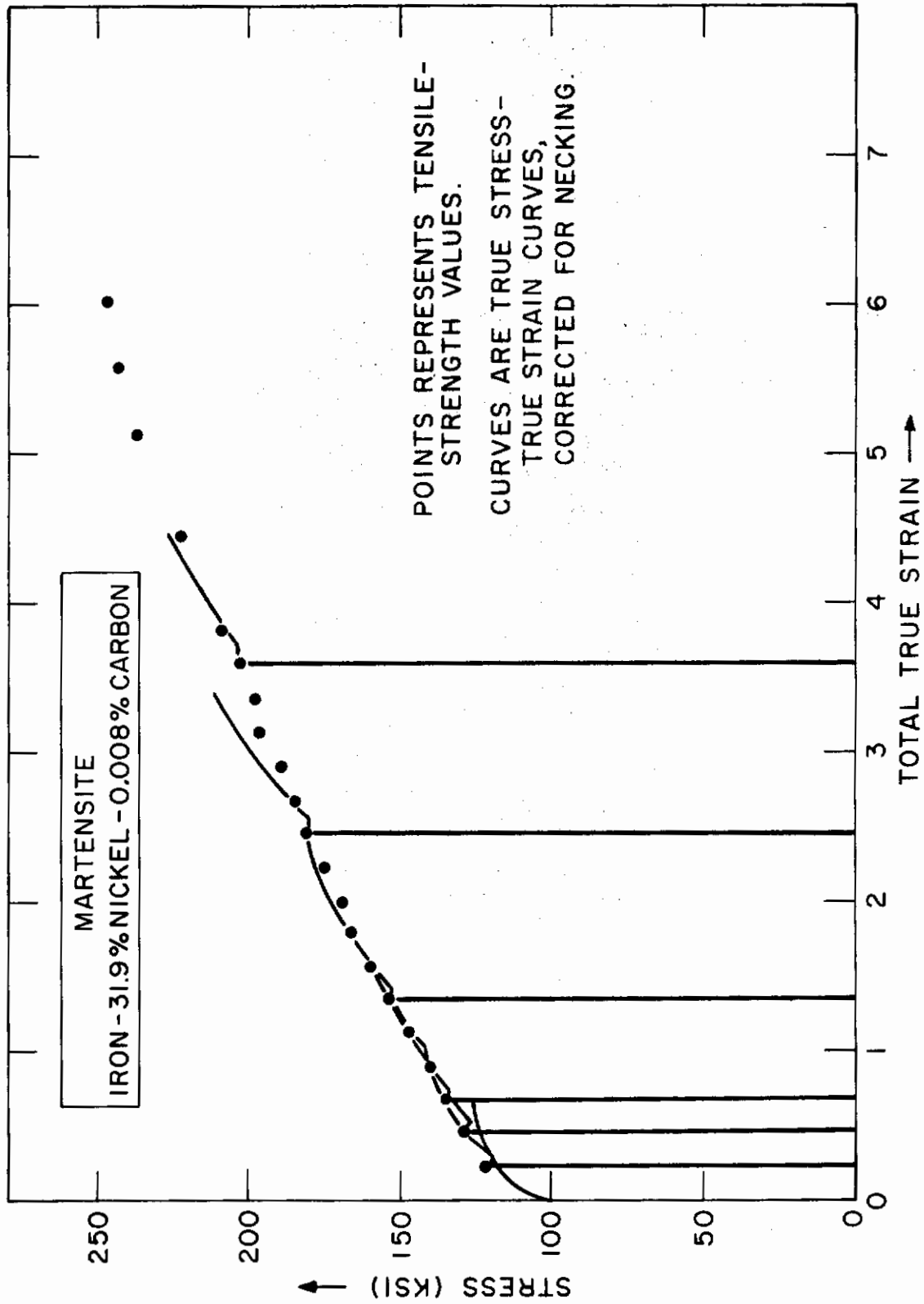
FIGURE VI-4. STRAIN HARDENING OF BCC MARTENSITE, WIRE DRAWN AND TESTED AT ROOM TEMPERATURE.

MARTENSITE
IRON-31.9%NICKEL-0.008%CARBON

POINTS REPRESENTS TENSILE-
STRENGTH VALUES.

CURVES ARE TRUE STRESS-
TRUE STRAIN CURVES,
CORRECTED FOR NECKING.

TOTAL TRUE STRAIN ⟶

STRESS (KSI) ⟵

$\epsilon = 0.9 \, (A/A_o = 1/2.4)$ — 1μ $\epsilon = 2.0 \, (A/A_o = 1/7.4)$ — 1μ

$\epsilon = 4.9 \, (A/A_o = 1/130)$ — 1μ $\epsilon = 6.0 \, (A/A_o = 1/420)$ — 1μ
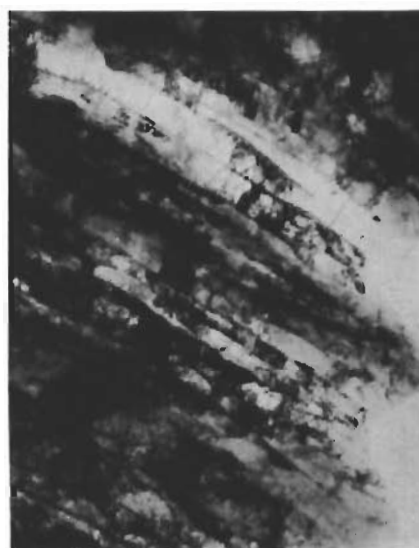
FIGURE VI-5. Transmission Electron Micrographs Showing Structural Changes Due to Wire Drawing of FCC Austenite (Iron - 31.9 Percent Nickel - 0.008 Percent Carbon) at 130° C. 20,000X.

104

wires after strains ranging from 0.9 to 6.0. A drawing temperature of 130°C was chosen in order to avoid the formation of martensite; this temperature was also adopted for the tensile testing of the austenite. The evident lack of any systematic refinement of the substructure is consistent with the failure of the material to strain harden at high strains. The only apparent change is a lengthening of the cells in the drawing direction. That the cells do not continue to narrow down in cross section suggests that many of the cell walls have migrated or merged into one another in a process of dynamic recovery during the wire drawing. The cells seem to remain equiaxed in cross section.

3. <u>Strain Hardening of BCC Iron</u> - The transmission electron micrographs of the drawn iron wires in Figure VI-6 indicate a strong refinement of the cell structure with increasing strain. In a qualitative sense, such refinement would be expected if little dynamic recovery had taken place during the wire drawing, unlike the case of the austenite.

However, the shape change of the cells in Figure VI-6 does not correspond exactly to that of the wire itself. Peck and Thomas[5] have found that the grains in a BCC material become ribbon-shaped during wire drawing, and that these ribbons interfold with one another to maintain continuity. Hosford[6] has accounted for this geometry in terms of the usual wire texture of BCC metals in which only two of the four <111> slip directions are oriented for tensile deformation, the other two contributing no tensile strain because they are perpendicular to the wire axis. Axially symmetric flow of the textured grains would then result in 50 percent more slip than in the case of unconstrained deformation. However, the grains apparently find it easier (at least initially) to curl around one another in contributing to the over-all plastic flow of the wire, even though some redundant bending deformation takes place locally. Therefore, it may be expected that if the cell walls do not migrate, the substructure will consist of ribbon-shaped cells, whose curvature in a transverse section is similar to that of the grains themselves. This situation can be inferred from the longitudinal sections in Figure VI-6, where a group of several narrow cells alternates with a few wide cells, as observed by Meieran in connection with drawn tungsten and columbium wires.[7]

If the ribbon-like nature of the cells in the drawn BCC iron is taken into account and if it is assumed that the cell <u>width</u> does not change appreciably (which would follow from the texture theory as long as the cells continue to interfold with one another rather than to deform with axial symmetry), then the <u>thickness</u> of the cells should bear the following relationship to the over-all strain:

$$t = d_o \exp(-\epsilon) \qquad\qquad VI-4$$

where ϵ is the natural strain attained in the wire drawing, and d_o is the diameter of the cells when first formed, i.e., at a strain of about 0.1. Keh and Weissman[8] found d_o to be about 15,000 Å in a similar type of iron.

If the cells were actually ribbon-shaped, the minimum transverse spacings in the electron micrographs should correspond to the

$\epsilon = 4.9$ (A/A$_o$ = 1/130)
20,000X. $\longmapsto$ 1μ

$\epsilon = 6.9$ (A/A$_o$ = 1/1000)
20,000X. $\longmapsto$ 1μ
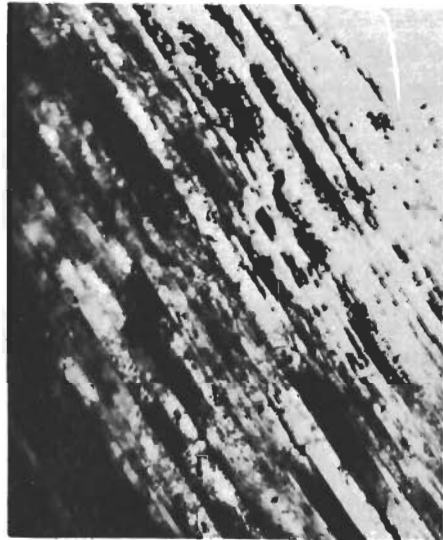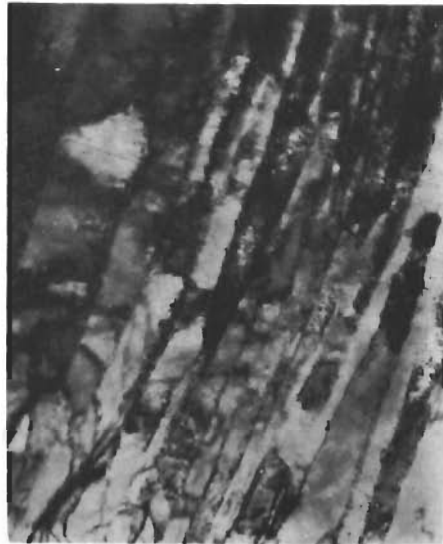
FIGURE VI-6.   Transmission Electron Micrographs Showing Structural
Changes Due to Wire Drawing of BCC Iron (0.006 Percent
Carbon) at Room Temperature.

106

thickness dimension of the cells, and the logarithm of this parameter plotted as a function of strain, as in Figure VI-7, should give a straight line of slope -1, according to Equation VI-4. This trend was observed up to a strain of 2, but not beyond. In the latter range the minimum cell spacings were much less sensitive to the drawing strain, suggesting that symmetrical axial flow had then begun to take place. However, it is also possible that some of the cell walls could have been missed in measurements at the higher strains, thus contributing to the apparent relative lack of refinement of the cell thickness when this dimension became relatively small.

On the other hand, the mean transverse cell dimension (given by the average linear intercept) in Figure VI-7 should vary with strain as:

$$\overline{d} = d_o \exp(-\epsilon/2) \qquad\qquad VI-5$$

assuming that the cell volume remains constant and that no new cells are formed. This is analogous to the relationship derived by Embury and Fisher[9] for the case of cylindrical grains or cells being reduced in proportion to the wire diameter. The experimental points do not provide an unambiguous confirmation of Equation VI-5 because a straight line is not obtained, but the slope is closer to -1/2 than -1 at the higher strains.

The tensile strengths of the wires are plotted against their respective transverse cell sizes in Figure VI-8, using $(\overline{d})^{-1/2}$ as the cell parameter as is customarily done in grain-size studies. The best straight line drawn through the resulting points has a slope of 400 lb/in$^{3/2}$ and an intercept of about 10,000 psi. These values correspond to the k_y and σ_o parameters in the Petch equation for the lower yield stress:

$$\sigma = \sigma_o + k_y (2\overline{d})^{-1/2} \qquad\qquad VI-6$$

where σ_o is the friction stress. The factor of 2 has been introduced here, after Embury and Fisher[9], to take into account the fact that the slip systems are actually inclined to the transverse direction in which the cell size is measured. The slope and intercept given by Figure VI-8 agree approximately with the k_y and σ_o values obtained for iron through grain-size variations.[10]

Embury and Fisher[9] have combined the equivalent of Equations VI-5 and 6 to express the strength developed by wire drawing, on the assumption that the cells or other slip-limiting entities are subjected to axially symmetrical flow:

$$\sigma = \sigma_o + k_y (2d_o)^{-1/2} \exp(\epsilon/4) \qquad\qquad VI-7$$

This equation is tested in Figure VI-9, where log $(\sigma - \sigma_o)$ is plotted against ϵ. A reasonable straight line is obtained for $\epsilon > 2$, and the slope is then 1/5, compared to a slope of 1/4 ex-
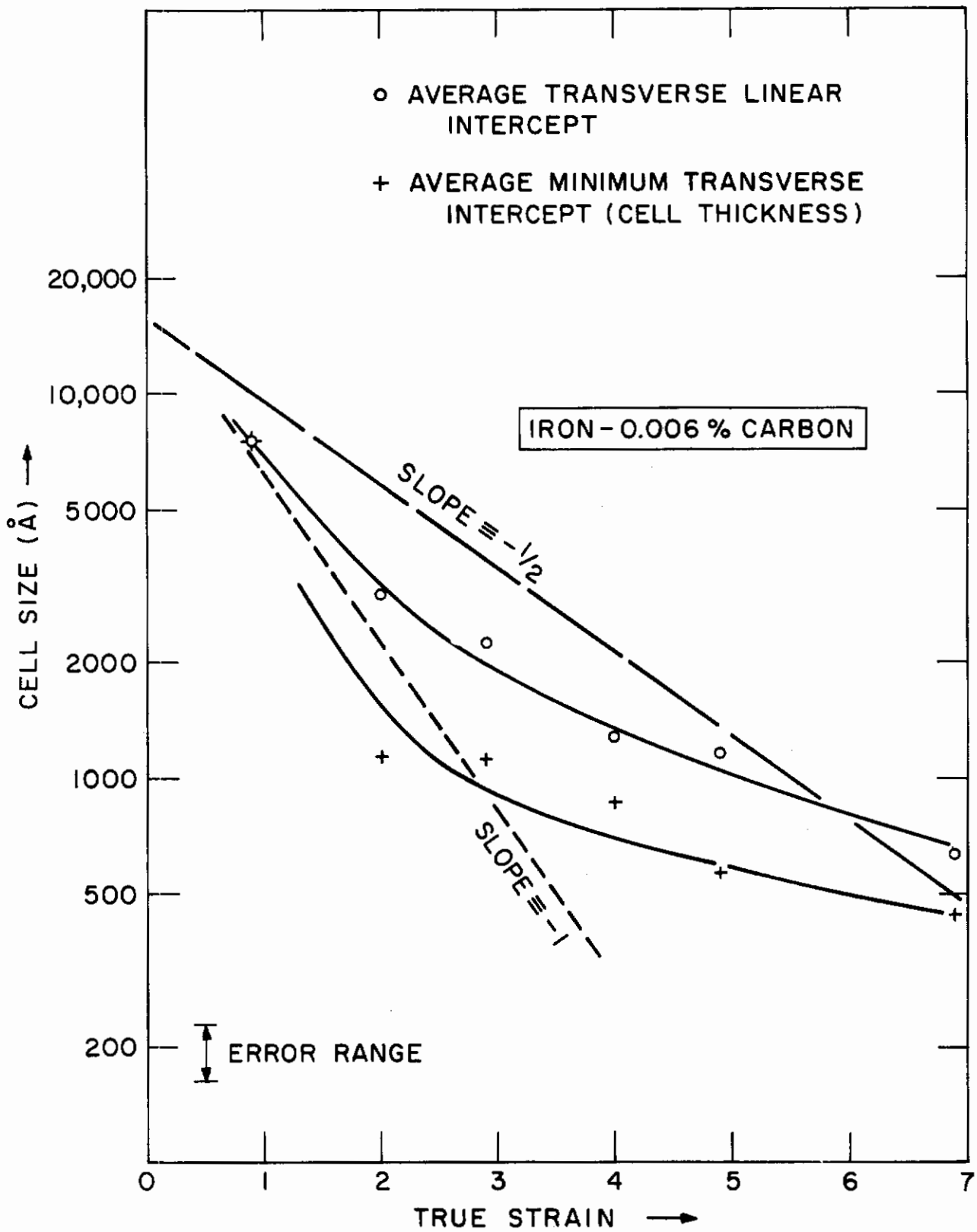
FIGURE VI-7. CELL SIZE VS. STRAIN FOR BCC IRON, WIRE DRAWN
AT ROOM TEMPERATURE.

108
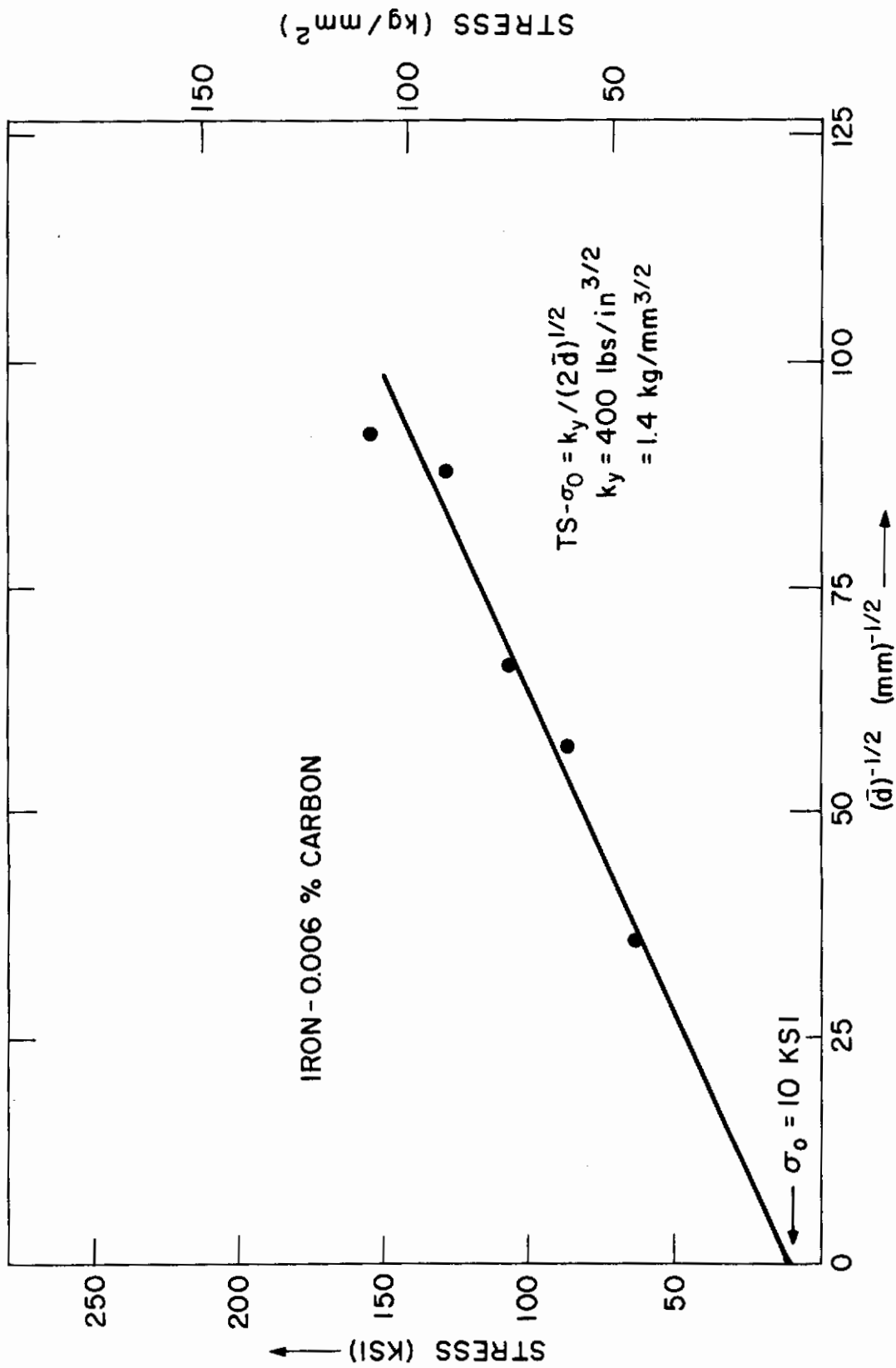
FIGURE VI-8. TENSILE STRENGTH OF WIRE-DRAWN BCC IRON AS A FUNCTION OF AVERAGE TRANSVERSE CELL SIZE, DRAWN AND TESTED AT ROOM TEMPERATURE.

FIGURE VI-9. TENSILE STRENGTH MINUS FRICTION STRESS ($\sigma_0 = 10$KSI) AS A FUNCTION OF WIRE-DRAWING STRAIN FOR BCC IRON, DRAWN AND TESTED AT ROOM TEMPERATURE.
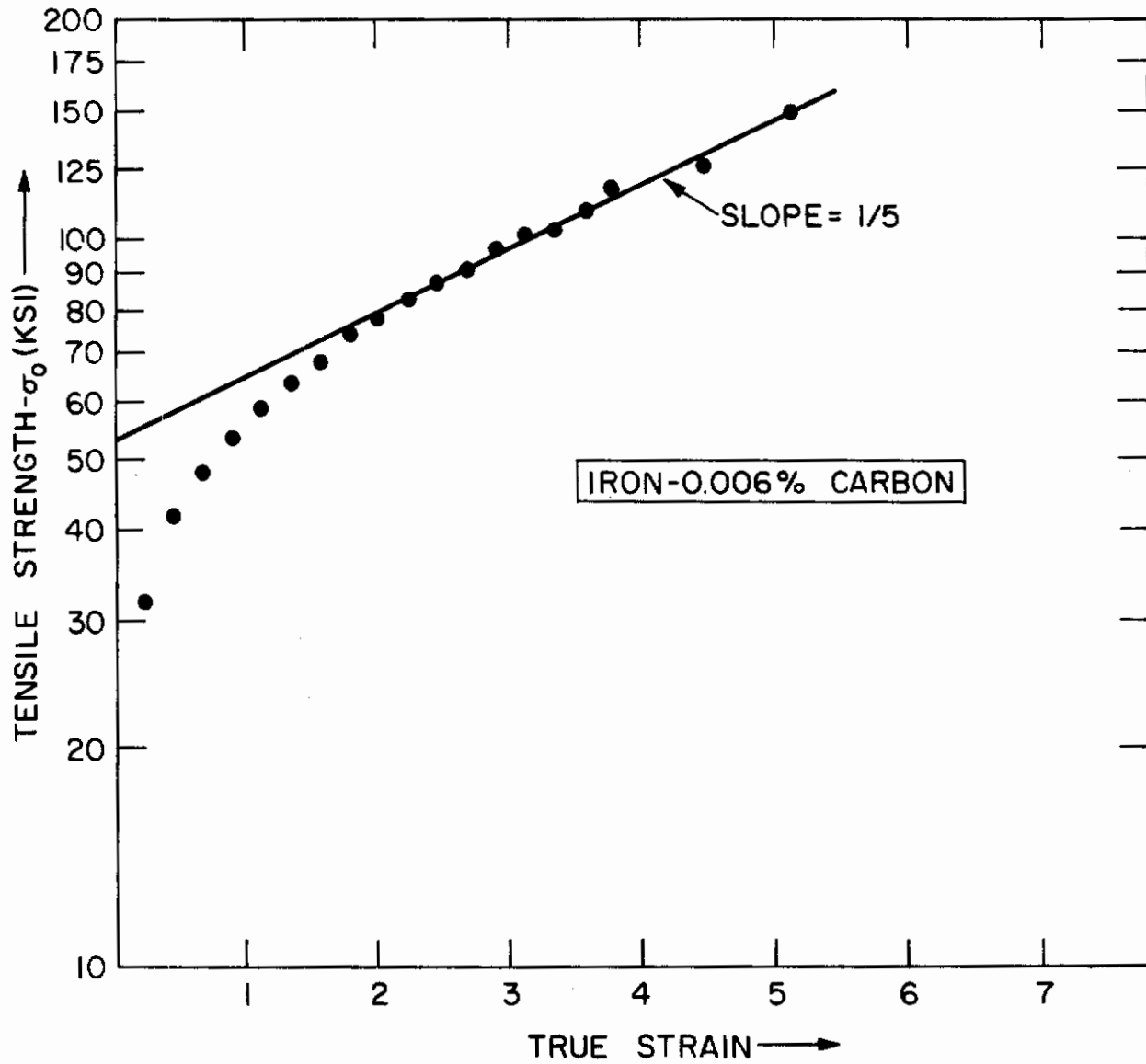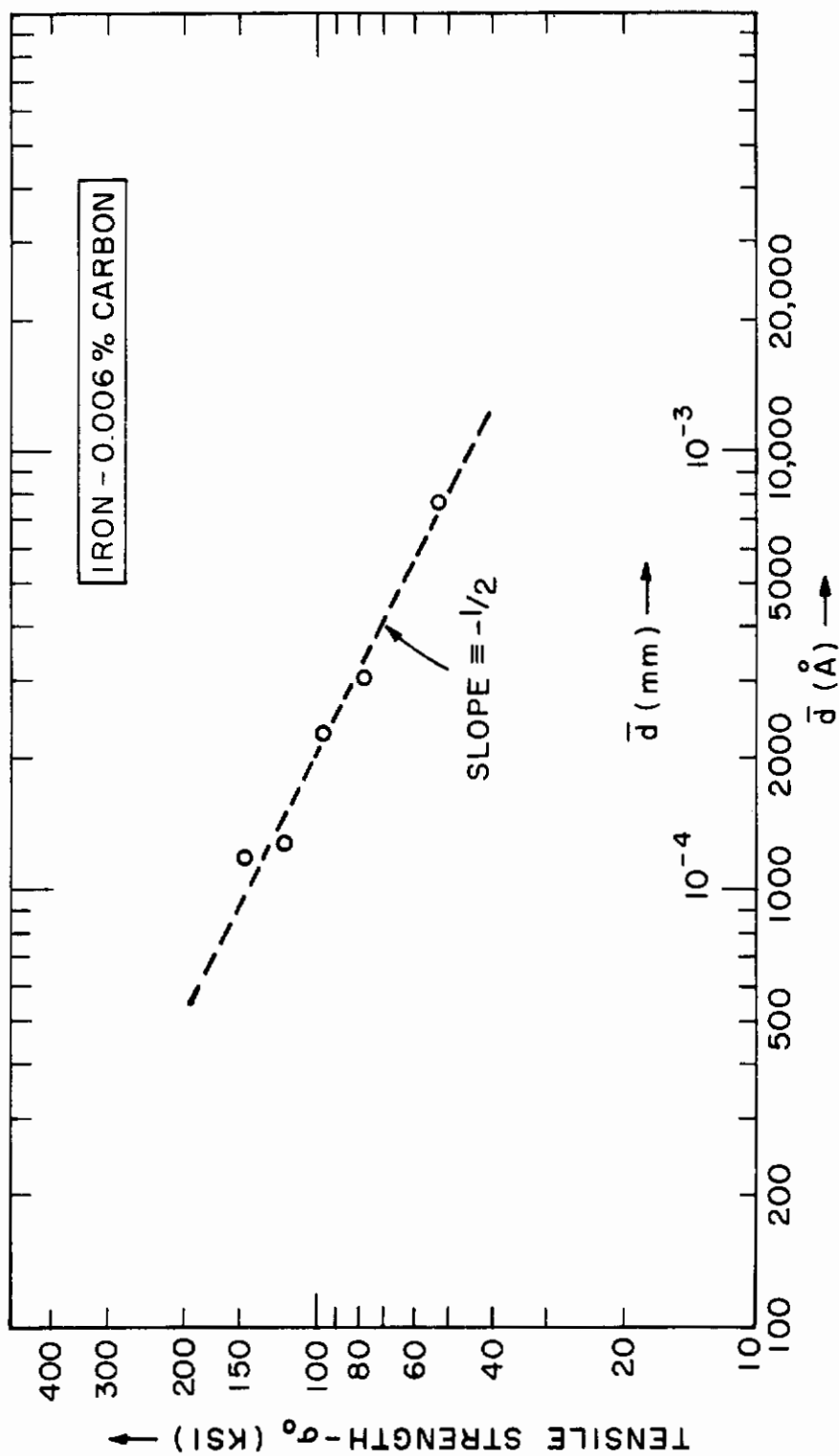
FIGURE VI-I0. TENSILE STRENGTH MINUS FRICTION STRESS ($\sigma_o = 10$ KSI) OF BCC IRON AS A FUNCTION OF AVERAGE TRANSVERSE CELL SIZE, WIRE DRAWN AND TESTED AT ROOM TEMPERATURE.

111

pected from Equation VI-7.

In Figure VI-10, $(\sigma - \sigma_o)$ is related directly to the mean transverse cell intercept $(\bar{d})$ on a log-log plot. The points fall reasonably close to a line having a slope of $-1/2$, thus indicating a Petch-type of relationship.
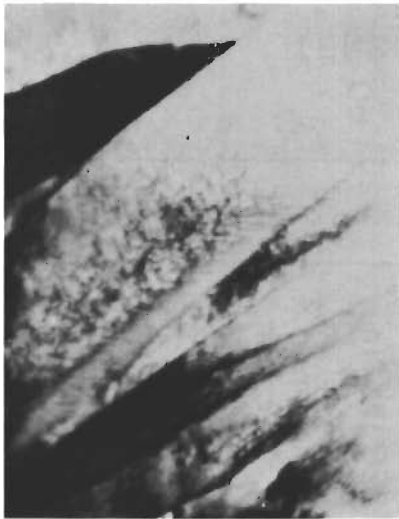
It is evident, then, that in combining Equations VI-5 and 6 to give Equation VI-7, the main uncertainty arises in Equation VI-5. There are at least three reasons for this uncertainty: (a) at low strains (less than 1) the cells are nearly equiaxed and the factor of 2 in Equation VI-6 is then inappropriate; (b) subsequently, the formation of ribbon-shaped cells generates more cell boundaries per unit transverse distance than would be the case with a symmetrical reduction of the cells; (c) there seems to be a change-over to the symmetrical reduction of cells at the higher strains; and (d) the rate of reduction of the cell size is less than predicted at strains greater than 2 (while axially symmetric flow is taking place). These complications could account for the rapidly rising flow stress in Figure VI-9, followed by the settling down to a constant slope (but less than 1/4) at strains above 2.

In summary, the strain hardening of the BCC iron (containing 0.006 percent carbon) appears to be governed by the transverse dimensions of the cells generated by the deformation. In turn, these cell dimensions depend in a complex way on the shape change of the wire specimen, but there is a progressive and persistent decrease in this parameter with increasing reduction of the wire. Despite the wire texture developed by the drawing operation, axially symmetric flow evidently ensues at strains greater than 2. In this high-strain range the strain dependence of the flow stress follows the form predicted by Embury and Fisher,[9] but with a somewhat smaller exponent. The latter fact suggests that some dynamic recovery takes place, but it is relatively minor compared to that occurring in the FCC austenite.

4. <u>Strain Hardening of BCC Martensite</u> - Figure VI-11 shows a series of electron transmission micrographs of the wire-drawn iron-nickel martensite. The sample with the lowest strain (5 percent) contains an internally twinned structure in some of the plates and a high dislocation density in the balance of the material. However, the twins are not visible after the higher strains. The cell structure of the deformed martensite appears to correspond to that of the deformed iron (Figure VI-6), except that the martensite exhibits a much higher dislocation density within the cells than does the iron. For the most part, the martensitic cells seem to correspond to the original martensitic plates.

The work of Speich and Swann[11] indicates that the σ_o component of the flow stress (due to lattice friction and solid-solution hardening) is about 60,000 psi for an iron-nickel martensite of this composition; this high friction stress might account for the many dislocations "trapped" <u>within</u> the cells. A value of 60,000 psi for σ_o was adopted for deducing the best line through the points in Figure VI-12, where the tensile strengths of the drawn martensitic wires are plotted against $(\bar{d})^{-1/2}$, as in Figure VI-8. The

112

$\epsilon = 0.05 \ (A/A_o = 1/1.05)$ ⊢—1μ—⊣ $\epsilon = 0.9 \ (A/A_o = 1/2.4)$ ⊢—1μ—⊣

$\epsilon = 2.9 \ (A/A_o = 1/18)$ ⊢—1μ—⊣ $\epsilon = 4.9 \ (A/A_o = 1/130)$ ⊢—1μ—⊣
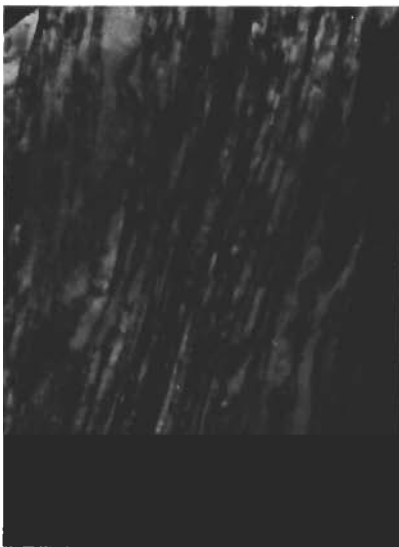
FIGURE VI-11.   Transmission Electron Micrographs Showing Structural
Changes Due to Wire Drawing of BCC Martensite
(Iron - 31.9 Percent Nickel - 0.008 Percent Carbon)
at Room Temperature.   20,000X.

113
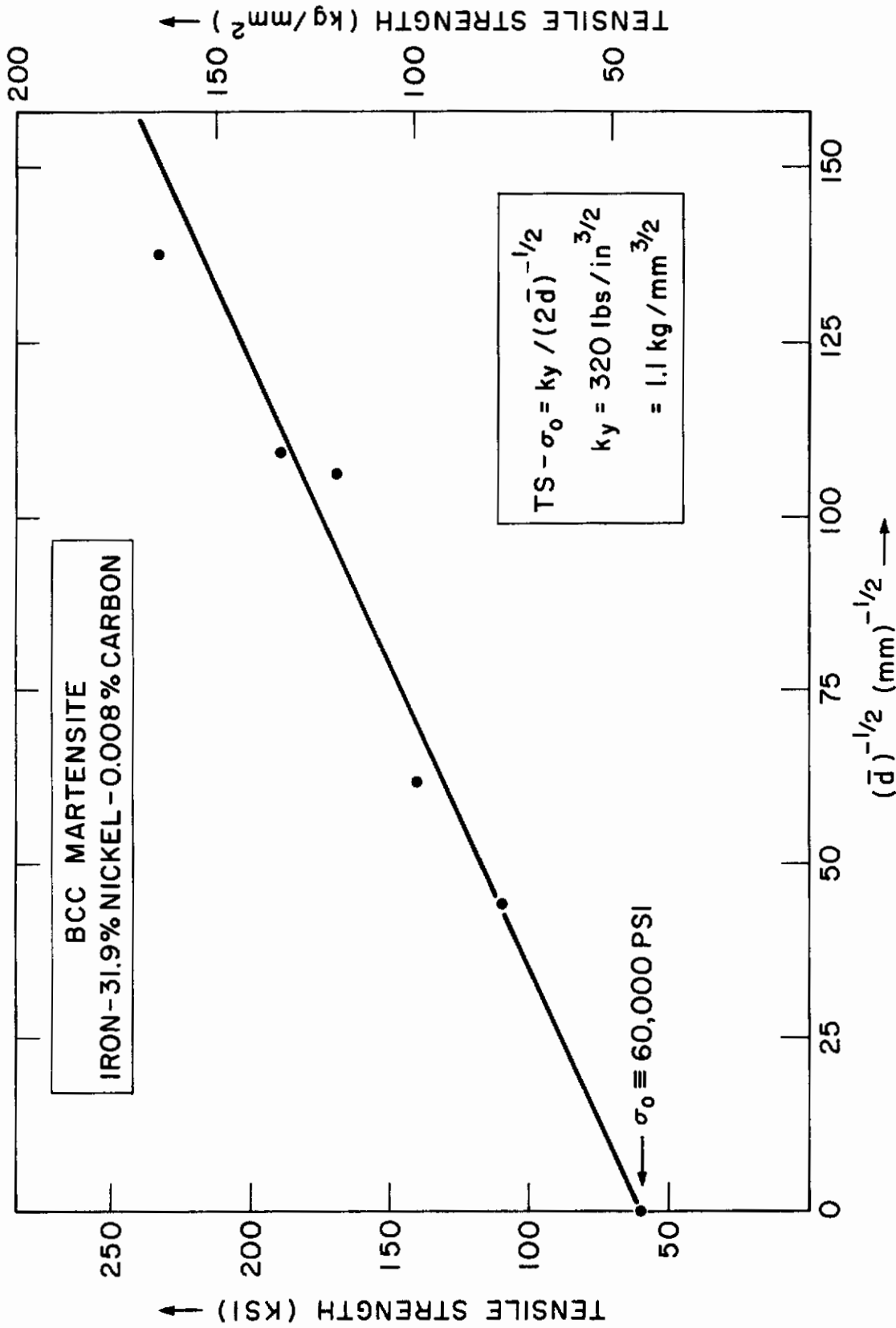
FIGURE VI-12. TENSILE STRENGTH OF WIRE-DRAWN BCC MARTENSITE AS A FUNCTION OF AVERAGE TRANSVERSE CELL SIZE, DRAWN AND TESTED AT ROOM TEMPERATURE.

114
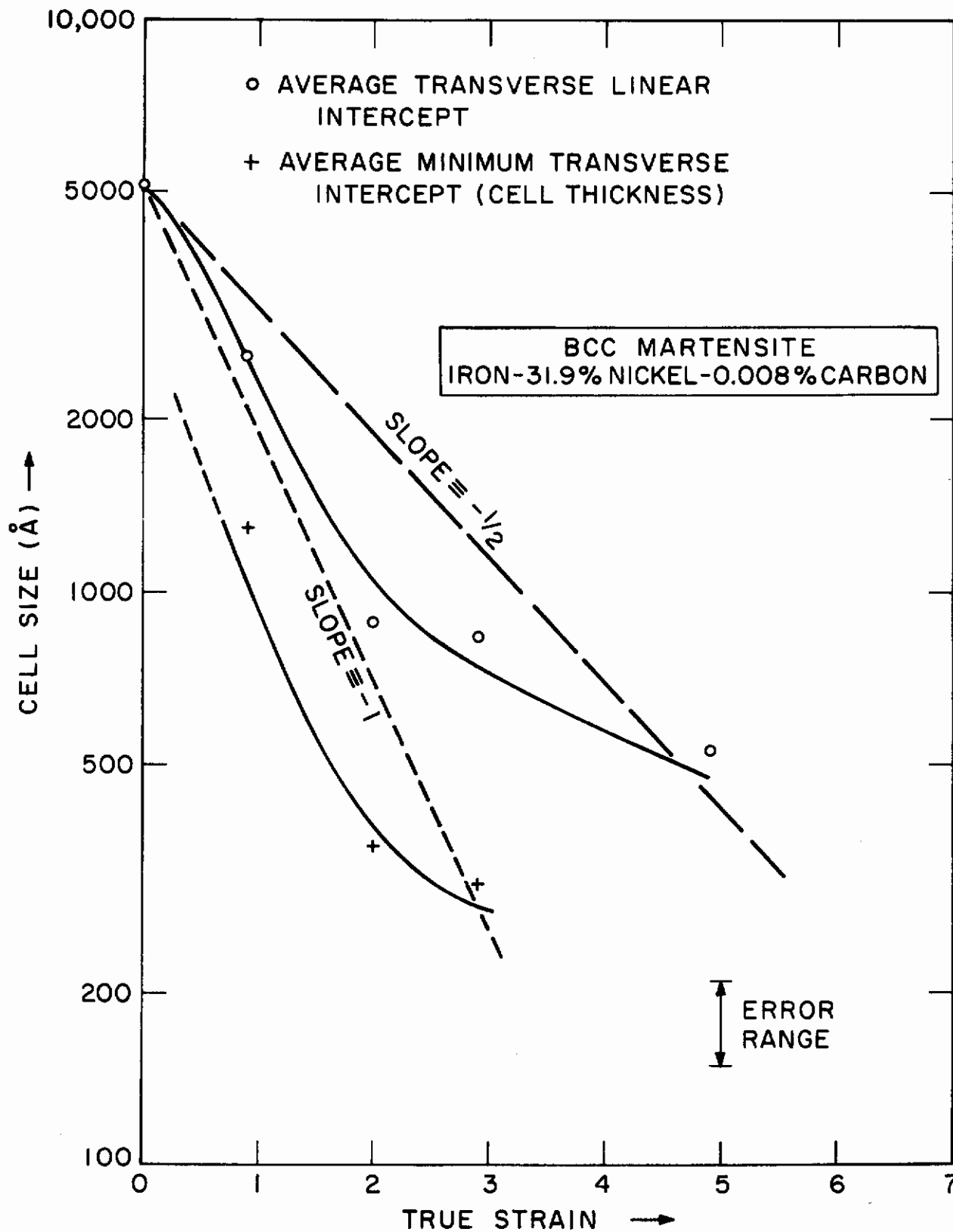
FIGURE VI-13. CELL SIZE VS. STRAIN FOR BCC MARTENSITE, WIRE DRAWN AT ROOM TEMPERATURE.

115

slope of this line corresponds to a k_y value of 320 lb/in$^{3/2}$, which is smaller than that obtained for iron in Figure VI-8.

Cohen and Taranto[2] have measured the effect of prior austenitic grain size on the ultimate tensile strength of BCC iron-nickel martensite, and the k_y value computed from their data is about 280 lb/in$^{3/2}$, when the martensitic plate thickness is taken as the effective grain-size parameter.

Figure VI-13 shows the average transverse linear intercept of the martensitic cell dimension, $\bar{d}$, as a function of strain on a log-log plot. The results are essentially the same as for the iron in Figure VI-7, except for the smaller size of the martensitic cells. No measurements of the minimum transverse cell dimensions could be made beyond a strain of 3 due to insufficient resolution in the electron micrographs. Thus it was not possible to ascertain unambiguously whether axially symmetric deformation takes place at the higher strains in the martensite, as appears to be the case in the iron.

The tensile strength minus σ_o (taken as 60,000 psi) is plotted logarithmically in Figure VI-14 against strain. The resulting curve is very similar to that for iron in Figure VI-9, except that there is a slight decrease in the logarithmic strain-hardening rate (excluding, perhaps, the region between $\epsilon = 2$ and 3). The BCC martensite (having nearly the same carbon content as the iron studied here) might be expected to undergo more dynamic recovery during the wire drawing because of its smaller cell size and higher dislocation density, compared to the iron. Alternatively, partial reversion of the martensite to austenite may take place at the high drawing strains, because the accompanying hydrostatic pressure could lower the reversion temperature of martensite to austenite by as much as 100-150°C, as estimated from the effect of pressure on the transformation characteristics.[12]

The last two stress-strain curves in Figure VI-4, which indicate more strain hardening than is evident from the tensile strength vs drawing-strain relationship, are consistent with the above martensite-to-austenite reversion mechanism. Since the tensile test involves a hydrostatic tension component, any austenite formed during drawing should be retransformed to martensite during the tensile test, thereby strengthening the specimen. The retained austenite (~15 percent) in the as-quenched martensite, on the other hand, is probably transformed to martensite in the first drawing pass, where the die pressure is much lower. Hence, the subsequent tensile curves should manifest no effect of retained-austenite transformation until sufficiently high strains (or hydrostatic pressures) are attained in the wire-drawing process to generate additional austenite.

Figure VI-15, in which the tensile strength minus σ_o is plotted against $\bar{d}$ on a log-log scale, demonstrates that there is an inverse square-root dependence of strength on the martensitic cell size, in line with the results on iron in Figure VI-12. Evidently, the main reasons for the higher strength levels reached by the BCC martensite than the BCC iron in the wire-drawing operation are to be found in the smaller cell size produced in the martensite and its larger friction stress.
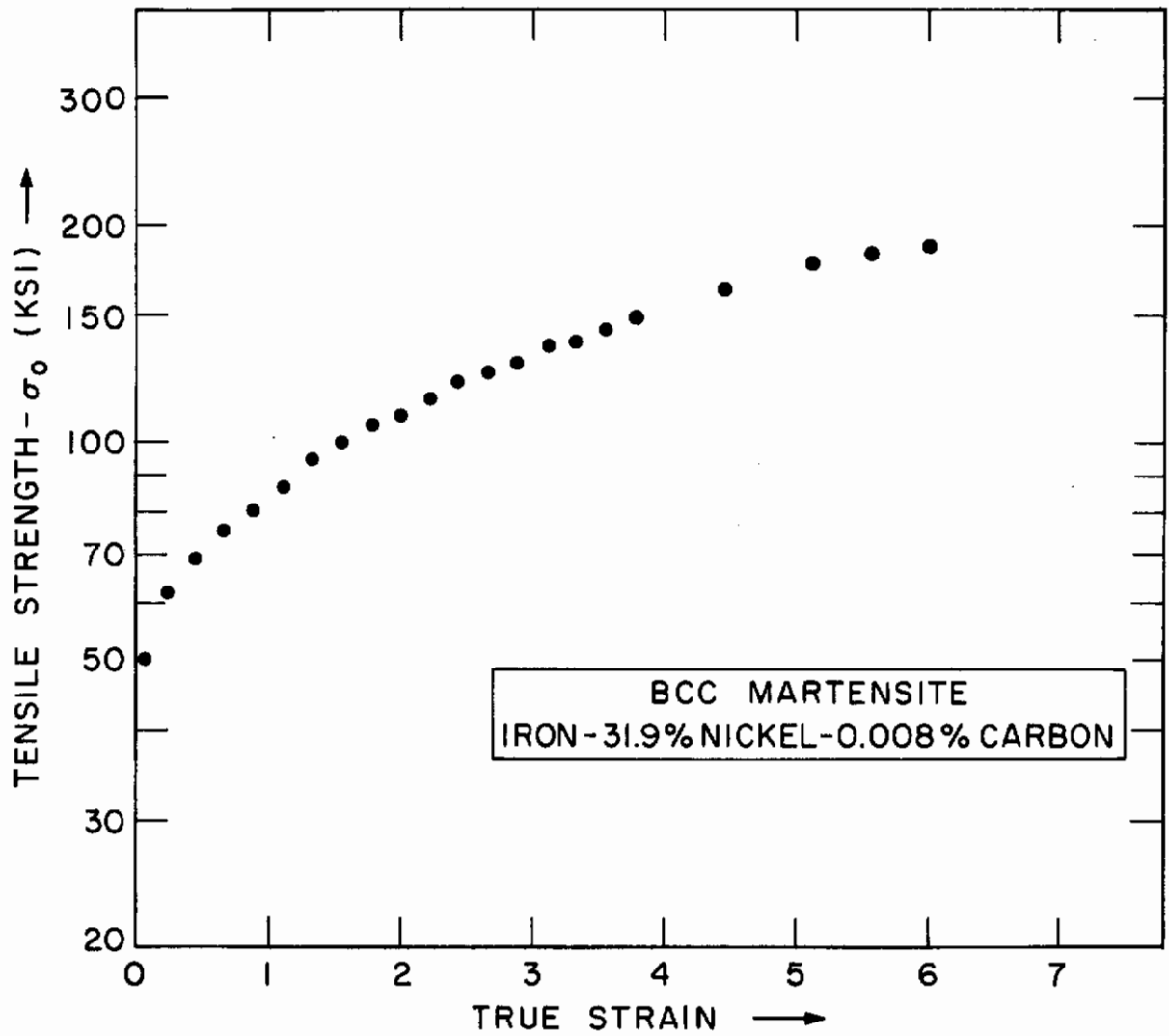
FIGURE VI-14. TENSILE STRENGTH MINUS FRICTION STRESS ($\sigma_0 = 60$KSI)
AS A FUNCTION OF WIRE-DRAWING STRAIN FOR BCC MARTENSITE,
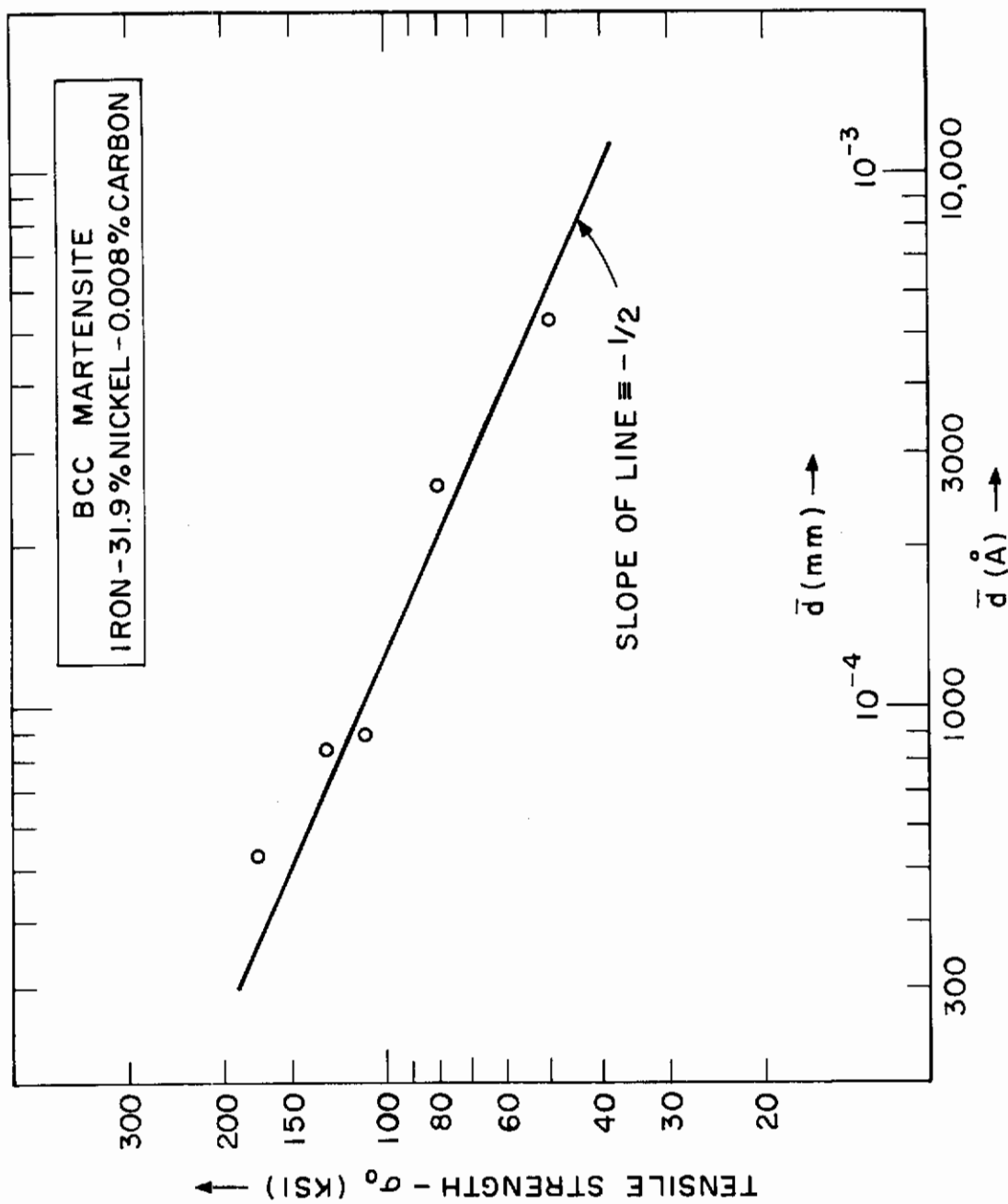DRAWN AND TESTED AT ROOM TEMPERATURE.

117

FIGURE VI-15. TENSILE STRENGTH MINUS FRICTION STRESS ($\sigma_0 = 60$ KSI) OF BCC MARTENSITE AS A FUNCTION OF AVERAGE TRANSVERSE CELL SIZE, WIRE DRAWN AND TESTED AT ROOM TEMPERATURE.

5. <u>Comparison of FCC and BCC Strain Hardening</u> – The saturation in strain hardening shown by the austenite, together with its lack of refinement in substructure, is typical of other FCC metals.[1,13] The difference in behavior between the FCC austenite and BCC martensite of the same composition is quite striking. The high degree of strain hardening in the BCC iron and martensite as well as the saturation of strain hardening in the FCC austenite depend primarily on the extent of transverse refinement of the cellular substructure. Judging from the relationship between strength and the wire-drawing strain (tensile strength vs $(\bar{d})^{-1/2}$ and $\bar{d}$ vs ϵ), there appears to be little change in the effectiveness of the slip-limiting boundaries with strain, and the strain-hardening rate is controlled mainly by the rate of refinement of the cell structure. The refinement, in turn, is governed by the complexities of the flow process and by dynamic recovery. The detailed rearrangement of the dislocations in the cell walls does not seem to be an essential factor at the high strains investigated here. However, the movement of the cell walls is an important consideration because this determines whether dynamic recovery (and, hence, only limited cell refinement) will be found, as in the case of austenite. Interstitial impurities may contribute to the strain hardening, depending on the extent to which they can inhibit cell-boundary migration. It is likely that the residual carbon is much more potent in this respect in the BCC iron and martensite than in the FCC austenite. Moreover, this difference in the role of interstitial impurities in BCC and FCC metals may be a more significant factor at play than any intrinsic difference in the strain hardenability of the two lattices.

Figure VI-16 shows some data on the strain hardening of a FCC copper –6.5 percent silver alloy taken from the work of Hodge et al.[14] This alloy was wire drawn in the solution-treated condition, and also in the aged condition after a prior strain of 1.35. The slope of the log (tensile strength minus friction stress) vs wire-drawing strain curve for the aged material is about 1/5.3, if σ_o is estimated at 20,000 psi (of Figure VI-9). The slope for the solution-treated material is much lower, and cannot be forced into the range of 1/5 unless a considerably higher friction stress (> 50,000 psi) is assumed for that condition, which is improbable. Hence, it appears that the precipitates formed in the cell walls of the drawn and aged material have pinned the boundaries. This indicates that FCC metals, like BCC metals, can be made to undergo strain hardening out to very large strains if dynamic recovery is inhibited, even if not prevented entirely.

Clearly, BCC martensites are capable of attaining high strength levels through the cell structure developed by plastic deformation, and the beneficial refinement of the cells is enhanced by the fine structure originally present in the martensite. But it is doubtful that such substructural phenomena contribute in a dominant way to the strength of martensite in quench-hardened steels. In the first place, despite the tremendous strains achieved in wire drawing, the maximum strength level reached by the BCC martensite falls far short of the strength of a regular 0.4 percent carbon tetragonal martensite. Secondly, although some tetragonal martensites contain high densities of entangled dislocations arranged in cellular
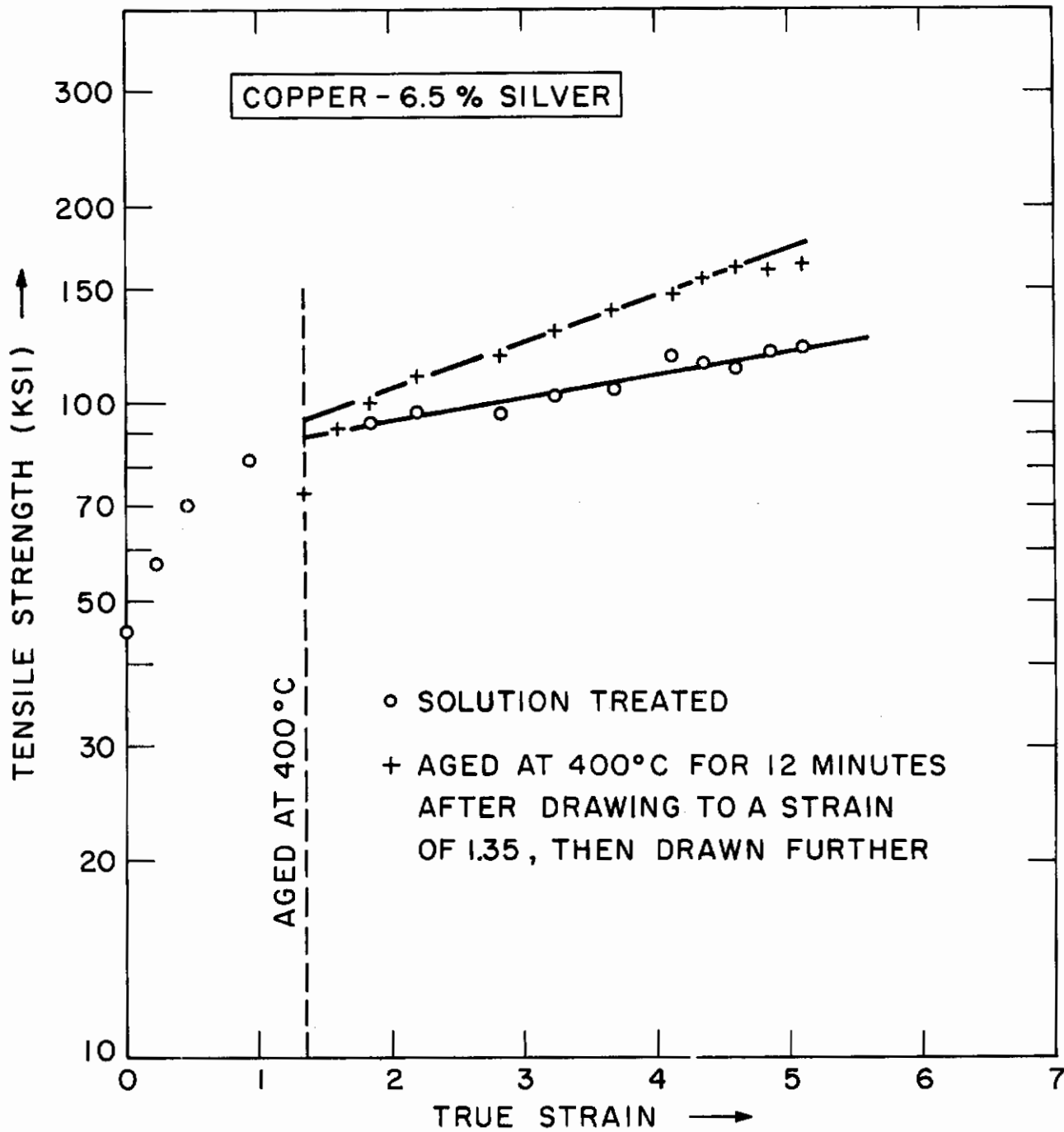
119

FIGURE VI-16. STRAIN HARDENING OF A COPPER-SILVER ALLOY, WIRE DRAWN AND TESTED AT ROOM TEMPERATURE. AFTER HODGE et al.[17]

fashion, the cell sizes are much larger than the fine dimensions obtained by wire drawing. Thirdly, as previously noted, the marked cellular refinement observed in the latter case is probably dependent on the presence of carbon to inhibit migration of the cell walls. Accordingly, even here, carbon remains a major factor in the strengthening of martensite by plastic deformation.

D. Conclusions

1. In the wire drawing of iron (0.006 percent carbon) as well as low-carbon (0.008 percent carbon) iron-nickel martensite and austenite, elongated cells or subgrains are formed, and the transverse dimensions of these cells appear to govern the strain-hardening characteristics. However, the shape of the cells may vary in a complex way with the drawing strain.

2. The cell boundaries are effective barriers in inhibiting slip, and the resulting strength is inversely proportional to the square root of the average transverse dimension of the cells, as in the Petch relation for grain-size strengthening.

3. In the BCC metals, the shape change of the cells is influenced by the wire texture at strains less than about 2, but at strains above 2 there is no apparent effect of the texture on strain hardening.

4. At high strains, the refinement of the cell structure in both the BCC and FCC phases is controlled by dynamic recovery; i.e., the cell cross section does not reduce in proportion to the wire section because the number of cells decreases through the merging of cell boundaries. However, the rates of such dynamic recovery are quite different in the two cases, probably due to the marked ability of interstitial impurities in BCC metals to interfere with cell-wall movements.

E. References

1. J.F.Peck "The Structure, Hardness and Texture of Columbium Wires," MIT Ph.D.Thesis, 1963 (Metallurgy).

2. M.Cohen and J.Taranto "Strain Hardening and Ausforming in an Iron-Nickel Alloy," ARL-63-124 (July, 1963). Wright-Patterson AFB, Ohio.

3. J.G.Wistreich "An Investigation of the Mechanics of Wire Drawing I, II," Wire Industry 22 (1955) 421,509.
See also: "The Fundamentals of Wire Drawing," Metallurgical Review 3 (1958) 97.

4. P.W.Bridgman, "The Stress Distribution at the Neck of a Tension Specimen," Trans.ASM 32 (1944) 553.

5. J.F.Peck and D.A.Thomas, "A Study of Fibrous Tungsten and Iron," Trans.AIME 221 (1961) 1240.

6. W.F.Hosford,Jr. "Microstructural Changes During Deformation of [Oll] Fiber-Textured Metals," Trans.AIME 230 (1964) 12.

7. E.S.Meieran "Transmission Electron Microscope Study of Deformed and Annealed Tungsten," MIT ScD.Thesis, 1963 (Metallurgy); also E.S.Meieran and D.A.Thomas, "Structure of Drawn and Annealed Tungsten Wire," Trans.AIME 233 (1965) 937.

8. A.S.Keh and S.Weissman "Deformation Substructure in Body-Centered Cubic Metals," in Electron Microscopy and Strength of Crystals, Ed. by G.Thomas and J.Washburn, Interscience,New York (1963) p.231.

9. J.D.Embury and R.M.Fisher "The Structure and Properties of Drawn Pearlite," E.C.Bain Laboratory of U.S.Steel Corp.Report No.PR 288 (March,1965) to be published in Acta Met.

10. D.McLean, Mechanical Properties of Metals, Wiley, New York (1962) 199.

11. G.R.Speich and P.R.Swann, "The Yield Strength and Transformation Substructure of Quenched Fe-Ni Alloys" E.C.Bain Laboratory of U.S.Steel Corp.Report No. PR 261 (July,1964), to be published in JISI.

12. L.Kaufman,A.Leyenaar and J.S.Harvey, "The Effect of Hydrostatic Pressure on the Potency of Martensitic Embryos," Acta Met.8 (1960) 270.

13. J.D.Embury,A.S.Keh,and R.M.Fisher, "Substructural Strengthening in Materials Subject to Large Plastic Strains," E.C.Bain Laboratory of U.S.Steel Corp.Report No. 1236 (September,1965), to be published in Trans.AIME.

14. W.Hodge, R.I.Jaffee, J.G.Dunleavy, and H.R.Ogden, "A High Strength - High Conductivity Copper-Silver Alloy Wire," Trans. AIME 180 (1949) 21.

VII. MODES OF FRACTURE IN MARTENSITE

U. H. Lindborg[*] and B. L. Averbach

A. Introduction

Detailed studies of fracture in martensitic steels are rendered difficult because of the small crystallite size, often about 1μ. However, transmission electron microscopy and selected-area diffraction provide a possible technique for dealing with the fine scale of martensitic structures and the related paths of fracture.

Previous work[1-8] has shown that room-temperature fracture in martensite proceeds both by ductile and by brittle mechanisms. Replicas of fracture surfaces often reveal characteristic cavities or dimples, caused by extensive void formation in ductile modes of fracture.[3-6] Flat areas are also present in the case of as-quenched or lightly tempered martensites.[2,3] These areas resemble true cleavage, as observed in ferrite, but show additional ductile features.[2] The fractographic studies suggest that the path of fracture in martensite is transgranular at room temperature, at least with respect to the prior austenite grains. This interpretation is supported by replication work on side surfaces or on sections through the fracture after the fracture surface has been plated.[3] At -195°C, however, untempered or temper-embrittled specimens break partly in an intergranular mode following prior austenitic grain boundaries,[7,8] as determined from replicas of fracture surfaces and sections. The relation between the fracture path and the aggregate of martensitic platelets remains uncertain. Side-surface replicas[3] suggest that the fracture path may be at least partly transgranular with respect to the platelets, but this interpretation is only tentative. The crystallography of fracture in martensite does not appear to have been treated previously.

The present investigation was based on transmission electron microscopy of thin areas formed near the fracture of martensitic specimens $5 - 10\mu$ thick. The properties considered were (a) the crystallographic planes preferred for fracture, (b) the width of the deformed zone near the crack, thereby giving a measure of the amount of local deformation to fracture, and (c) the over-all path of fracture. The results were obtained on fairly thin specimens, which may not have been wholly representative of bulk material. Where a cross-check was possible, however, as in the case of ferrite, the thin-foil results agreed with the findings on bulk specimens.

B. Experimental Procedures

1. <u>Material for Study</u> - The material chosen for the present investigation was a high-purity iron-carbon alloy containing 0.3 percent carbon (Table VII-1). This carbon content was sufficiently high to avoid the formation of pearlite and bainite during quenching to produce martensite, and yet was sufficiently low to minimize the amount of retained austenite.

---

[*] Now at Aktiebolaget Atomenergi, Stockholm, Sweden.

The as-quenched microstructure consisted of martensitic plate-
lets and needles with a high internal dislocation density. Some
groups of {211} twins were noted in the martensite, but the spac-
ings were rather large, about 500 Å, suggesting that these twins
were not transformation twins but resulted from inadvertent de-
formation. Presumably the second or heterogeneous shear in the mar-
tensitic transformation took place by dislocation movements rather
than by twinning. The arrangement of crystallites was similar to
that observed by Kelly and Nutting[9] in martensitic low-carbon
steels, with needles or sheet-like groups of needles having a $<111>_M$
axis.

TABLE VII-1

Composition of Iron-Carbon Alloy for Fracture Studies

(weight percent)

C	Mn	P	S	Si	Al
0.293	0.002	0.002	0.004	0.006	0.002

Cr	Ni	Cu	O	N
0.013	0.001	0.005	0.001	None found

2. <u>Specimen Preparation</u> - The specimens for these fracture
studies consisted of foils less than 10μ thick. The hardening oper-
ation was usually performed on 2 mm thick specimens. Austenitizing
was carried out at 900°C for 20 minutes in an argon atmosphere, and
was followed by quenching in iced brine. Tempering was subsequently
conducted in air furnaces for 1 hour at various temperatures.

The specimens were thinned in several stages: (a) surface
grinding, (b) chemical polishing (1.1 part orthophosphoric acid 85
percent, 1 part hydrogen peroxide 30 percent), and (c) electrothin-
ning in a solution of chromic acid and acetic acid according to the
method of Glenn and Raley.[10]

Pieces of thin foil were cut from the edges of the originally
12 mm square specimen with a pair of fine scissors. The foil pieces
were typically 1 × 3 mm, and the average thickness was about 5μ. In
some instances the foils were transparent to the electron beam over
large areas, i.e., less than 0.3μ thick.

3. <u>Fracturing and Examination of Specimens</u> - When the foils
were to be fractured, they were placed on a glass microscope slide
and cracks were generated by means of a sharp needle. Certain

groups of specimens were fractured in a shallow dish under a layer of liquid nitrogen with no other changes in the procedure.

The specimens were subsequently examined in a Siemens electron microscope at 100 kV without any further thinning. Transparent areas formed along the fracture paths partly because of local plastic deformation preceding the fracture and partly because of the obliqueness of the fracture surface. Selected-area electron diffraction of these regions usually gave complicated diffraction patterns. The edge of each crack was followed in search of areas giving simple single-crystal patterns.

The direct output of this transmission electron microscopy was a set of electron micrographs and the corresponding diffraction patterns. It was found that the fracture path consisted of more-or-less distinct segments. The angles between each of these segments and the photograph border were measured and similar orientation measurements were made on the diffraction patterns, taking into account the inherent rotation between the micrograph and the diffraction pattern in the electron microscope.[11] Figure VII-1 illustrates how the fracture segments were related to the crystallographic lattice and to the general or over-all direction of crack propagation. Histograms were constructed for the angular distributions of the segments relative to the crystal lattice and to the general direction of crack propagation. The width of the transparent zone along the fracture path was estimated at five equidistant points and then averaged.

C. Discussion of Results

1. **Appearance of Fracture** - Figure VII-2 shows two cracks in an untempered martensitic foil which was transparent to the electron beam before the fracture. The cracks cut right across several groups of martensitic needles, indicating that the mode of fracture is transcrystalline here, even with respect to the martensitic crystallites.

Figure VII-3 illustrates the fracture in thicker, tempered (260° for 1 hour) foils. There is evidence that some plastic deformation and dislocation motion took place prior to, or along with, the fracturing process. The crack edge in Figure VII-3a, however, gave a sharp single-crystal diffraction pattern, with no sign of distortion. If dislocations took part in the fracturing process their relative absence suggests that they were annihilated at the free fracture surface. The existence of the sharp diffraction patterns along the fracture path was the rule rather than the exception, and made orientation determinations possible. In Figure VII-3b, on the other hand, both the micrograph and the diffraction pattern denote a heavily cold-worked structure. Regions like this were encountered occasionally in as-quenched martensite fractured at 25°C and -195°C, and in ferrite fracture at -195°C. Such areas may be the remains of slip bands formed ahead of the propagating cracks. The strongly localized deformation could then have strain hardened the material to the point that the dislocations may have become locked in tangles, preventing annihilation.

Figure VII-4 illustrates the appearance of room-temperature fracture in a relatively soft specimen, martensite tempered at 480°C.
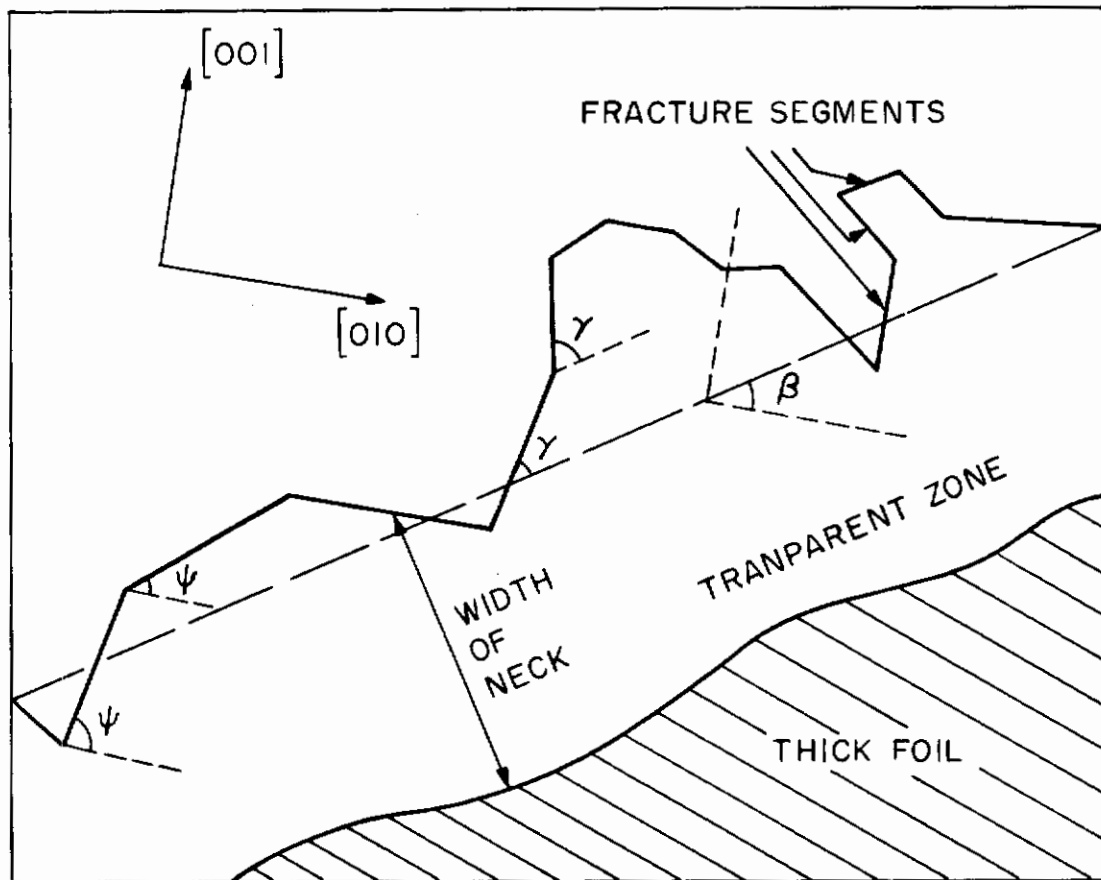
—— GENERAL DIRECTION OF CRACK PROPAGATION

ψ   ANGLE BETWEEN FRACTURE SEGMENT
AND [010]

γ   ANGLE BETWEEN FRACTURE SEGMENT AND
GENERAL DIRECTION OF CRACK PROPAGATION

β   ANGLE BETWEEN GENERAL DIRECTION OF
CRACK PROPAGATION AND [010]

FIGURE VII-1 DEFINITION OF ANGULAR MEASUREMENTS
IN ELECTRON MICROSCOPY OF FRACTURE PATHS IN
MARTENSITE.
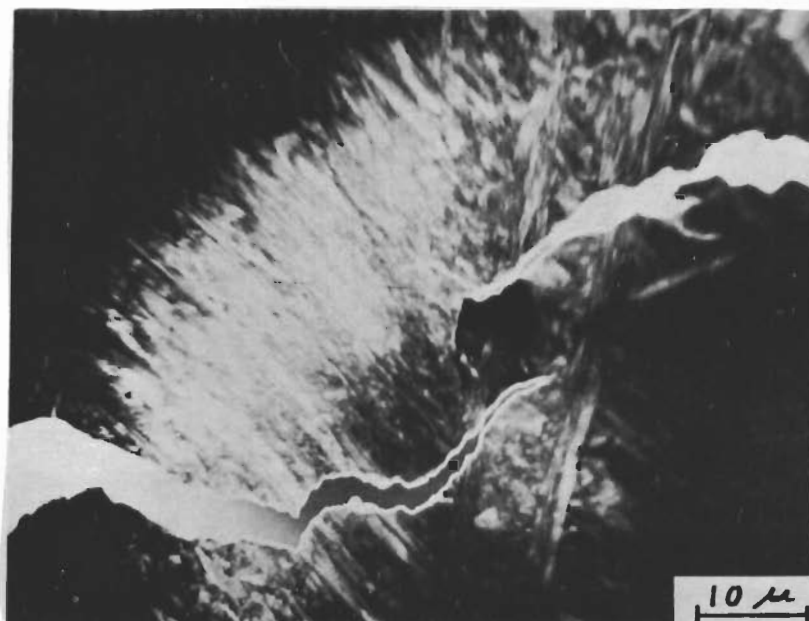
FIGURE VII-2. Transcrystalline Cracks in As-quenched
0.3 Percent Carbon Martensite. Transmission
Electron Micrograph, 1600X
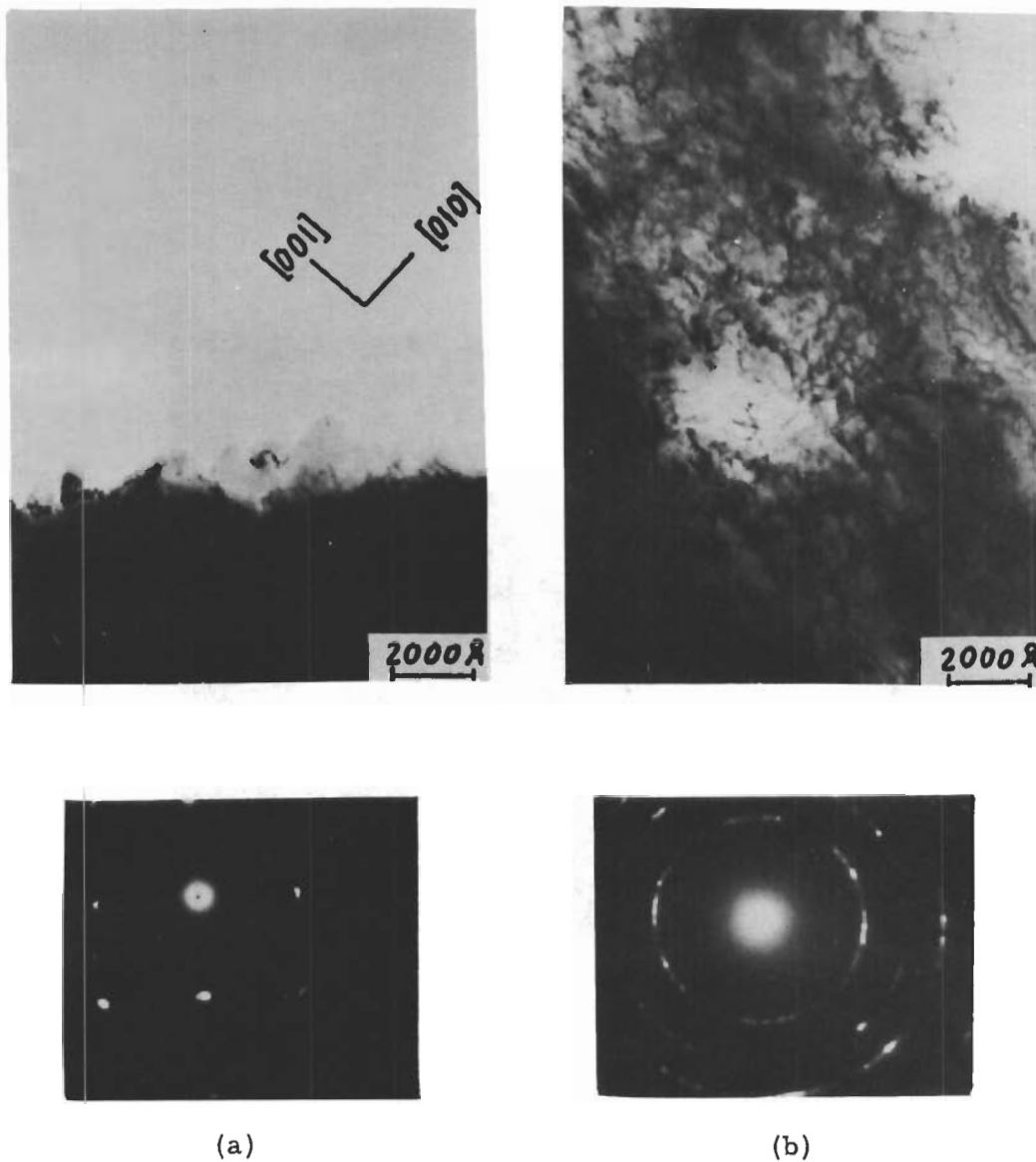
FIGURE VII-3. Transmission Electron Micrographs and Diffraction
Patterns from Fracture Edges of Specimen Tempered
at 260° C, 1 Hour. 60,000X
(a) Left, Single-crystal Edge; Diffraction Pattern
Corrected for Rotation in Microscope.
(b) Right, Heavily Cold-worked Tongue in Fracture
Path, Polycrystalline Diffraction Pattern.

128
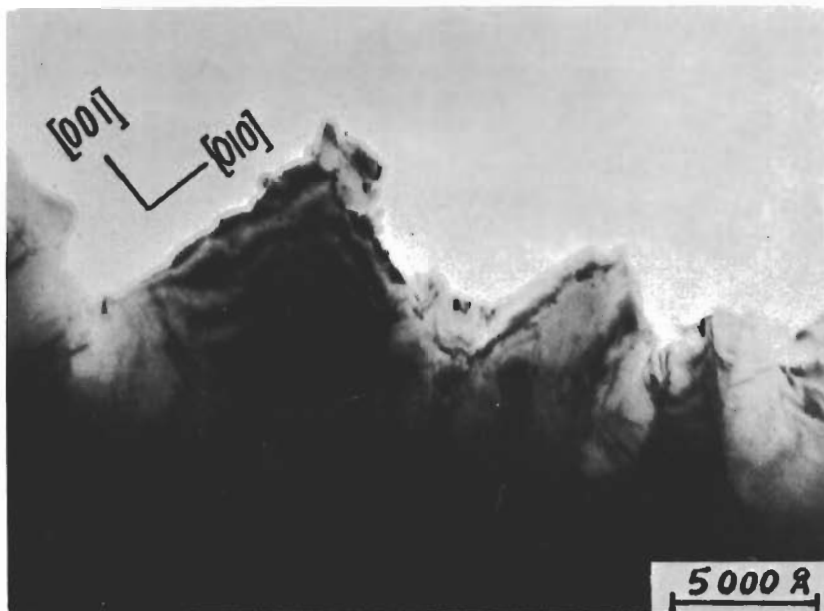
FIGURE VII-4. Transmission Electron Micrograph of Fracture
Edge in Specimen Tempered at 480° C.   60,000X

129
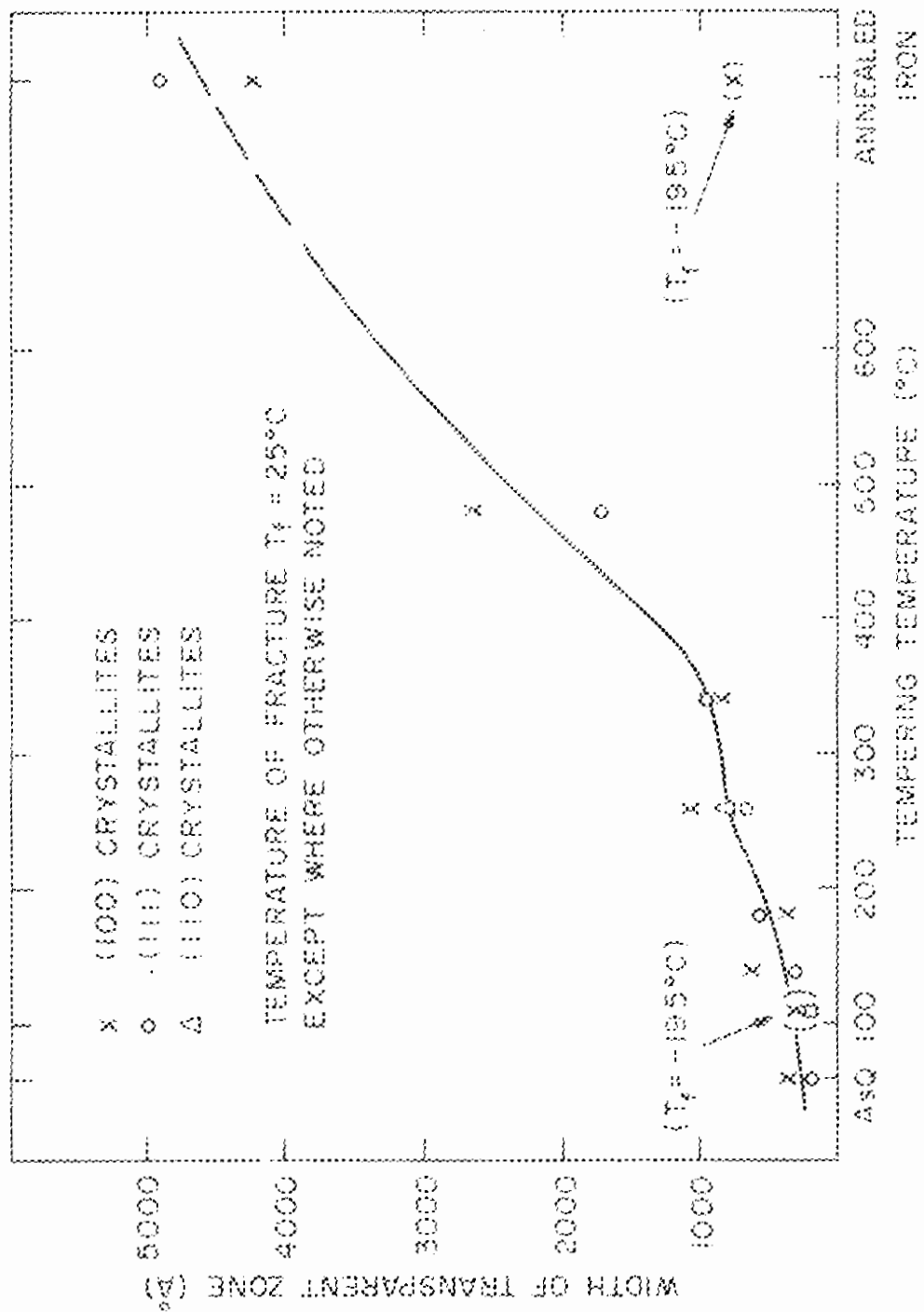
FIGURE XIII-5 WIDTH OF ELECTRON-TRANSPARENT ZONE ALONG FRACTURE PATH
VS TEMPERING TEMPERATURE
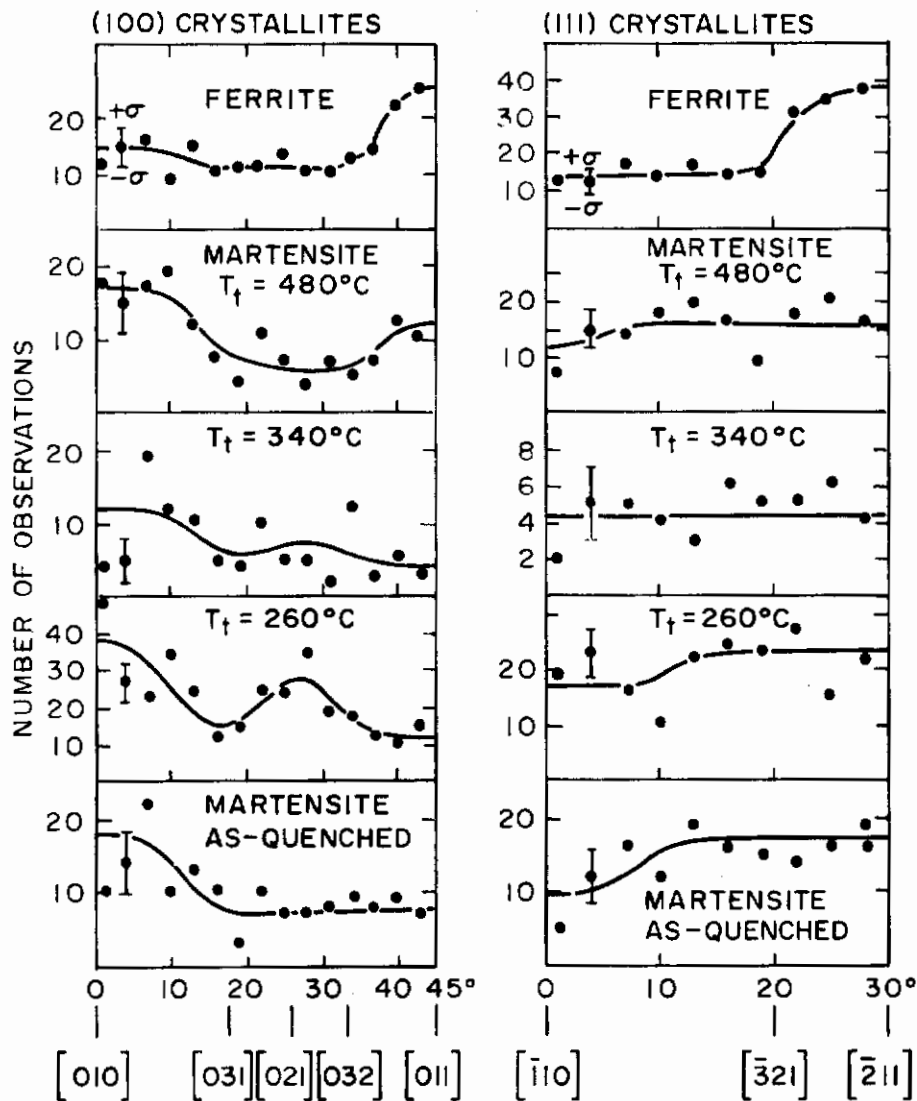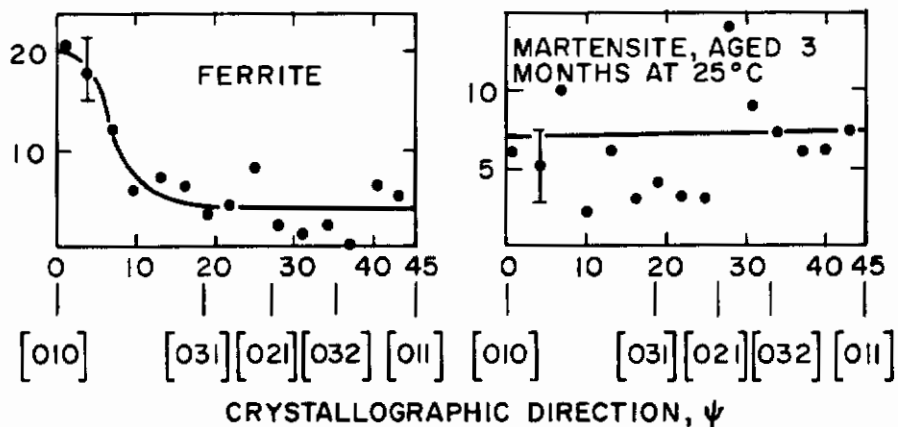
FIGURE VII-6 DISTRIBUTION OF FRACTURE SEGMENTS OVER CRYSTALLOGRAPHIC DIRECTIONS. T_t = TEMPERING TEMPERATURE.

The transparent area along the crack edge was considerably wider than in the material tempered at 260°C.   In fact, there was a pronounced tendency for this zone to widen with increasing tempering temperature, as shown in Figure VII-5.   This zone represented a measure of the local elongation to fracture, i.e., the local ductility, and increased from 200 - 300 Å for as-quenched foils to 4000 - 5000 Å for iron foils on fracturing at 25°C.   When the fracturing temperature was lowered to -195°C, the transparent zone in the iron narrowed significantly, but the zone in the martensite was hardly affected.

The crack edge was found to change direction repeatedly, even side each crystallite of martensite.   Typically, 20 or more of such segments could be distinguished in each crystallite, and the segments tended to be straight.   This observation offered further evidence of the transcrystallinity of fracture in the martensite, whether tempered or untempered.   Most of the crystallites had their {100} planes parallel to the foil surface, but other orientations, particularly {111}, were regularly encountered.

2. $\underline{\text{Crystallography of Fracture}}$ -   The distribution of the crystallographic angle ψ , defined in Figure VII-1, is presented in Figure VII-6.   The analysis is restricted to crystallites in the two most common orientations, (100) and (111), and ψ is the angle between any given fracture segment and the [010] direction.   Each plot corresponds to a particular combination of tempering temperature, fracturing temperature and crystallite orientation.   On the average, each plot is based on about 200 fracture segments.

The symmetry involved made it possible to reduce the measurements to the region 0 - 45° for the (100) crystallites and 0 - 30° for the (111).   In the case of (100), for instance, measurements of 18°, 72°, and 108° could then be counted as 18°.   The histograms were based on 3° intervals to obtain the orientation distributions. The error bars in Figure VII-6 indicate the standard deviation of a plotted point, estimated as the square root of the number of readings.   A chi-square analysis was employed to test for the validity of the peaks in Figure VII-6.   In this test a uniform, horizontal-line distribution of the angular measurements was assumed, and the probability calculated that a random sample would give no better fit to this line than the experimental points.   The probability turned out, for example, to be as low as 0.1 percent for the (100) crystallites tempered at 260°C, and for the (111) crystallines in ferrite; the distribution peaks determined for such specimens must be considered to be well established.   On the other hand, for the case of the (100) crystallites in ferrite, the probability of random orientations was as high as 10 percent, rendering the peak at 45° of borderline significance.

Nevertheless, certain general features become evident.   In each box of Figure VII-6 there is a background of a considerable "intensity," indicating that fracture can take place in many crystallographic directions.   In addition, there are some pronounced peaks, showing that special fracture directions and planes are preferred. The peaks are fairly broad, the full width at half-height being approximately 15°, and the peaks at 0° are about 25°, compared to an estimated error in the angle measurements of ± 3 - 4°.   Thus, the broader peaks designate real deviations from the most favorable crys-

132

tallographic directions. The positions of the peaks vary as the
martensite structure is changed by tempering treatments. An attempt
will now be made to deduce the preferred fracture planes from the a-
vailable data.

(100) Crystallites: Looking first at the curves for the (100)
crystallites in Figure VII-6, one notices that ferrite exhibits a
diffuse peak at 0°, i.e., in the [010] direction, and another more
pronounced peak at 45°, i.e., in the [011] direction, superimposed
on a fairly high background. Martensite tempered at 480°C shows
the same peaks, but their relative heights are now different. Tem-
pering at 260°C produces a strong peak at an intermediate angle,
about 27°, and traces of this peak may also be present after temper-
ing at 340°C. As-quenched martensite gives only one peak, at 0°.

In order to rationalize these peaks we consider the intersec-
tions of possible fracture planes with the (100) surface of these
crystallites. The {110}, {211} and {321} families have been ob-
served to be slip planes in ferrite, with some preference for {110}
at room temperature, and we now inquire whether any of these planes
would provide a good fit with the experimental results. {110} frac-
ture planes would give ψ angles at 0° and at 45°; {211} at 26.6°
and 45°, and {321} at 18.4°, 26.6° and 33.7°. On the other hand,
{100} cleavage planes should only yield a ψ angle of 0°. For the
(100) crystallites, then, the peaks at 0° and 45° may be attributed
to fracture on {110} planes, while the high background suggests that
planes like {211} and {321} may also contribute to the fracture. It
therefore appears likely that the fracture process is one of shear
rupture after deformation on these slip planes, although cleavage
separation on these planes cannot be ruled out.

The prominent 0° peak found in as-quenched and tempered marten-
sites fractured at room temperature suggests that {100} cleavage
also occurs, but not in the more ductile ferrite. The 27° peak
after tempering at 260°C must be ascribed to fracture on planes like
{211} or {321}, inasmuch as the {110} and {100} planes do not in-
terest the (100) crystallite surface anywhere close to the ψ posi-
tion of the peak. This effect will be explained later in terms of
the precipitation of cementite.

(111) Crystallites: The results for (111) crystallites in
the right-hand half of Figure VII-6 show less detail than those for
(100) because a larger number of available fracture systems can in-
tersect the (111) foil surface. Fracture on {110} planes would
give ψ angles at 0° and at 30°; {211} at 0° and 19.1°; and {321}
at 10.9°, 13.9°, 23.4° and 30°. Cleavage on {100} would only give
a ψ angle of 0°.

The pronounced peak for ferrite at ψ = 30° is consistent with
{110} being the preferred fracture plane, but then a peak at 0°
would also be expected to appear. Fracture is governed, however,
by the resolved stresses in the plane of fracture, and the absence
of fracture on certain members of a family of planes may be due to
low resolved stresses on those planes.

There are no definite ψ-peaks for the (111) crystallites in
untempered and tempered martensite. The absence of a peak at ψ = 0,

the direction for {100} cleavage, implies that such cleavage occurs less frequently than in the case of (100) crystallites. The reason for this discrepancy probably lies in the fact that the {100} planes in (111) crystallites are subjected to lower resolved normal stresses during the fracture loading than are the {100} planes in the (100) crystallites. This comes about because the potential cleavage planes are normal to the foil surface in the latter case, whereas they are inclined in the former case.

Effects of Fracturing Temperature: Similar fracturing experiments were conducted at -195°, and the ψ-angles measured. However, no experimentally significant difference from the room-temperature behavior were observed, except for the ferrite (Figure VII-6). In this instance a ψ-peak appeared at 0° in the (100) crystallites of ferrite, in contrast to a peak at 45° when the ferrite was fractured at room temperature. This difference in ψ-distribution reflects the change in the predominant fracture mode from shear to cleavage with decreasing test temperature, as is well known in bulk ferrite.

In the martensite case there is no similar increase in the amount of cleavage on lowering the fracture temperature to -195°C. This lack of a transition temperature for the fracture mode in martensite, at least down to -195°C, may account for the absence of a sudden embrittlement range in bulk martensite when tested at subzero temperatures.

3. **Propagation of Fracture** - In addition to the crystallographic distribution of the individual fracture segments in the crystallites, the average fracture-propagation direction was also measured for each crystallite (Figure VII-1) and expressed in crystallographic coordinates, β. This average direction would be expected to be a function of the state of stress during the fracturing operation, as well as the crystallographic anisotropy just discussed. The width of the transparent zone along the fracture path might, in turn, be sensitive to the general direction of fracture, since the latter could be related to the amount of deformation preceding fracture.

The transparent width versus the average direction of propagation (relative to [010] in (100) crystallites is shown in Figure VII-7 for ferrite and for martensite tempered at 480°C. Each point here represents one crystallite. For these ductile materials the propagation directions occur uniformly over the entire range of β-angles, indicating that anisotropy of the crystallites does not have much influence on the direction of fracture, at least for the conditions at hand. However, the transparent zone widths are markedly dependent on the propagation angle, reaching a maximum at $\beta = 45°$, i.e., in an <011> direction. Figure VII-4 is an example of a wide transparent zone, resulting from such a propagation angle. It turns out that, in (100) crystallites, slip in the regular [111] and 111 directions is favored when the fracture path extends in the [011] direction, and hence the transparent zone should be maximized(due to the thinning that accompanies plastic deformation) when $\beta = 45°$, as in Figure VII-7.

4. **Carbide Precipitation and Fracture** - There are several

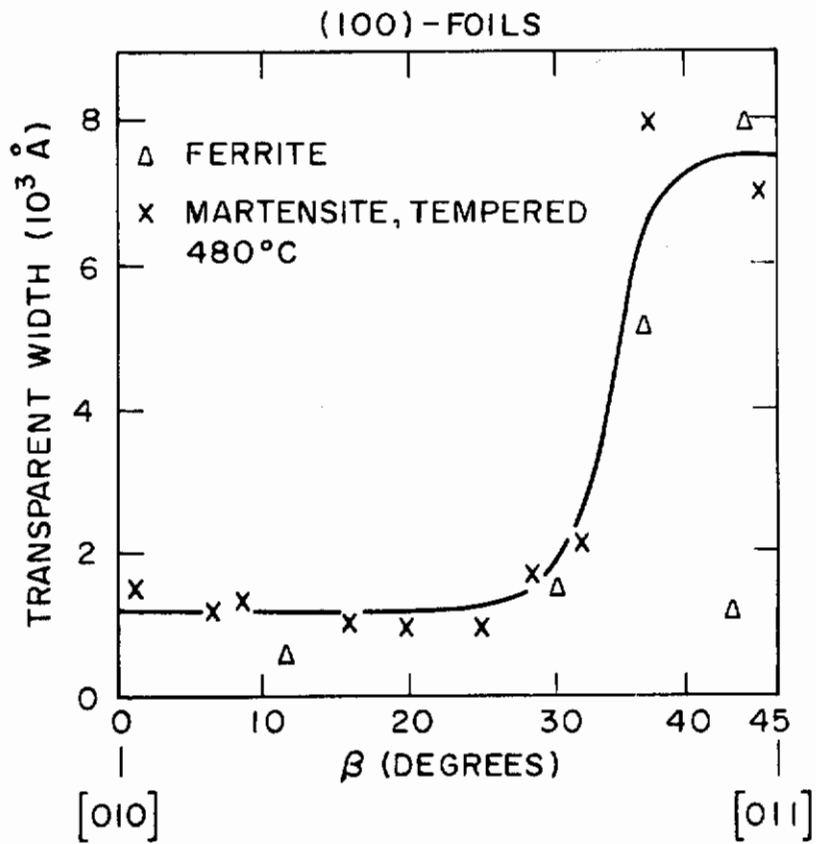FIGURE VII-7 WIDTH OF ELECTRON-TRANSPARENT
ZONE AS FUNCTION OF CRACK-PROPAGATION
DIRECTION, β. SPECIMENS FRACTURED AT 25°C.

ways by which precipitated carbides may influence the fracture process in tempered martensite. An obvious assumption is that they may cause cracking along the carbide-habit plane due to some weakness in the carbide-matrix interface. The habit planes are $\{100\}_M$ and $\{110\}_M$ for ϵ-carbide and cementite, respectively, but such

fracture planes do not become more prominent as a result of tempering. Another possibility is that the fracture of tempered martensite might be nucleated by the cleavage of carbide particles, but no evidence of this was found. Alternatively, coherency strains near the particle-matrix interfaces might favor some particular mode of fracture. Both ϵ-carbide and cementite precipitate on well-defined crystallographic habit planes and with definite lattice relationships to the matrix, apparently to minimize coherency strains. Such strains might exist during the early stages of precipitation, i.e., at a tempering temperature of about 100°C for ϵ-carbide and 200°C - 300°C for cementite. It would then be the shear components of the coherency strains on the crystallographic slip planes that should be considered since fracture appears to occur by a shear mechanism for these intermediate tempering temperatures.

The coherence strains have been calculated for each of the carbide phases, assuming perfect coherency and a BCC lattice parameter of 2.86 Å for the matrix. The results listed in Table VII-2 are further based on the carbide lattice parameters and orientations relationships reported by Pitsch and Schrader.(12,13) The strains are taken to reside in the matrix, but the arguments below will remain valid if only a portion of the coherency strain is accommodated by the matrix, provided that proportionality constant is the same for the components of strain in different directions.

It is now necessary to resolve these coherency strains into components lying along a <111> slip direction on the indicated slip planes $\{110\}$, $\{211\}$ and $\{321\}$. This can readily be done by tensor methods. However, in each case the strain normal to the habit plane is set equal to zero because no strain is required in that direction to maintain registry of the two lattices across the habit plane. The resulting shear strains are (101) - 13.4 percent, $(2\bar{1}\bar{1})$ - 13.3 percent and $(3\bar{1}\bar{2})$ - 13.8 percent for the ϵ-carbide; and $(\bar{1}10)$ - 2.88 percent, $(\bar{2}11)$ - 3.32 percent, and $(\bar{3}21)$ - 3.26 percent for the cementite.

From this tabulation we see that, when ϵ-carbide forms, the prominent slip-plane families are strained to nearly equal extents by the existence of coherency, and so tempering to this stage should not favor one set of planes over another for either slip or subsequent fracture. This situation changes when cementite precipitates (say at 260°C) because then the coherency strains are about 15 percent higher on the $\{211\}$ and $\{321\}$ planes than on the 110 planes. Such coherency effects could account for the observed intermediate ψ-peak in the (110) crystallites after tempering at 260°C (Figure VII-6).

D. Conclusions

1. Martensitic foils 5 - 10μ thick have been fractured with a needle, and electron-transparent zones have been found along the

136

TABLE VII-2

Coherency Strains Produced by ϵ-carbide and Cementite

in a Body-Centered Cubic Lattice

Ferrite or Martensite BCC (a_o = 2.86 Å)		ϵ-Carbide, Hexagonal (a = 2.73 Å, c = 4.33 Å)		Relative Strain
Plane	Interatomic Distance (Å)	Plane	Interatomic Distance (Å)	Percent
100	2.86	$1\bar{1}1$	3.20	11.9
010	2.86	$11\bar{1}$	3.20	11.9 (normal to habit)
001	2.86	110	2.73	-4.5

Ferrite or Martensite BCC (a_o = 2.86 Å)		Cementite, Orthorhombic (2.54, 5.52, 6.74 Å)		Relative Strain
Plane	Interatomic Distance (Å)	Plane	Interatomic Distance (Å)	Percent
$01\bar{1}$	4.04	100	4.52	11.0 (normal to habit)
$\bar{1}11$	2.50	010	2.54	1.6
211	7.00	001	6.74	-3.7

137

fracture paths. The zones are thinned regions produced by plastic deformation prior to fracture, and increase in width with increasing tempering temperature.

2. The fracture paths in untempered or tempered martensite are transgranular with respect to the martensitic crystallites. Across each crystallite, the fracture is composed of many segments, whose crystallographic distributions provide information about the predominating fracture planes. At room temperature, the as-quenched martensite fractures on multiple planes, but exhibits some preference for {100} planes, thus indicating a cleavage mechanism. On tempering at 260°C, where cementite precipitates, {211} and {321} fracture planes also become operative. These modes of fracture are considered to be shear types, and they seem to be favored by cementite coherency strains. Similar analysis of the ϵ-carbide coherency strains indicates no preference for any of the main competing fracture planes. On tempering at 480°C, and also in ferrite, shear fracture on {110} planes dominates.

3. The fracture modes in martensite are not sensitive to the test temperature down to -195°C, but in ferrite the fracture changes to cleavage on {100} with decreasing test temperature. These findings are in line with previous observations on bulk specimens in which ferrite displays a conspicuous transition in fracture appearance, while martensite does not.

4. The general direction of fracture propagation in the foil specimens is a composite of many fracture segments, but shows no over-all crystallographic preference. There is, however, a strong correlation between the width of the electron-transparent zone along the fracture and the general direction of the fracture. The zone width is greatest when the over-all fracture path is such that <111> slip directions can easily operate.

E. References

1. F.R.Larson and F.L.Carr, "Tensile Fracture Surface Configurations of a Heat Treated Steel as Affected by Temperature," Trans.ASM 55 (1962) 599.

2. C.D.Beacham, B.F.Brown and A.J.Edwards, "Quasi-Cleavage," Characterizing Fractures by Electron Fractography, Part 12, U.S.Naval Research Laboratory, Washington, D.C. Memorandum Report 1432 (1963).

3. B.R.Banerjee and J.J.Hauser, Fracture Micromechanics in High-Strength Steels and Titanium, Technical Documentary Report ML-TDR-64-182 (1964). Obtainable from DDC Cameron Station, Bldg.5, 5010 Duke Street, Alexandria, Va. 22314.

4. C.D.Beacham, "An Electron Fractographic Study of the Influence of Plastic Strain Conditions upon Ductile Rupture Processes in Metals," Trans.ASM 56 (1963) 318.

5. C.S.Yen and S.L.Pendleberry, "Fracture Strength of High-Strength Steels Containing Shallow Cracks" Trans.ASM 55 (1962) 214.

6. J.H.Bucher, G.W.Powell and J.W.Spretnak, "Tensile Fracture of Three Ultra-high Strength Steels," Trans.Met Soc <u>233</u> (1965) 884.

7. J.R.Low, "A Review of the Microstructural Aspects of Cleavage Fracture," <u>Conference on Fracture</u>, Technology Press and Wiley, New York (1959) 88.

8. A.M.Turkalo, "The Morphology of Brittle Fracture in Pearlite, Bainite and Martensite," Trans.AIME <u>218</u> (1960) 24.

9. P.M.Kelly and J.Nutting, "The Martensite Transformation in Carbon Steels," Proc.Roy.Soc.A<u>259</u> (1960) 45.

10. R.C.Glenn and J.C.Raley, "An Improved Procedure for Thinning Metallic Specimens for Transmission Electron Microscopy," <u>Symposium on Techniques in Electron Microscopy</u>, ASTM Tech.Pub. No.339 (1962) 60.

11. G.Thomas, "<u>Transmission Electron Microscopy of Metals</u>," Wiley, New York (1962) 115.

12. W.Pitsch and A.Schrader, "The Morphology of ε-Carbide Precipitation on Tempering Ferrite and Martensite," (in German).Arch. Eisenh.<u>29</u> (1958) 715.

13. W.Pitsch and A.Schrader, "The Morphology of Cementite Precipitation in Ferrite," (in German).Arch.Eisenh.<u>29</u> (1958) 485.

DOCUMENT CONTROL DATA - R&D

(Security classification of title, body of abstract and indexing annotation must be entered when the overall report is classified)

1. ORIGINATING ACTIVITY (Corporate author)	2a. REPORT SECURITY CLASSIFICATION
Department of Metallurgy Massachusetts Institute of Technology Cambridge, Massachusetts	Unclassified
	2b. GROUP

3. REPORT TITLE

Strengthening Mechanisms in Steel

4. DESCRIPTIVE NOTES *(Type of report and inclusive dates)*

Final Report - February 1962 to February 1965

5. AUTHOR(S) *(Last name, first name, initial)*

Cohen, Morris; Moss, S. C.; Hoffman, D. W.; MacDonald, B. A.; Langford, G.;
Lindborg, U. H.; and Averbach, B. L.

6. REPORT DATE	7a. TOTAL NO. OF PAGES	7b. NO. OF REFS
June 1966	139	62

8a. CONTRACT OR GRANT NO. AF 33(657)-8285	9a. ORIGINATOR'S REPORT NUMBER(S)
b. PROJECT NO. 7351	AFML-TR-65-406
c. Task No. 735105	9b. OTHER REPORT NO(S) *(Any other numbers that may be assigned this report)*
d.	

10. AVAILABILITY/LIMITATION NOTICES

This document is subject to special export controls and each transmittal to foreign
governments or foreign nationals may be made only with prior approval of the Metals
and Ceramics Division (MAM), Air Force Materials Laboratory, Wright-Patterson AFB,
Ohio.

11. SUPPLEMENTARY NOTES	12. SPONSORING MILITARY ACTIVITY
	Air Force Materials Laboratory Research and Technology Division Wright-Patterson Air Force Base, Ohio

13. ABSTRACT

In order to further develop understanding of the strengthening mechanisms that
are responsible for high-strength levels in steel, five related areas of research
were undertaken:

(1) The anisotropic static displacements of iron atoms around interstitial
carbon atoms in body-centered tetragonal martensite, as measured by x-ray intensity
measurements, are found to be much larger than the dynamic displacements due to
thermal motion. The static displacements thus determined are root-mean-square aver-
ages, from which it is possible to calculate the local displacements of the six iron
atoms which are adjacent to individual carbon atoms in the martensitic lattice. The
resulting tetragonal strain around each carbon atom is sufficiently large to inter-
act strongly with the strain field around dislocations, thereby accounting for the
potent solid-solution hardening effect of carbon in martensite.

(2) Ausformed martensite in an iron - 23 percent nickel - 0.4 percent carbon
alloy is significantly stronger than regular martensite, when both are in the virgin
(unaged) condition and when corrections are made for the retained austenite present.
However, both types of virgin martensite are relatively weak at low (micro) strains,
and exhibit their characteristic strength levels only after further straining in the
tensile test. Both kinds of martensite also undergo strengthening on aging at room
temperature or somewhat above, while the increment of ausform-strengthening reaches
a maximum on tempering at 200°C. These findings show that ausform-strengthening

(Continued on next page)

DD FORM 1473 1 JAN 64

Security Classification

14. KEY WORDS	LINK A		LINK B		LINK C	
	ROLE	WT	ROLE	WT	ROLE	WT

INSTRUCTIONS

1. **ORIGINATING ACTIVITY:** Enter the name and address of the contractor, subcontractor, grantee, Department of Defense activity or other organization *(corporate author)* issuing the report.

2a. **REPORT SECURITY CLASSIFICATION:** Enter the overall security classification of the report. Indicate whether "Restricted Data" is included. Marking is to be in accordance with appropriate security regulations.

2b. **GROUP:** Automatic downgrading is specified in DoD Directive 5200.10 and Armed Forces Industrial Manual. Enter the group number. Also, when applicable, show that optional markings have been used for Group 3 and Group 4 as authorized.

3. **REPORT TITLE:** Enter the complete report title in all capital letters. Titles in all cases should be unclassified. If a meaningful title cannot be selected without classification, show title classification in all capitals in parenthesis immediately following the title.

4. **DESCRIPTIVE NOTES:** If appropriate, enter the type of report, e.g., interim, progress, summary, annual, or final. Give the inclusive dates when a specific reporting period is covered.

5. **AUTHOR(S):** Enter the name(s) of author(s) as shown on or in the report. Enter last name, first name, middle initial. If military, show rank and branch of service. The name of the principal author is an absolute minimum requirement.

6. **REPORT DATE:** Enter the date of the report as day, month, year; or month, year. If more than one date appears on the report, use date of publication.

7a. **TOTAL NUMBER OF PAGES:** The total page count should follow normal pagination procedures, i.e., enter the number of pages containing information.

7b. **NUMBER OF REFERENCES:** Enter the total number of references cited in the report.

8a. **CONTRACT OR GRANT NUMBER:** If appropriate, enter the applicable number of the contract or grant under which the report was written.

8b, 8c, & 8d. **PROJECT NUMBER:** Enter the appropriate military department identification, such as project number, subproject number, system numbers, task number, etc.

9a. **ORIGINATOR'S REPORT NUMBER(S):** Enter the official report number by which the document will be identified and controlled by the originating activity. This number must be unique to this report.

9b. **OTHER REPORT NUMBER(S):** If the report has been assigned any other report numbers *(either by the originator or by the sponsor),* also enter this number(s).

10. **AVAILABILITY/LIMITATION NOTICES:** Enter any limitations on further dissemination of the report, other than those imposed by security classification, using standard statements such as:

  (1) "Qualified requesters may obtain copies of this report from DDC."

  (2) "Foreign announcement and dissemination of this report by DDC is not authorized."

  (3) "U. S. Government agencies may obtain copies of this report directly from DDC. Other qualified DDC users shall request through

    _____."

  (4) "U. S. military agencies may obtain copies of this report directly from DDC. Other qualified users shall request through

    _____."

  (5) "All distribution of this report is controlled. Qualified DDC users shall request through

    _____."

If the report has been furnished to the Office of Technical Services, Department of Commerce, for sale to the public, indicate this fact and enter the price, if known.

11. **SUPPLEMENTARY NOTES:** Use for additional explanatory notes.

12. **SPONSORING MILITARY ACTIVITY:** Enter the name of the departmental project office or laboratory sponsoring *(paying for)* the research and development. Include address.

13. **ABSTRACT:** Enter an abstract giving a brief and factual summary of the document indicative of the report, even though it may also appear elsewhere in the body of the technical report. If additional space is required, a continuation sheet shall be attached.

It is highly desirable that the abstract of classified reports be unclassified. Each paragraph of the abstract shall end with an indication of the military security classification of the information in the paragraph, represented as *(TS), (S), (C),* or *(U)*.

There is no limitation on the length of the abstract. However, the suggested length is from 150 to 225 words.

14. **KEY WORDS:** Key words are technically meaningful terms or short phrases that characterize a report and may be used as index entries for cataloging the report. Key words must be selected so that no security classification is required. Identifiers, such as equipment model designation, trade name, military project code name, geographic location, may be used as key words but will be followed by an indication of technical context. The assignment of links, rules, and weights is optional.

___